

# **Stony Brook University**



OFFICIAL COPY

**The official electronic file of this thesis or dissertation is maintained by the University Libraries on behalf of The Graduate School at Stony Brook University.**

**© All Rights Reserved by Author.**

Hepatocyte-Specific Endocytic Activity Exhibited by the Coxsackie and  
Adenovirus Receptor (CAR)

A Dissertation Presented to

The Academic Faculty

By

Paul John Lawrence

To

The Graduate School

In Partial Fulfillment of the

Requirements for the Degree

Doctor of Philosophy

In

Molecular Genetics and Microbiology

Stony Brook University

May 2007

Copyright by  
**Paul John Lawrence**  
2007

**Stony Brook University**

The Graduate School

**Paul John Lawrence**

We, the dissertation committee for the above candidate for the Doctor of Philosophy degree, hereby recommend acceptance of this dissertation.

Paul Freimuth - Dissertation Advisor  
Biochemist, Associate Chairman  
Biology Department, Brookhaven National Laboratory

Carol Carter - Chairperson of Defense  
Professor  
Department of Molecular Genetics and Microbiology

Eckard Wimmer  
Distinguished Professor  
Department of Molecular Genetics and Microbiology

Patrick Hearing  
Professor  
Department of Molecular Genetics and Microbiology

Deborah Brown  
Professor  
Department of Biochemistry and Cell Biology

This dissertation is accepted by the Graduate School

Lawrence Martin  
Dean of Graduate School

## **Abstract of the Dissertation**

Hepatocyte-Specific Endocytic Activity Exhibited by the Coxsackie and Adenovirus  
Receptor (CAR)

By

Paul John Lawrence  
Doctor of Philosophy

In

Molecular Genetics and Microbiology  
Stony Brook University

2007

Much of the current knowledge of the coxsackie and adenovirus receptor (CAR) stems from the study of infection of cell cultures by human subgroup B coxsackieviruses and many adenovirus (Ad) serotypes, which use CAR for attachment to susceptible cells. Apart from viral infection, knock-out mutations in mice determined that CAR plays a vital role in the development of cardiac tissue during embryogenesis. Many adult tissues also maintain CAR expression at relatively high levels and the importance of sustained CAR expression in these tissues has not been elucidated. A notable limitation of most investigations of CAR cell biology reported to date is that the studies were confined to cell culture models, which may not fully reconstitute the *in vivo* environment. Here, the behavior of CAR expressed in rodent adult liver and prostate tissue was investigated using the Ad-derived knob domain as a mono-specific ligand for CAR. The results of these experiments revealed two distinct tissue-specific CAR functions in cell culture as well as *in vivo*. Intravenous injection of knob in male mice stimulated the secretion of two proteins indigenous to the prostate ventral lobe into the mouse urine. The manner by which knob affects this secretion appears to reinforce traditional models established in cell culture, where CAR functions as an epithelial cell adhesion molecule contributing to the maintenance of the paracellular permeability barrier. In strong contrast, CAR on the surface of hepatocytes demonstrated rapid, receptor-mediated endocytosis of knob ligand with subsequent delivery to lysosomes where knob was degraded. This is the first direct evidence of efficient ligand endocytosis mediated by CAR that is recapitulated in an animal model.

## **Dedication**

*To my father,  
A veritable warehouse of knowledge,  
Who always kept me on my toes  
With his command of numerous subjects  
And challenged me  
To continually re-evaluate my beliefs.*

# Table of Contents

Abstract of the Dissertation.....	iii
Dedication .....	iv
Table of Contents .....	v
List of Figures.....	viii
List of Tables.....	ix
Acknowledgements.....	x
<b>Chapter 1: Introduction.....</b>	<b>1</b>
1. <i>The coxsackie adenovirus receptor (CAR)</i> .....	2
1.1.    CAR gene.....	2
1.2.    CAR protein.....	3
2. <i>CAR and adenovirus infection</i> .....	4
2.1.    Attachment.....	4
2.2.    Internalization.....	6
3. <i>CAR expressed on polarized epithelium</i> .....	7
4. <i>CAR expressed on hepatocytes</i> .....	9
5. <i>Background Figures</i> .....	11
<b>Chapter 2: Materials and Methods I—CAR Hepatocyte Study.....</b>	<b>16</b>
1. <i>Materials</i> .....	17
2. <i>Cell Cultures</i> .....	17
3. <i>Recombinant knob domain</i> .....	17
3.1.    Constructing the recombinant knob domain.....	17
3.2.    Biotinylation of the recombinant knob domain.....	18
4. <i>Animal studies</i> .....	18
4.1.    Swiss-Webster mice.....	18
4.2.    Preparation of liver tissue lysate.....	18
4.3.    Western blot analysis of liver tissue lysate.....	18
5. <i>Knob degradation assay</i> .....	19
6. <i>Knob internalization assays</i> .....	19
6.1.    Indirect immunofluorescent microscopy.....	19
6.2.    Pronase surface-stripping analysis.....	19
7. <i>Trafficking assessment</i> .....	20
7.1.    Mode of uptake.....	20
7.2.    Site of proteolysis.....	22
8. <i>Antibody-induced receptor crosslinking</i> .....	22
8.1.    Single-layer crosslinking.....	22
8.2.    Double-layer crosslinking.....	23

9.	<i>3'-RACE PCR assay</i> .....	23
9.1	First strand cDNA synthesis.....	23
9.2	Amplification of the target cDNA.....	24
9.3	Nested PCR of the amplified cDNA.....	24
10.	<i>Palmitoylation reduction assay</i> .....	25
11.	<i>Detergent-resistant membrane (DRM) isolation</i> .....	25
<b>Chapter 3: Results I—CAR Hepatocyte Study</b> .....		<b>26</b>
1.	<i>The adenovirus knob domain</i> .....	27
1.1.	Biotinylation of Ad2 and Ad12 knob.....	27
1.2.	Evaluation of biotinylated knob-CAR binding.....	27
2.	<i>Evaluating the fate of the biotinylated knob ligand in vivo</i> .....	28
3.	<i>Hepatocytes are responsible for the apparent degradation of biotinylated knob in the mouse liver</i> . 28	
3.1.	Primary rat hepatocytes.....	28
3.2.	H4-II-E cell line.....	29
3.3.	A549 cell line.....	30
3.4.	HEK-293 cell line.....	30
3.5.	HeLa S3 cell line.....	30
4.	<i>Evaluating CAR potential to internalize knob protein</i> .....	31
4.1.	Indirect immunofluorescent microscopy with acid surface-stripping.....	31
4.2.	Western blot analysis of cells surface-stripped with pronase.....	32
5.	<i>Route of CAR endocytosis</i> .....	32
5.1.	Knob degradation assay with specific inhibitors of endocytosis.....	33
5.2.	Knob internalization assay with specific inhibitors of endocytosis.....	33
5.3.	Co-localization with EEA-1 marker.....	34
6.	<i>Site of proteolysis</i> .....	34
6.1.	Co-localization with LysoTracker Red marker.....	34
6.2.	Knob degradation assay with lysosome inhibitors.....	34
7.	<i>Receptor crosslinking</i> .....	35
7.1.	A549 cell line.....	35
7.2.	H4-II-E cell line.....	36
8.	<i>Figures</i> .....	38
<b>Chapter 4: Discussion I—CAR Hepatocyte Study</b> .....		<b>47</b>
<b>Chapter 5: Supplementary Data—CAR Hepatocyte Study</b> .....		<b>53</b>
1.	<i>Regulation hypothesis #1: CAR splice variants</i> .....	54
2.	<i>Regulation hypothesis #2: CAR palmitoylation and raft association</i> .....	55
2.1.	Palmitoylation.....	55
2.2.	Lipid raft association.....	56
3.	<i>Supplemental Figures of Preliminary Data</i> .....	57
<b>Chapter 6: Materials and Methods II—CAR Prostate Study</b> .....		<b>60</b>
1.	<i>Materials</i> .....	61
2.	<i>Recombinant knob domain</i> .....	61
2.1.	Constructing the recombinant knob domain.....	61
2.2.	Biotinylation of the recombinant knob domain.....	61

3.	<i>Animal studies.</i>	61
3.1.	Swiss-Webster mice.	61
3.2.	Preparation of tissue lysates.	62
4.	<i>Urinary protein analysis.</i>	62
5.	<i>Kallikrein fluorescence assay and zymogram.</i>	62
6.	<i>Western blot analysis.</i>	62
7.	<i>Mass spectrometry and protein identification.</i>	63
<b>Chapter 7: Results II—CAR Prostate Study</b>		<b>64</b>
1.	<i>Large bladder volumes.</i>	65
2.	<i>Urinary protein analysis.</i>	65
2.1.	Protein gel electrophoresis.	65
2.2.	Knob assessment.	66
2.3.	Kallikrein assessment.	66
2.4.	CAR assessment.	66
3.	<i>Identification of SBP and P12.</i>	66
3.1.	Mass spectrometry analysis.	66
3.2.	Western blot analysis with anti-spermine binding protein.	67
4.	<i>Phosphate enhances knob effect.</i>	67
5.	<i>Figures and Tables.</i>	69
<b>Chapter 8: Discussion II—CAR Prostate Study</b>		<b>78</b>
<b>References</b>		<b>83</b>

## List of Figures

Figure 1 (Chapter 1).....	page 11
Figure 2 (Chapter 1).....	page 12
Figure 3 (Chapter 1).....	page 13
Figure 4 (Chapter 1).....	page 14
Figure 5 (Chapter 1).....	page 15
Figure 1 (Chapter 3).....	page 38
Figure 2 (Chapter 3).....	page 39
Figure 3 (Chapter 3).....	page 40
Figure 4 (Chapter 3).....	page 41
Figure 5 (Chapter 3).....	page 42
Figure 6 (Chapter 3).....	page 43
Figure 7 (Chapter 3).....	page 44
Figure 8 (Chapter 3).....	page 45
Figure 9 (Chapter 3).....	page 46
Figure 1 (Chapter 5).....	page 57
Figure 2 (Chapter 5).....	page 58
Figure 3 (Chapter 5).....	page 59
Figure 1 (Chapter 7).....	page 69
Figure 2 (Chapter 7).....	page 70
Figure 3 (Chapter 7).....	page 71
Figure 4 (Chapter 7).....	page 72
Figure 5 (Chapter 7).....	page 73
Figure 6 (Chapter 7).....	page 74

## List of Tables

Table I (Chapter 7).....	page 75
Table II (Chapter 7).....	page 76
Table III (Chapter 7).....	page 77

## **Acknowledgements**

I want to thank Dr. Paul Freimuth for being a superb mentor over the years. His instruction and guidance have matured my research aspirations and provided me with a solid footing for my career as a scientist.

I also want to acknowledge my colleagues in the biology department of Brookhaven National Laboratory for their kind support and most importantly for their friendship. In particular, I want to thank Ryan Schulz, Beth Mulligan, Celine Lesaulnier, Irene Rosati, Sydell Lamb, Kathy Folkers, and Dr. Yian-Biao Zhang.

Finally, I want to thank my committee members: Drs. Carol Carter, Patrick Hearing, Eckard Wimmer, and Deborah Brown whose advice has steered me to the successful completion of my doctorate.

## **Chapter 1: Introduction.**

## **1. The coxsackie adenovirus receptor (CAR).**

The coxsackie and adenovirus receptor (CAR) is a member of the immunoglobulin (Ig) superfamily that is highly conserved among vertebrates. CAR is also part of the CTX subset of the Ig superfamily (1), thus possessing two Ig-like ectodomains: D1 and D2, which are attached to a single pass transmembrane domain, followed by a cytoplasmic tail composed of 94 or 107 amino acids depending on which of two dominant splice variants is expressed (chapter 1, figure 1) (2). Much of the current knowledge regarding CAR has been derived from investigations of infection by subgroup B coxsackieviruses (CVB) and several serotypes of adenovirus (Ad). With respect to these viruses, CAR serves as the site of primary attachment to host cells (3-6). Apart from its role in virus infection, early studies in mice found that CAR knock-out mutations are embryonic lethal, where the receptor molecule was found to be necessary for development of cardiac tissue (7-9). Conditional knock-out mutations in cardiac tissue narrowed the criticality of CAR to the first two weeks of embryonic development (10). During this time period, it is believed that CAR forms homotypic contacts that are likely very important for intercellular adhesion at this stage of embryonic development. After day 12, disruption of the CAR gene in heart tissue was not lethal. Additionally, quantitative real-time PCR and Western blot analysis of rat cardiac tissue demonstrated that CAR expression gradually decreases during post-natal development (9). These findings have substantiated an important role for CAR in early embryogenesis, but many rodent and human adult tissues exhibit sustained CAR expression. Several tissues demonstrate relatively high levels of CAR such as the liver, kidney, heart, lung, and prostate (11,12). Maintenance of CAR expression strongly suggests that this molecule fulfills a critical role in adult tissue that has yet to be elucidated.

### **1.1. CAR gene.**

The CAR gene locus, designated CXADR, was identified on chromosome 21q11.2 in humans and on chromosome 16 in mice (13,14). CXADR consists of seven exons in both humans and mice, and both loci possess an additional eighth exon approximately 27 kb downstream of exon 7. Northern blot analysis has confirmed the existence of at least two principal mRNA transcripts, commonly referred to as mCAR1 and mCAR2 in mice and hCAR1 and hCAR2 in humans, which exhibit differential splicing within the region of exon 7 (2). Approximately 75% of exon 7 is removed and substituted with exon 8 in the smaller mCAR2 transcript in mice. Smaller less abundant transcripts have been also been identified through RT-PCR in both humans and mice that are lacking exons 5 and 6, which encode the transmembrane domain and part of the cytoplasmic tail, but retain exon 7 (15,16). Some of these smaller isoforms also omit exons 3 and 4. As such, the smaller human and mouse CAR transcripts are not cell-associated like hCAR1/hCAR2 and mCAR1/mCAR2 and are reported to be secreted. Alternative functions for these secreted CAR isoforms have not yet been described, though several studies have demonstrated inhibition of CVB

infection in cell culture and *in vivo* by recombinant soluble CAR isoforms (17-19).

As described above, expression of the CXADR gene is important in the first 12 days of embryogenesis, particularly with respect to cardiac tissue (7,9,10). In other tissues, CAR expression is maintained into adulthood, thus this molecule continues to serve a purpose in other organs beyond embryonic development. In fact, CAR expression is considerably high relative to other tissues in the liver and the prostate (2,11,12). The reason for the increased level of CAR production in these tissues is not currently understood. Additionally, immortalized cell lines from human tissues typically sustain CAR expression such as HeLa, A549, HEK-293, and HepG2. By contrast, most rodent cell lines such as NIH-3T3, CHO, and A9 exhibit no detectable CAR expression, but there are a few rare exceptions such as the H4-II-E rat hepatoma cell line. It has yet to be determined why immortalized human cell lines sustain CAR expression and murine cell lines do not, though there is some evidence supporting regulation by chromatin remodeling (20). Taken together, it is clear that there are many aspects of CAR gene regulation that need to be examined in greater detail.

## **1.2. CAR protein.**

As described above, CAR is a type 1 transmembrane protein and an Ig superfamily member. Notably, this family of proteins includes many other virus receptors including: poliovirus receptor (PVR) (21,22), intercellular adhesion molecule-1 (ICAM-1) used by rhinoviruses (23), and junctional adhesion molecule-A (JAM-A) used by mammalian reoviruses (24). Like JAM-A, CAR is a member of the CTX subset of the Ig superfamily(1), and as such has two extracellular Ig-like domains: D1 and D2 (25,26). CAR D1 is at the distal N-terminus of the protein, is defined as an Ig variable (Ig-V) type domain, and is the site of a single N-linked glycan modification. Both CVB and Ad particles attach to CAR via an interaction with the D1 ectodomain, though in different regions of the domain (3,4). The co-crystal structure of the Ad12 derived knob domain complexed with the CAR D1 domain identified the critical amino acid residues for Ad attachment (27). In fact, with the exception of the D1 domain, the rest of the CAR molecule is dispensable with respect to productive Ad infection, as demonstrated by a published report in which Ad particles were able to efficiently infect cell cultures that do not endogenously express CAR, but ectopically expressed the CAR D1 domain tethered to the cell surface by a glycosyl-phosphatidylinositol (GPI) anchor (28). The D2 ectodomain has been categorized as an Ig constant (Ig-C2) type domain and is found below D1 proximal to the membrane surface. The D2 domain is also modified by N-linked glycosylation at a single site, similar to D1. The D1 and D2 glycosylations are responsible for the apparent 46 kDa molecular weight of CAR in SDS gels, while the calculated molecular weight of the receptor is 38 kDa. Although, D2 does not physically interact with virus attachment proteins, studies have suggested that D2 positions the D1

domain in an orientation favorable for virus attachment (29). Following D2 is the single pass transmembrane helix and the cytoplasmic tail.

Although the cytoplasmic tail is not essential for viral pathogenesis, it has been implicated in the sorting of newly synthesized CAR molecules to specific regions of the plasma membrane and may participate in signaling cascades (30). The first two residues of the tail domain are cysteines, which were found to be acylated by the 16-carbon fatty acid palmitate (31). Additionally, the final three amino acid residues of the C-terminus of the two major splice variants represent a class I PDZ domain interaction motif: Ser-Ile-Val (SIV) in mCAR1/hCAR1 and Thr-Val-Val (TVV) in mCAR2/hCAR2 (32,33). Several cytosolic PDZ domain containing proteins, including MUPP-1, MAGI-1, PSD-95, LNX and ZO-1, have been reported to interact with CAR through this PDZ interaction motif (34-37). Considering that MUPP-1 contains 13 PDZ domains, CAR is conceivably a component of large supramolecular lattices on the cytosolic face of the plasma membrane (38).

The X-ray structure of recombinant CAR D1 was solved to an atomic resolution of 1.7 angstroms, and revealed the D1 domain formed dimers in solution, in a head-to-tail orientation (39). Additionally, equilibrium centrifugation analysis determined the dissociation constant ( $K_d$ ) of the CAR D1 dimers was 16  $\mu$ M, similar to the  $K_d$  of several known intercellular adhesion molecules. These structural findings lend credence to proposed model of CAR mediating homophilic interactions between cells in developing embryonic tissue.

## **2. CAR and adenovirus infection.**

As mentioned above, CVB and Ad virions utilize CAR for primary attachment to susceptible cells (3,4). Human Ad serotypes from subgroups A, C, D, E, and F bind CAR with high affinity through the trimeric globular knob domain that sits atop a fiber shaft that projects from the vertices of the capsid (6,40). Subgroup B adenoviruses do not interact with CAR, and some subgroup B serotypes have been reported to attach to host cells via a component of the complement cascade: CD46 (41-43).

### **2.1. Attachment.**

The adenovirus particle is a non-enveloped double-stranded DNA virus, which is composed of several different proteins including the hexon, penton, and fiber antigens that are exposed to environment. Early studies of Ad infection of cell cultures found that certain structural components of the Ad capsid are overproduced during viral synthesis and can be purified from infected cells. Among these viral components, the Ad fiber protein was able to be purified apart from other capsid proteins (44). Given that this protein extends away from the virus capsid, it was presumed that this fiber mediated attachment to the cellular receptor site, which had yet to be identified as CAR. Indeed, it was discovered that pre-treatment of cell cultures with the purified Ad fiber protein from Ad serotypes 2 and 5 (Ad2 and Ad5) completely abrogated the attachment of the Ad virions (40). Based on these findings, it

was concluded that the Ad fiber was responsible for virus binding to host cells.

With the advent of protein overexpression and purification technologies in bacterial and insect cells, the recombinant knob domain from CAR-binding Ad serotypes has frequently been employed as a CAR ligand. Sequence and conformational analyses of the Ad fiber shaft have revealed poly-lysine motifs, which were demonstrated to mediate interactions with heparin sulfate glycosaminoglycans on the cell surface (45,46). Therefore, the globular knob domain in absence of the fiber shaft represents a truly monospecific CAR ligand. The knob domain from subgroup C serotypes 2 and 5 have been crystallized, and the subgroup A serotype 12 knob domain has been crystallized in complex with the D1 domain of CAR (27,47). Recently, the structures have been solved for the heterodimers of human Ad37 knob-CAR D1 and canine Ad2 knob-CAR D1 (48). These structural studies have provided a wealth of information regarding the knob-CAR interaction (chapter 1, figure 2). The Ad5 knob X-ray structure revealed a cavity on the ventral 3-fold axis of the homotrimeric knob domain, which suggested a possible binding pocket for the Ad cellular receptor (which had yet to be identified as CAR). However, the Ad12 knob-CAR D1 co-crystal structure revealed that the binding interface is along the lateral side surface of each monomer subunit, with some overlap onto the neighboring knob monomer. Specifically, the CAR D1 interaction occurs through the AB, CD, and DG loops of one knob monomer, and the second monomer interacts via the FG loop. This indicated that a single knob homotrimer was capable of simultaneously binding as many as 3 different CAR molecules, which subsequent investigations have found to promote an avidity mechanism to the interaction of knob-CAR (49). Interestingly, the amino acid residues within the CAR D1 domain that are utilized by knob for attachment have been evolutionarily conserved, and overlap with the CAR-CAR binding sites delineated by the CAR D1 dimer crystal structure (27,39). Topologically, the binding regions of knob do not form a snug fit on the CAR D1 surface. The co-crystal structure identified a pocket of space between the two molecules that could potentially accommodate several water molecules, which the authors describe could act as “molecular glue” (27,50). A notable consequence of such a binding interaction would be that it allows for antigenic variation to occur in the virus attachment domain without necessarily sacrificing the ability to attach to the receptor molecule. Furthermore, analysis of the critical contact residues in the knob domain has allowed for the rational design and production of recombinant knob mutants with enhanced or severely diminished affinity for CAR (50,51). For example, the  $K_d$  for wild-type Ad12 knob in complex with CAR D1 was measured by fluorescence anisotropy to be 290 nM. The substitution of Pro417 and Pro418 residues in the AB-loop of Ad12 knob with Glu and Ala residues (P417E/P418A), respectively, resulted in a dramatic reduction in knob affinity for CAR to a millimolar affinity. Extrapolating from the Ad12 knob-CAR D1 co-crystal

structure, similar mutations (S408E/P409A) were introduced into Ad2 knob that completely ablated its ability to bind CAR. Cumulatively, these structural studies have allowed for the dissection of the knob-CAR interaction, partially in the hopes of using that knowledge for the re-targeting of Ad-based gene therapy vectors to desired sites in host organisms.

## **2.2. Internalization.**

While the fiber knob was demonstrated repeatedly to be necessary for attachment, it became clear that the processes of attachment and entry of the Ad particle into susceptible host cells was mediated by two distinct viral antigens and two distinct cellular receptors. Enzymatic treatment of adherent HeLa cells with subtilisin was found to inactivate nearly all available cellular receptor sites (40) (now known to be CAR). By cellular fractionation, it was confirmed that the CAR molecules were confined to the plasma membrane. Since subtilisin does not penetrate the plasma membrane, it was concluded that the Ad receptor was confined to the cell surface. In another study, purified Ad fiber was radiolabeled, applied to HeLa cell cultures, and incubated at warm temperatures to allow for endocytosis (52). After warming for specified durations, the cells were surface-stripped with subtilisin as described above. A very limited amount of the radiolabeled fiber survived the enzymatic treatment, suggesting that receptor molecule, CAR, with which Ad fiber attaches cannot facilitate rapid ligand endocytosis.

Attention turned to the penton base protein present at the capsid vertices, where the Ad fiber inserts. In a hypervariable region that protrudes from the penton base, a tripeptide Arg-Gly-Asp (RGD) motif was identified, which is present on the surface of vitronectin and fibronectin; known substrates of  $\alpha_v$ -containing integrins. Repeating the subtilisin time course analysis that was conducted for Ad fiber, purified penton base and fiber-penton base complexes were radiolabeled and incubated on HeLa cells. Both the penton base and fiber-penton base complexes were internalized rapidly within 15 minutes. Furthermore, pre-treatment with antibodies specific for  $\alpha_v$ -containing integrin heterodimers that bind vitronectin and fibronectin abrogated the observed binding and uptake. The authors concluded that, while the Ad fiber protein mediated cell attachment, a secondary interaction with  $\alpha_v\beta_3$  and  $\alpha_v\beta_5$  integrins through the RGD motif in the Ad penton base was required for the rapid endocytosis of viral particles (52). Both the cryo-EM and the X-ray crystallographic structure of the Ad2 and Ad12 virions engaged with the  $\alpha_v\beta_5$  integrin heterodimer reinforced the contention that the RGD motifs are the critical binding site for the integrin co-receptor (53,54). Kinetic analysis demonstrated that a single penton base molecule is capable of binding approximately 4 integrin heterodimers, clustering the integrins, which might signal for uptake.

In the context of whole virus, mutant Ad2 virions were constructed with the RGD motif altered to RAE, RVD, and RGE (55). These RGD-negative Ad2 particles were applied to different non-polarized cell lines and evaluated for initiation of viral DNA replication relative to wild-type Ad2.

When applied to the lung carcinoma A549 cell line, although still viable, the mutant virions experienced a considerable delay in the onset of viral DNA replication of 10 hours relative to wild-type. Similar results were obtained for the adherent HeLa cell line. During the 10 hours, the mutant Ad2 virions were susceptible to the treatment of neutralizing antibodies, thus confirming that the delay was at the level of endocytosis. Curiously, when the RGD-negative Ad2 particles were applied to cultures of the HEK-293 cell line, uptake was prolonged by less than 2 hours relative to wild-type Ad2. The same mutants were endocytosed with wild-type efficiency when applied to the suspension-adapted HeLa S3 cell line. The results with the latter two cell lines imply that the co-receptor interaction is not necessarily an absolute requirement for the acceleration of viral endocytosis depending on the cell type. It also could be inferred from this study that the endocytosis of the RGD-negative Ad2 virions was mediated by CAR. However, these studies were limited to cell lines, and as such it was unclear if the phenotype observed could be recapitulated in an *in vivo* model system.

Interestingly, there are Ad serotypes, such as human Ad40 and Ad41 and canine Ad2, which do not possess the RGD motifs required for the integrin co-receptor interaction (56,57). While retaining affinity for CAR through the knob domain, these viruses have an as yet uncharacterized alternative mode of efficient entry into host cells. These serotypes typically exhibit an enteric tropism suggesting the possibility that CAR displayed on the epithelia of the gastro-intestinal tract may be endocytically active.

### **3. CAR expressed on polarized epithelium.**

Most of our understanding of CAR cell biology is within the context of polarized lung epithelium. The strong interest in CAR expressed in adult lung tissue derives in part from the inefficiency with which lung tissue was transduced by Ad-based gene therapy vectors. An examination of cultures of polarized lung epithelia revealed CAR to be limited to the basal-lateral surface, where apical localization of the receptor was observed only on damaged or regenerating cells (58). Further analysis found CAR sequestered in the paracellular space below the tight junction in the adherens junction (36,38,59). The poor transduction efficiency of Ad-based gene therapy vectors therefore was explained by the absence of the virus receptor on the apical surface of lung epithelial cells.

The sorting of newly synthesized CAR molecules to the basal-lateral surface has been attributed to specific sequences within the cytoplasmic tail domain. Bergelson and colleagues ectopically expressed various mutant CAR molecules truncated at different lengths within the tail domain (30). The deletion of the entire cytoplasmic tail domain resulted in the localization of CAR to both the apical and the basal-lateral surface. Targeted substitutions of particular regions of the cytoplasmic tail revealed that residues 345-349 (LSRMG) and tyrosine (Y) 318 were essential for the basal-lateral sorting of CAR. As previously mentioned, two dominant CAR splice variants exist in mice, which differ only in the cytoplasmic domain. Both retain residue Y318, but the smaller isoform, mCAR2, lacks the LSMRG motif. When examined, both isoforms

mCAR1 and mCAR2 localized to the basal-lateral surface. In a separate study, the importance of the palmitoylation of the twin cysteines of the cytoplasmic tail for membrane sorting of CAR was assessed by substitution with twin alanine residues (31). The ablation of CAR palmitoylation resulted in a split distribution of the receptor molecule between the cell surface and several unidentified intracellular compartments. The authors proposed two explanations: that the fatty acid modification is responsible for directing newly synthesized CAR molecules to the cell surface or that the palmitate anchors CAR at the plasma membrane and its removal triggered the constitutive endocytosis of CAR.

It was presumed that CAR might contribute to the maintenance of the paracellular permeability barrier through the formation of homotypic contacts with its counterparts on adjacent cells within the paracellular space. Indeed, the purified CAR D1 domain crystallized as dimers in head-to-tail orientation, thus strengthening the notion that CAR formed homophilic interactions with adjacent partners. Interestingly, experiments described in previous sections revealed that endogenous CAR molecules have a 1000-fold higher affinity for purified Ad fiber protein than for homophilic interactions, suggesting that the Ad fiber protein could competitively dissociate CAR homotypic contacts and open up the paracellular space (60). In fact, when fiber protein was applied to the basal-lateral surface of polarized epithelial cells grown in voltage-gated trans-well plates, there was a substantial decrease in trans-epithelial resistance confirming that CAR-CAR interactions blocked the passage of ions and other solutes through the paracellular space between polarized cells (36). Indirect immunofluorescent microscopy has been used to demonstrate that CAR co-localizes with cytosolic proteins, such as ZO-1, known to associate with tight junction and adherens junction molecules. Moreover, in epithelial cell lysates, CAR was immunoprecipitated with ZO-1 and other tight junction and adherens junction proteins.

Interestingly, the progression of certain types of cancers including malignant glioblastoma, and prostate and bladder cancer has been shown to correlate with the down-regulation of CAR leading some investigators to attribute tumor suppressor function to CAR (61-63). The effect has been purported to derive from the loss of intercellular adhesion from diminished CAR-CAR contacts. In the case of malignant glioma cells, the critical domain for CAR tumor suppressor function has been reported to be the cytoplasmic domain, where expression of recombinant CAR isoforms with deleted cytoplasmic tails failed to curtail cancer progression (64). Research into a potential role for CAR in prostate cancer has revealed that the receptor molecule is abundantly expressed in prostate epithelium, where it is not limited to the basal-lateral surface, but also exhibits apical localization (65). However, as described above, down-regulation of CAR has been found to be coincident with cancer progression in prostate tissue. The decrease in CAR expression has been reported to occur through the epigenetic modification of the CAR promoter site by histone de-acetylation in several urogenital cancer cell lines (20). This was reinforced by evidence that treatment of cell cultures with a chemotherapeutic agent functioning as a histone de-

acetylase inhibitor stimulated CAR expression. Taken together, these reports strongly suggest that in the context of polarized epithelium of certain adult tissues, CAR exerts tumor suppressor activity through the maintenance of intercellular adhesion. Further analysis will be required to determine, apart from impeding cancer progression, why the prostate epithelium sustains such high levels of CAR expression on both the apical and basal-lateral surfaces, relative to the levels and distribution of CAR in the polarized epithelium of other adult tissues.

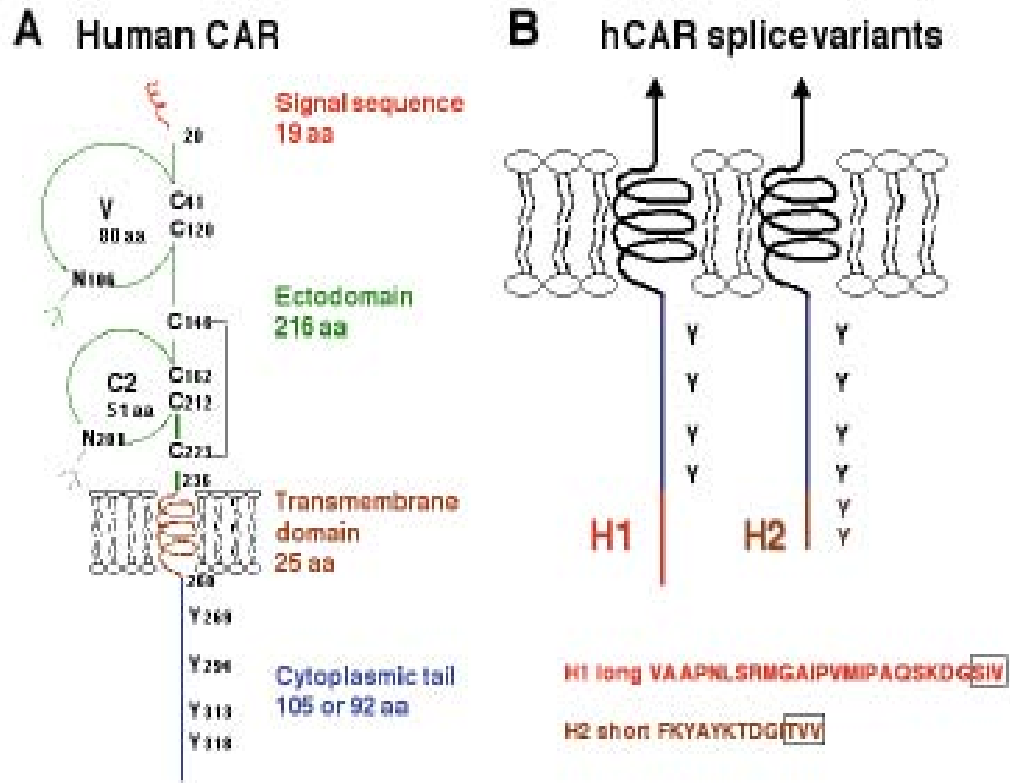
#### **4. CAR expressed on hepatocytes.**

Northern blot analysis with probes for CAR mRNA transcripts and immunohistochemical staining with peroxidase conjugated anti-CAR antibodies have established that, particularly in rodents, the liver is the site of the highest level of CAR expression in the adult animal (11,12). Additionally, the receptor does not appear to be buried within the junctional space between polarized cells. An *in vivo* investigation of CAR biodistribution utilized technetium-99m (<sup>99m</sup>Tc) labeled recombinant Ad5 knob protein as a mono-specific ligand for CAR, which was administered by tail-vein injection (66). Dynamic imaging tracked the rapid depletion of the knob ligand from the bloodstream and saturation of specific binding sites in the liver after less than 1 minute post-injection. Pre-injection of cold Ad5 knob prevented the accumulation of <sup>99m</sup>Tc-Ad5 knob in the liver, while pre-injection with recombinant knob from the non-CAR binding Ad3 subgroup B serotype did not, thus supporting that this was CAR-dependent. The kinetics of knob sequestration to the liver suggests a population of CAR molecules that is highly accessible to blood borne ligands. The importance of maintaining elevated amounts of CAR in the liver has yet to be determined.

Another *in vivo* CAR biodistribution study provided additional indirect evidence in support of the hypothesis that CAR expressed on hepatocytes facilitates rapid receptor-mediated endocytosis (67). Recombinant Ad2 and Ad12 knob were radioiodinated (<sup>131</sup>I) and IV administered similar to the previously reported CAR biodistribution study using <sup>99m</sup>Tc-Ad5 knob. After a period of time, the mice were sacrificed, their organs dissected, and evaluated for radioactivity by gamma counting. In contradiction to previous results, the bulk of the radioactivity accumulated in the stomach, rather than the liver, in <sup>131</sup>I-Ad2 knob injected mice. Mice injected with <sup>131</sup>I-Ad12 knob exhibited radioactivity split between the liver and the stomach. Radioiodinated mutants of Ad2 and Ad12 knob, where the critical amino acid residues for CAR binding were substituted, were employed as negative controls and their associated radioactivity persisted in the blood. This was perplexing in that of the many adult tissues that sustain CAR expression, the stomach produces relatively little compared with liver, lung, prostate, heart, and kidney tissue (2,11,12). However, the stomach has been reported to possess large quantities of sodium-iodide symporters which are used by the host organism to scavenge free iodine for the production of thyroid hormone (68). Given that the iodo-tyrosine bond is particularly labile and that hepatocytes are established to have large intracellular pools of deiodinase activity, the authors speculated that the radioiodinated Ad2 and Ad12 knob had actually

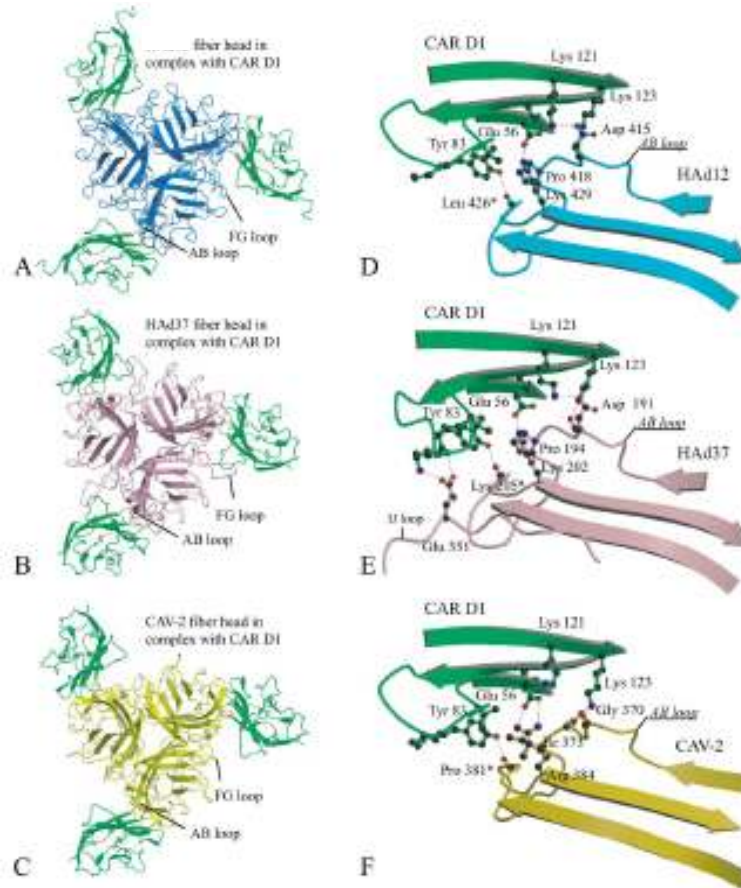
been captured in the liver. However, once bound, the knob ligands were delivered to an intracellular compartment containing deiodinases, which liberated the radioiodine allowing it to diffuse back into circulation to eventually be scavenged by sodium-iodide symporters in the stomach. They concluded that the rapid endocytosis of the knob ligand required CAR interaction, in that the radioactivity associated with IV administered knob mutants persisted in the blood. The notion that CAR on hepatocytes is endocytically active is strengthened taking into consideration a parallel *in vivo* study of low density lipoprotein receptor (LDLR) (69). In the LDLR study, LDL molecules were labeled with either  $^{99m}\text{Tc}$  or  $^{131}\text{I}$ , and were IV injected into mice. Mirroring the pattern observed with the knob ligands, the  $^{99m}\text{Tc}$ -LDL injected animals saw the accumulation of radioactivity in the liver, while radioactivity was observed in the stomach of the  $^{131}\text{I}$ -LDL injected animals. Given that LDLR has been extensively characterized as an endocytically active receptor molecule, to obtain identical results with CAR strongly implies that it may also catalyze rapid ligand endocytosis. Moreover, CAR has been demonstrated to associate with a specialized microdomain of the plasma membrane distinct from that of caveolin-1 associated lipid rafts, which also appears to be occupied by LDLR (70). The capacity of CAR to facilitate receptor-mediated endocytosis of bound ligand in the context of liver tissue has not been directly investigated until this present study.

5. Background Figures.



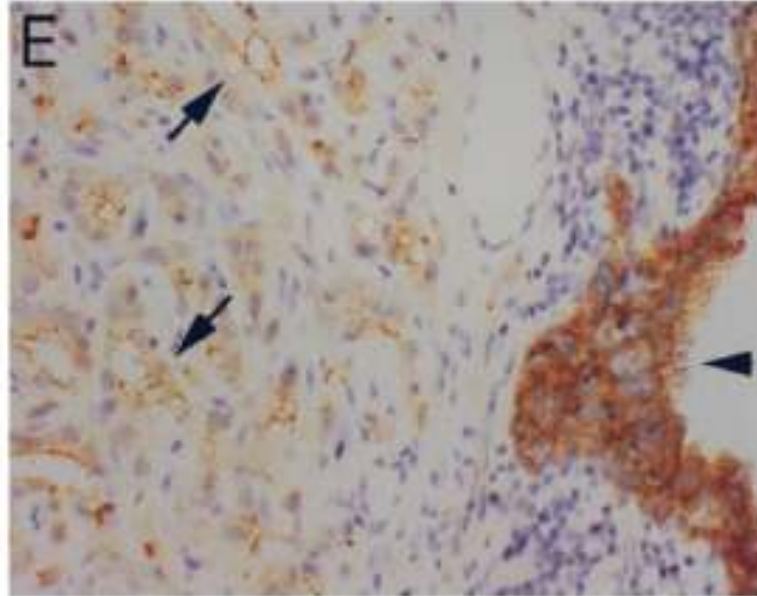
Philipson, L, and R.F. Pettersson. The Coxsackie-Adenovirus Receptor—A New Receptor in the Immunoglobulin Family Involved in Cell Adhesion (2004). *Current Topics in Microbiology and Immunology* 273: 87-111.

**Background Figure 1.** A, schematic of full length CAR inserted into the cell membrane with two Ig-like ectodomains (denoted V and C2) and transmembrane domain and a cytoplasmic tail of varying length. B, schematic of the two cell-associated isoforms of human CAR inserted into the cell membrane with conserved tyrosine residues indicated as well as two class I PDZ interaction motifs found in both isoforms (SIV for hCAR1 and TVV for hCAR2).



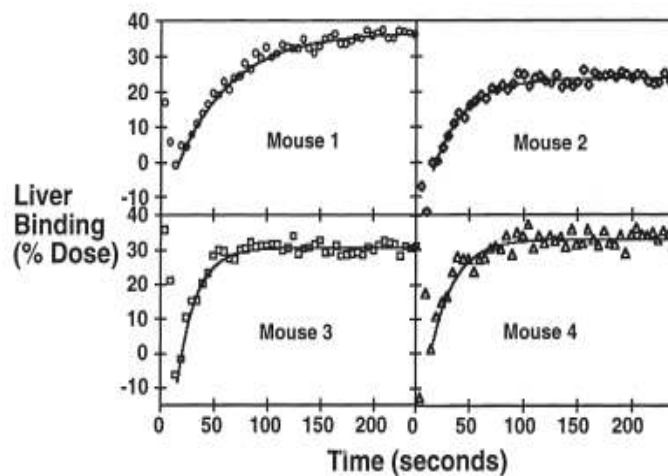
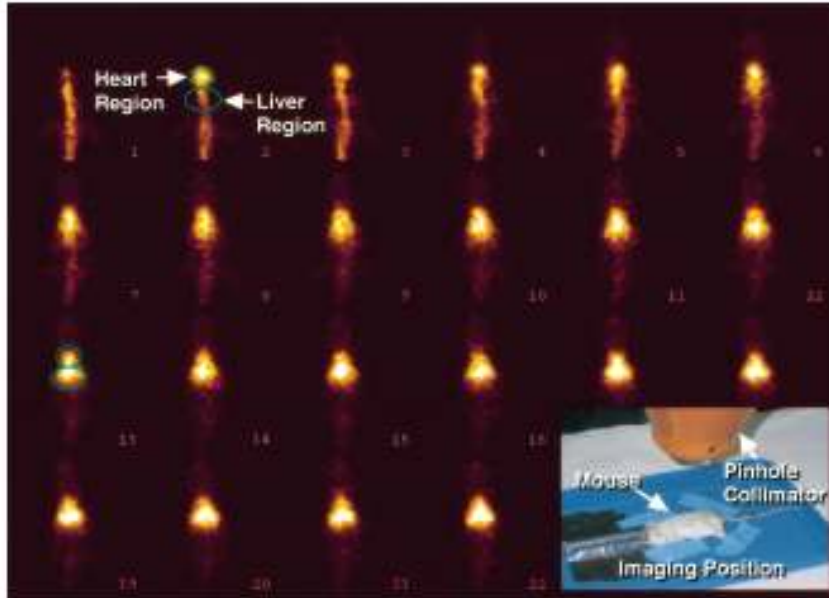
Seiradake, E., H. Lortat-Jacob, O. Billet, E. J. Kremer, and S. Cusack (2006). Structural and Mutational Analysis of Human Ad37 and Canine Adenovirus 2 Fiber Heads in Complex with the D1 Domain of Coxsackie and Adenovirus Receptor. *The Journal of Biological Chemistry* **281**(44): 33704-33716.

**Background Figure 2.** *A, B, C*, Ribbon diagrams of the X-ray crystallographic structures of hAd12 knob-CAR D1, hAd37 knob-CAR D1, and cAd2 knob-CAR D1 heterodimers looking down from the viral fiber. These diagrams illustrate the trivalence of the Ad knob domain, where one knob homotrimer can bind up to 3 CAR molecules simultaneously. *D, E, F*, Part of the knob-CAR binding interface showing the key interacting amino acid residues.



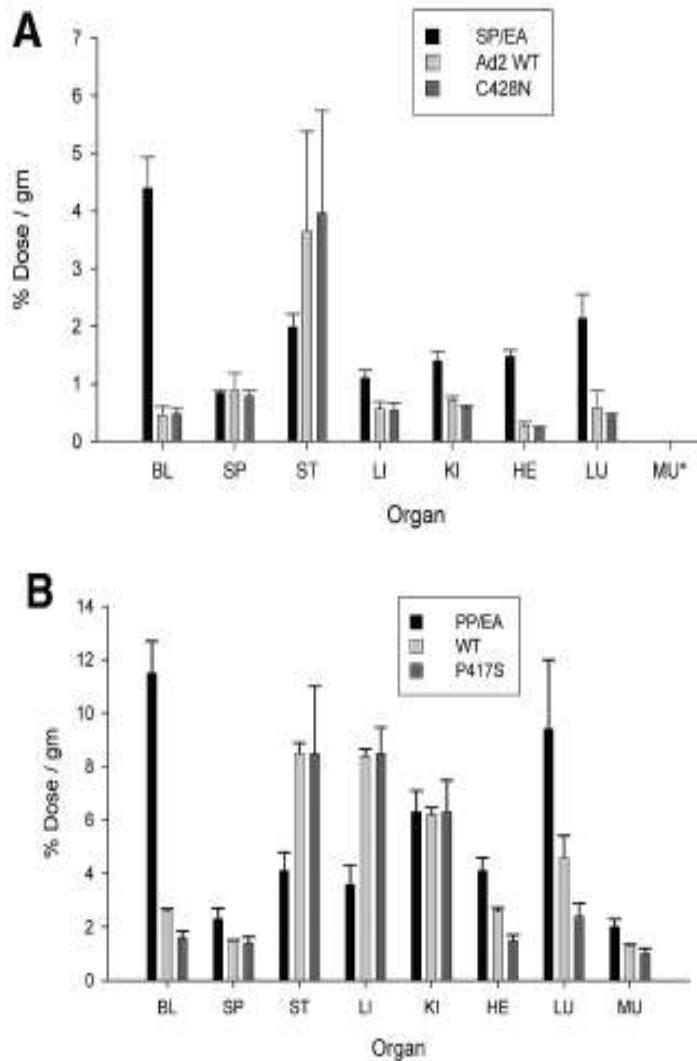
Rauen, K.A., D. Sudilovsky, J.L. Le, K.L. Chew, B. Hann, V. Weinberg, L.D. Schmitt, and F. McCormick (2002). Expression of the coxsackie adenovirus receptor in normal prostate and in primary and metastatic prostate carcinoma: potential relevance to gene therapy. *Cancer Research* **62**(13): 3812-3818.

**Background Figure 3.** Immunohistochemical staining for CAR in prostate epithelium. Panel E (from Rauen et.al, 2002) shows the difference in the level of CAR staining between a high-grade prostate adenocarcinoma (arrows) and normal prostate (arrowhead).



Zinn, K.R., J.T. Douglas, C.A. Smyth, H.G. Liu, Q. Wu, V.N. Krasnykh, J.D. Mountz, D.T. Curiel, and J.M. Mountz (1998). Imaging and tissue biodistribution of  $^{99m}\text{Tc}$ -labeled adenovirus knob (serotype 5). *Gene Therapy* 5(6): 798-808.

**Background Figure 4.** *Top:* sequential images taken every 5 seconds after IV injection of  $^{99m}\text{Tc}$ -Ad5 knob by dynamic imaging. *Bottom:* The liver uptake was quantified from the sequential dynamic imaging showing that  $^{99m}\text{Tc}$ -Ad5 knob is rapidly sequestered to the mouse liver approximately 1 minute post-injection.



Awasthi, V., G. Meinken, K. Springer, S.C. Srivastava, and P. Freimuth (2004). Biodistribution of radioiodinated adenovirus fiber protein knob domain after intravenous injection in mice. *Journal of Virology* **78**(12): 6431-6438.

**Background Figure 5.** Detection of IV administered  $^{131}\text{I}$ -labeled knob in mice. *A*, WT-Ad2 knob and an enhanced CAR binding mutant (C428N) are found almost exclusively in the stomach. *B*, WT-Ad12 knob and an enhanced binding mutant (P417S) are found 50% in the liver and 50% in the stomach. Non-CAR binding mutants of both knob proteins (Ad2-SP/EA and Ad12-PP/EA) are detected in the blood.

## **Chapter 2: Materials and Methods I—CAR Hepatocyte Study**

## **1. Materials.**

“ImmunoPure” streptavidin-coupled to horse radish peroxidase, Sulfo-NHS-LC-biotin and the EZ-link HABA quantification kit were purchased from Pierce (Rockford, IL). Ammonium chloride, bovine serum albumin (BSA), chlorpromazine, filipin, nystatin, and wortmannin were purchased from Sigma Aldrich (St. Louis, MO). Nitrocellulose membranes (Protran BA83, 0.2  $\mu\text{m}$ ) were purchased from Schleicher and Schuell BioScience (Keene, NH). LysoTracker-Red lysosomotropic labeling reagent, AlexaFluor-488 and AlexaFluor-555 antibody conjugation kit and goat-anti-rabbit coupled to fluorescein isothiocyanate (FITC) or rhodamine were purchased from Molecular Probes (Carlsbad, CA). Mouse monoclonal anti-EEA-1 was purchased from BD Biosciences (San Jose, CA). CAR gene-specific primers and the 3'RACE PCR kit was purchased from Invitrogen (Carlsbad, CA).

## **2. Cell Cultures.**

Primary rat hepatocyte cultures were generously provided by Hoffman-La Roche Pharmaceuticals (Nutley, NJ), which were prepared by the collagenase perfusion method (71), and were cultured in Williams medium supplemented with 10% calf serum at 37°C in 5% CO<sub>2</sub>. The A549, HEK-293, and H4-II-E cell lines were purchased from the American Tissue Culture Collection (ATCC, Manassas, VA). The human A549 and HEK-293 cell lines were cultured in Dulbecco's F12 minimal essential medium (Gibco, Carlsbad, CA) supplemented with 10% calf serum at 37°C in 5% CO<sub>2</sub>. The rat H4-II-E cell line was cultured in Dulbecco's minimal essential medium supplemented with 10% fetal calf serum at 37°C in 5% CO<sub>2</sub>. The human suspension-adapted HeLa S3 cell line was purchased from ATCC, and was cultured in Joklik's minimal essential medium (Gibco) supplemented with 5% calf serum spinning in a flask at 37°C.

## **3. Recombinant knob domain.**

### **3.1. Constructing the recombinant knob domain.**

Previously, the genetic sequences for the wild-type knob domain of human adenovirus serotypes 2 (Ad2) and 12 (Ad12) as well as their non-CAR binding mutants, Ad2-S408E/P409E and Ad12-P417E/P418A, respectively were amplified by polymerase chain reaction (PCR) and cloned into a pET15b vector (Novagen, Madison, WI) between NdeI and XhoI restriction sites. The plasmid constructs were separately transformed into the BL21-DE3 strain of bacteria (Invitrogen, Carlsbad, CA) by the electroporation method. Bacteria were grown on Luria broth (LB) agar plates supplemented with penicillin to select for transformed bacteria using the ampicillin resistance cassette provided by the pET15b vector. Selected colonies were grown in LB supplemented with penicillin shaking at 37°C for 2 hours, after which IPTG was added to trigger overexpression of the encoded knob domains. Cells were pelleted at 6000 rpm at 4°C and the bacterial cell pellets were lysed in BugBuster™ (Invitrogen) reagent supplemented with lysozyme and benzonase™ (Invitrogen). Lysates were centrifuged at 12000 rpm at 4°C for 20 minutes. The recovered supernatant was applied to a DEAE-cellulose column (Sigma-Aldrich) and eluted with 0-0.2 M gradient of NaCl. The knob

protein was further purified through the hexahistidine N-terminal tag using a Ni-NTA column (Qiagen, Valencia, CA) and eluted with imidazole.

### **3.2. Biotinylation of the recombinant knob domain.**

Sulfo-NHS-LC-biotin (Pierce) was diluted to 1 mg/mL in PBS, and mixed with 1 mg/mL dilution of wild-type Ad2 knob, wild-type Ad12 knob, S408E/P409A-Ad2 knob, or P417E/P418A-Ad12 knob. The mixture was tumbled at room temperature for 1 hour. Subsequently, the reaction was quenched by adding 1 M ammonium chloride (NH<sub>4</sub>Cl) and tumbling at room temperature for an additional 30 minutes. Excess biotin was removed by dialysis of the biotin-knob solutions overnight at 4°C against 10 mM phosphate buffer. The following day the degree of biotin-labeling was evaluated using the EZ-link HABA quantification assay (Pierce), a colorimetric assay that measures the positive correlation in color change of the HABA dye from orange to yellow in response to the concentration of biotin.

## **4. Animal studies.**

### **4.1. Swiss-Webster mice.**

Male Swiss-Webster mice were purchased from Jackson Laboratories (Bar Harbor, ME). In accordance with the Brookhaven National Laboratory Institutional Animal Care and Use Committee protocols (Upton, NY), mice were tail-vein injected with approximately 20 µg of biotinylated knob protein in 0.1 mL of PBS. Mice were then sacrificed by oxygen deprivation in triplicate at 10, 60, and 180 minutes post-injection. The livers were dissected, washed in Hanks balanced salt solution (Gibco), snap frozen in liquid nitrogen, and stored for later analysis at -60°C.

### **4.2. Preparation of liver tissue lysate.**

Frozen livers were thinly sliced with a razor blade in a Petri-dish, and then solubilized in RIPA buffer (1X PBS, 1% Nonidet-P40, 0.5% sodium deoxycholate, 0.1% SDS) supplemented with a protease inhibitor cocktail (Invitrogen). The mixture was transferred to a glass Dounce homogenizer and homogenized with 3-4 strokes. The homogenate was then transferred to a 1.5 mL eppendorf tube and centrifuged at 12000 x g at 4°C for 30 minutes. The supernatant was transferred to a new 1.5 mL eppendorf tube and centrifuged a second time to remove any residual particulates. The final supernatant is representative of the total tissue lysate.

### **4.3. Western blot analysis of liver tissue lysate.**

Of the total tissue lysate, 5 µL was diluted with 5 µL of distilled water and 5 µL of 3X Laemmli sample buffer (72); and then boiled for 10 minutes. The lysate was separated on a 12% SDS-PAGE gel and then transferred by electrophoretic transfer onto nitrocellulose membranes (Schleicher and Schuell BioScience) using the semi-dry blotting apparatus (CBS Scientific, Del Mar, CA) and the discontinuous Tris-CAPS buffer system described by BioRad (Hercules, CA). The nitrocellulose membrane was blocked in 3% solution of bovine serum albumin (BSA) dissolved in PBS supplemented with 0.05% Tween-20 (PBS-T) for 30 minutes at room temperature, and then probed with a 1:200000 dilution of streptavidin-coupled to horseradish

peroxidase (SA-HRP) for 60 minutes at room temperature. The blot was washed successively in PBS-T, and reacted with West-Dura chemiluminescent reagent (Pierce). X-ray film was exposed to the blot for various durations, developed, and fixed.

## **5. Knob degradation assay.**

Cell cultures were treated with either saturating (1  $\mu\text{g}/\text{mL}$ ) or sub-saturating (0.04  $\mu\text{g}/\text{mL}$ ) doses of biotinylated wild-type Ad2 or Ad12 knob for 60 minutes at 4°C. Excess unbound knob was removed through three successive PBS washes. Plates of cells selected to represent an initial time point ( $T_0$ ) were immediately harvested by scraping cells into solution with PBS. The recovered cell solution was centrifuged at 600g for 1 minute at room temperature. Cell pellets were chilled on ice for later analysis. The remaining plates of cells were provided fresh knob-free media and allowed to incubate at 37°C for 120 minutes. Afterwards, the cells were washed twice and scraped in PBS. Cell pellets were solubilized in Laemmli sample buffer (72) and boiled. The lysates were analyzed by Western blot as described in the animal studies section 4.3.

## **6. Knob internalization assays.**

### **6.1. Indirect immunofluorescent microscopy.**

H4-II-E and A549 cells were grown on glass coverslips in 33 mm plates overnight. The cells were treated with 0.1-1  $\mu\text{g}/\text{mL}$  unlabeled recombinant Ad2 or Ad12 knob protein at 4°C to synchronize the start of internalization. Unattached knob was removed by consecutive three PBS washes. Subsequently, cells were warmed to 37°C for 0, 30, 60, or 120 minutes. The cells were then fixed to the glass coverslips with 1% paraformaldehyde (Sigma-Aldrich) at room temperature for 10 minutes. The fixed cells were washed in PBS and permeabilized with 0.1% Triton X-100 (TX-100) on ice for 15 minutes. The cells were then blocked with 3% BSA in PBS for 30 minutes, and probed with 1  $\mu\text{g}/\text{mL}$  rabbit anti-Ad2 or Ad12 knob for 60 minutes at room temperature. After three consecutive PBS washes, a 1:10000 dilution of goat-anti-rabbit coupled to AlexaFluor-488 or AlexaFluor-555 (Molecular Probes) was applied to the cells for 60 minutes at room temperature. The cells were then washed in PBS, air-dried at room temperature, and mounted onto glass slides with the ProLong anti-fade mounting medium (Molecular Probes) supplemented with 4',6'-diamidino-2-phenylindole (DAPI) stain. The slides were examined the following day using FITC, Cy3.5 and DAPI filters on a 63X objective of a Zeiss microscope (Thornwood, NY). Before fixation, designated samples were surface-stripped with 0.2 M glacial acetic acid in 0.5 M sodium chloride (NaCl) on ice for 5 minutes, which dissociates most receptor-ligand interactions, to distinguish between surface-bound and internalized ligand.

### **6.2. Pronase surface-stripping analysis.**

H4-II-E and A549 cells were treated with biotinylated recombinant Ad2 or Ad12 knob protein for 60 minutes at 4°C to synchronize internalization. In this case, cells were treated with a sub-saturating concentration of 0.04  $\mu\text{g}/\text{mL}$  biotinylated Ad2 or Ad12 knob. Duplicate sets

of cells designated for an initial  $T_0$  time point were fixed immediately with 1% paraformaldehyde to prevent any ligand uptake during further processing of the samples. All other duplicate sets of cells were warmed at 37°C for 30, 60, and 90 minutes, then washed, and fixed with 1% paraformaldehyde. Subsequently, cells were incubated with either 0.5 mM EDTA in PBS or 0.1 mg/mL pronase (Roche Diagnostics, Mannheim, Germany) in PBS for 20 minutes at 37°C. Both treatments result in cell detachment from the substratum avoiding the need for cell scraping, which ruptures some cells, and allows harvesting by pipeting the cell solution off the plate and into an eppendorf tube. The pronase treatment digests all surface bound ligands, leaving receptor molecules intact and not disrupting the membrane. Trypan blue staining of unfixed H4-II-E and A549 cells confirmed that at the concentration employed, pronase did not negatively affect membrane integrity. Harvested cells were centrifuged and the supernatant discarded; followed by no less than four consecutive PBS washes to assure that digested remnants of surface bound knob were completely removed from the samples. Cell pellets were resuspended in volumes of PBS proportional to the size of the pellet. A fraction of the cell suspension was analyzed by Western blot probing with SA-HRP. The appearance of a biotinylated knob band on the blot in a lane corresponding to a pronase-treated sample confirms the existence of a pronase-resistant intracellular population of knob.

## **7. Trafficking assessment.**

### **7.1. Mode of uptake.**

Chlorpromazine (CPZ) and hypertonic sucrose (HS) inhibit endocytosis through clathrin-coated pits (CCPs) by disrupting the assembly of the adaptor protein-2 (AP-2) in the clathrin scaffold (73-75). Nystatin (NYS) and filipin (FIL) block uptake through lipid raft-dependent pathways by sequestering membrane cholesterol (76-78). Separately, these inhibitors were added to the media of H4-II-E cells to determine which mode of uptake is utilized by CAR to internalize knob.

#### **7.1.1. Biochemical analysis of sensitivity to specific endocytic inhibitors.**

The first method selected to test the effects of different endocytic inhibitors was an evaluation of the impact on the rate of knob metabolism over time. Cell cultures were pre-treated with 0.2 M or 0.4 M sucrose; 10  $\mu\text{g}/\text{mL}$  or 25  $\mu\text{g}/\text{mL}$  CPZ; 12.5  $\mu\text{g}/\text{mL}$  or 25  $\mu\text{g}/\text{mL}$  NYS; or 2.5  $\mu\text{g}/\text{mL}$  or 5  $\mu\text{g}/\text{mL}$  FIL for no greater than 30 minutes at 37°C. The cells were then treated with either biotinylated Ad2 or Ad12 knob at the sub-saturating dose 0.04  $\mu\text{g}/\text{mL}$  in the continued presence of the inhibitors for 60 minutes at 4°C. Excess knob was removed by successive PBS washes. Cells designated for an initial time point ( $T_0$ ) were harvested by scraping in PBS. The recovered cell pellets were chilled on ice. The remaining cell sets were warmed to 37°C in knob-free serum-free media for 120 minutes ( $T_{120}$ ) in continued presence of the specified endocytic inhibitors. At the conclusion of the time course, the  $T_{120}$  sets were harvested by scraping in

PBS. Cell pellets were resuspended in PBS and a fraction of each cell suspension was analyzed by Western blot probing with SA-HRP. At every step where the media was replaced, the cells were examined for any change in morphology or loss of adherence due to the effects of each individual drug treatment. Trypan blue staining was conducted on a fraction of the recovered cells to evaluate the toxicity of the individual drug treatments.

The second method developed to evaluate the effects of specific inhibitors of endocytosis was a modification of the pronase surface-stripping assay. Designated plates of H4-II-E cells were pre-treated with 10  $\mu\text{g}/\text{mL}$  CPZ or 12.5  $\mu\text{g}/\text{mL}$  NYS for 30 minutes at 37°C. Cells were treated with 0.04  $\mu\text{g}/\text{mL}$  biotinylated Ad2 or Ad12 knob at 4°C for 60 minutes in the continued presence of a specific endocytic inhibitor, and then PBS washed several times consecutively. Specific sets were fixed with 1% paraformaldehyde immediately for an initial time point ( $T_0$ ). All other plates were supplied fresh knob-free serum-free media and allowed to incubate at 37°C for 120 minutes ( $T_{120}$ ). Incubation with knob and the following time course at 37°C were both conducted in continued presence of each drug, respectively. Afterwards, the  $T_{120}$  cells were washed with PBS and fixed in 1% paraformaldehyde. Selected plates were incubated with either 0.5 mM EDTA in PBS or 0.1 mg/mL pronase in PBS for no greater than 20 minutes at 37°C. Cells were harvested by pipeting directly off the plate and washed several times with PBS. Cell pellets were resuspended in a volume of PBS proportional to the size of the recovered pellet. A fraction of each cell solution was analyzed by Western blot probing with SA-HRP.

#### **7.1.2. Indirect immunofluorescent microscopic analysis of sensitivity to specific endocytic inhibitors.**

The previous indirect immunofluorescence knob internalization assay was modified to incorporate the aforementioned endocytic inhibitors to corroborate the results of the pronase surface-stripping assay described in section 7.1.1. H4-II-E cells grown on glass coverslips were pre-treated with 0.4 M sucrose; 10  $\mu\text{g}/\text{mL}$  or 25  $\mu\text{g}/\text{mL}$  CPZ; 12.5  $\mu\text{g}/\text{mL}$  or 25  $\mu\text{g}/\text{mL}$  NYS; or 2.5  $\mu\text{g}/\text{mL}$  or 5  $\mu\text{g}/\text{mL}$  FIL for 30 minutes at 37°C. Unlabeled Ad2 or Ad12 knob was applied to the cells for 60 minutes at 4°C in the continued presence of a specific endocytic inhibitor. Excess unbound knob protein was removed through consecutive PBS washes, and then the cells were either fixed with 1% paraformaldehyde for an initial time point or were incubated for 60 minutes at 37°C in media containing a specific uptake inhibitor. Afterwards, the cells representative of a 60 minute time point were fixed with 1% paraformaldehyde. All the samples were then permeabilized with 0.1% Triton-X100 in PBS for 20 minutes on ice, blocked for 30 minutes at room temperature with 3% BSA in PBS, and then probed with 1:100 dilution of anti-Ad2 knob-AF488 or anti-Ad12 knob-AF555. The coverslips were washed in PBS, air-dried, and were

mounted onto glass slides with ProLong mounting medium supplemented with DAPI stain (Molecular Probes). The slides were examined through FITC, Cy3.5, and DAPI filters under 63X objective of a Zeiss microscope.

## **7.2. Site of proteolysis.**

Typically, uptake through CCPs delivers cargo to early endosomes that stain positive for the early endosomal antigen 1 (EEA-1) (79). Additionally, the lysosomotropic LysoTracker red reagent (Molecular Probes) stains late endosomes and the lysosome. Lysosome-specific degradation of internalized ligands is sensitive to the effects of ammonium chloride (NH<sub>4</sub>Cl) and wortmannin (WM), which inhibit endosome maturation and lysosome fusion, respectively (80-83). Specifically, NH<sub>4</sub>Cl prevents the acidification of endosomes, which is required for their maturation, and WM inhibits the phosphatidyl inositol-3 kinase (PI-3K) cascade that triggers late endosome-lysosome fusion.

### **7.2.1. Co-localization with endosome and lysosome markers.**

For detection of knob co-localization with early endosomes, H4-II-E and A549 cells were probed with a 1:100 dilution of monoclonal anti-EEA1 (BD Biosciences) for 60 minutes at room temperature followed by incubation for 60 minutes with goat-anti-mouse-FITC (Sigma-Aldrich). When examining for co-localization with EEA-1 positive endosomes, the anti-Ad12 knob-AF555 would be used for knob detection. Separately, when assessing for knob co-localization with the lysosomotropic LysoTracker Red fluorescent marker (Molecular Probes), live cells would be incubated in medium supplemented with 50-75 nM LysoTracker Red for 30 minutes at 37°C, and anti-Ad2 knob-AF488 would be used for knob detection.

### **7.2.2. Analysis of sensitivity to specific lysosomal inhibitors.**

H4-II-E cells were pre-treated for 30 minutes at 37°C with either 20 NH<sub>4</sub>Cl or 100 nM WM. Biotinylated recombinant Ad2 or Ad12 knob was applied at 0.04 µg/mL for 60 minutes at 4°C, and then the cells were incubated at 37°C for 0 or 120 minutes; at both stages in the continued presence of NH<sub>4</sub>Cl or WM. Cells were harvested by scraping in PBS, and the collected cell pellets were analyzed by Western blotting with SA-HRP as previously described.

## **8. Antibody-induced receptor crosslinking.**

### **8.1. Single-layer crosslinking.**

The internalization of receptor-ligand complexes was evaluated after antibody-induced crosslinking, H4-II-E and A549 cells grown on glass coverslips in 33mm plates were treated with 0.1-1 µg/mL of biotinylated Ad2 or Ad12 knob protein at 4°C for 60 minutes to synchronize internalization. Successive PBS washes were used to remove excess knob. The cells were then treated with 1 µg/mL anti-Ad2 knob coupled to AF488 or anti-Ad12 knob coupled to AF555 at 4°C for 60 minutes, and excess unbound antibody was removed by successive PBS washes. The treated cells were then allowed to warm to 37°C for 0, 30, or 120 minutes. Afterwards, the cells were fixed to

the coverslips with 1% paraformaldehyde for 10 minutes at room temperature. The coverslips were washed in PBS, air-dried, and mounted onto glass slides using ProLong anti-fade mounting medium supplemented with DAPI stain (Molecular Probes). The cells were examined through DAPI, Cy3.5 and FITC filters on a 63X objective of a Zeiss microscope. Surface-stripping of designated samples with 0.2 M glacial acetic acid in 0.5 M NaCl was used to distinguish between surface-bound and internalized ligand.

To evaluate for ligand metabolism after antibody-induced crosslinking, H4-II-E and A549 cells were treated successively with biotinylated Ad2 or Ad12 knob then AF488-conjugated anti-Ad2 knob or AF555-conjugated anti-Ad12 knob as described above. After each treatment excess unbound ligand was removed by successive PBS washes. Cells were then warmed to 37°C for 0, 30 or 120 minutes and washed with PBS. Cells were recovered by scraping in PBS and pelleted. Cell pellets were resuspended in a volume of PBS proportional to the size of the recovered pellet and examined for knob metabolism by Western blot probing with SA-HRP.

### **8.2. Double-layer crosslinking.**

An evaluation of the effect of double-layer antibody-induced crosslinking on knob internalization and metabolism followed the procedure detailed in the single-layer crosslinking section above, except the additional treatment with fluorophore modified goat-anti-rabbit IgG. With both the indirect immunofluorescent microscopy and the Western blot analysis, subsequent to the addition of rabbit anti-knob, the cells were treated with a 1:10,000 dilution of goat-anti-rabbit-FITC for 60 minutes at 4°C. After this treatment, the cells were allowed to warm to 37°C for 0, 30, or 120 minutes. All the following steps were the same respective of the assay being performed. With indirect immunofluorescent microscopic analysis, acetic acid stripping of designated samples was used to distinguish between surface-bound and internalized ligand.

## **9. 3'-RACE PCR assay.**

RNA was extracted from H4-II-E and A549 cells grown on 150 mm plates by vortexing recovered cell pellets in Trizol™ reagent (Invitrogen). Afterwards, chloroform was vigorously mixed into the Trizol solution and subsequently centrifuged. Post-centrifugation of the cell lysates, the aqueous phase was removed and the RNA was precipitated an equal volume of isopropanol. The mixture was then centrifuged and the pellet resuspended in 70% ethanol, which was stored at -20°C. The washed RNA was pelleted, air-dried, and resuspended in DEPC-treated water. The concentration of the isolated RNA was quantified by measuring the absorbance at 260 nm, and the relative purity was evaluated by the ratio of the absorbance at 260 nm to the absorbance at 280 nm.

### **9.1. First strand cDNA synthesis.**

Approximately 1-5 µg of the isolated RNA was mixed with a 10 µM solution of the oligo-dT adapter primer, heated to 70°C for 10 minutes, and then cooled on ice for 1 minute. The mixture was then added to a cocktail of 10X PCR buffer, 25 mM magnesium chloride (MgCl<sub>2</sub>), 10 mM dNTP mix,

and 0.1 M DTT; and equilibrated for 5 minutes at 42°C. SuperScript™ II reverse transcriptase was added to the mixture and warmed at 42°C for 50 minutes. Afterwards, the mixture was incubated at 70°C for 15 minutes to terminate the reaction. The mixture was chilled on ice and residual RNA was by incubating with RNase H for 20 minutes at 37°C. The final mixture of cDNA was stored overnight at -20°C.

### **9.2. Amplification of the target cDNA.**

Approximately 1/25 of the final cDNA synthesis solution was mixed with a cocktail of 10X PCR buffer, 25 mM MgCl<sub>2</sub>, distilled water, 10 mM dNTP mix, a 10 μM solution of the gene specific 5' primer (5'-GAATTCCTCGAGCATGGCGCTCCTACTGT-3' for CAR from rat cell lines and 5'-GAATTCCTCGAGACCATGGCGCTCCTGCTGT-3' for CAR from human cell lines), a 10 μM solution of the abridged universal amplification 3' primer, and 5 units of Taq polymerase. The mixture was incubated for 3 minutes at 94°C. Subsequently, the samples were run through 35 standard PCR cycles. Of the amplified sample, 20 μL was run on a 1% agarose gel stained with ethidium bromide (EtBr) alongside the lambda-HindIII DNA ladder.

### **9.3. Nested PCR of the amplified cDNA.**

In the event that the 3'RACE-PCR reaction resulted in multiple bands of unexpected size, additional primers were designed to confirm that CAR transcripts had been amplified and to verify the presence of CAR splice variants.

#### **9.3.1. Amplification of the CAR D1 domain.**

The variation produced by alternative splicing is mostly confined to the cytoplasmic tail domain of CAR, not the D1 ectodomain. As such, to solely confirm the presence of amplified CAR transcripts, the forward primer 5'-CTAGTGCATATGGGTATCACTACTCCT-3' and reverse primer 5'-TGAATTCTCGAGCGCACCT-3' for the D1 domain of human CAR (for human cell lines) and forward primer 5'-GATCAGCTATATGAGTATCACTACACCTGAAC-3' and reverse primer 5'-GATCAGCTCGAGACCTGAAGGCTTAACAAG-3' for the D1 domain of rat CAR (for rodent cell lines) were used to in standard 35 cycle PCR reactions to amplify the D1 region of CAR. One third of the PCR products were analyzed alongside a lambda-HindIII DNA ladder on a 1.75% agarose gel stained with EtBr.

#### **9.3.2. Amplification of the CAR cytoplasmic tail domain.**

To confirm the presence of different splice forms of CAR, a constant forward primer for exon 7A was used in separate PCR reactions in conjunction with a reverse primer specific for the 3'-end of the two major known splice variants frequently designated: CAR mRNA-1 and CAR mRNA-2. For human cell lines, the forward exon 7A primer was 5'-AAGAGCCGTACGTCCACTGC-3' and the reverse primers 5'-3' for mRNA-1 and 5'--3' for mRNA-2 were employed. For rodent cell lines, the forward exon 7A primer was 5'-ACATCCACCGCCAGGAGCTA-3'

and the reverse primers 5'-CGCTCCCATTCGACTTA-3' for mRNA-1 and 5'-CTGCAATGCCATCGGTCAG-3' for mRNA-2 were employed. After a standard PCR reaction of 35 cycles, one third of the products were analyzed alongside the New England Biolabs 100 bp DNA ladder (Ipswich, Massachusetts) on a 1.75% agarose gel stained with EtBr.

#### **10. Palmitoylation reduction assay.**

To reduce the level of palmitate-modified proteins, H4-II-E and A549 cells were incubated at 37°C for 2 or 6 hours in media supplemented with either 50 or 100  $\mu$ M 2-bromopalmitate (2-BrP). After incubation, cells were examined by light microscopy for any morphological changes. Cell monolayers were washed with PBS, and treated with 1  $\mu$ g/mL biotinylated Ad2 or Ad12 knob for 60 minutes at 4°C. Cell lysates were analyzed by Western blot probing with SA-HRP.

#### **11. Detergent-resistant membrane (DRM) isolation.**

A549 and H4-II-E cells were treated with 0.04  $\mu$ g/mL biotinylated Ad2 or Ad12 knob at 4°C for 60 minutes. Excess unbound knob was removed by PBS washes. Cells were scraped into solution in PBS and pelleted. Cell pellets were resuspended in 0.1% Triton-X100 (TX-100) and incubated either on ice for 20 minutes or at 37°C for 20 minutes. Cell lysates were centrifuged, and the supernatant recovered. The insoluble pellet material was dispersed in an equivalent volume of 0.1% TX-100 by probe sonication. The supernatant and pellet fractions were analyzed by Western blot probing with SA-HRP.

## **Chapter 3: Results I—CAR Hepatocyte Study**

## **1. The adenovirus knob domain.**

To study CAR endocytosis *in vivo* and in cell culture models, the Ad fiber recombinant knob domain, which is mono-specific for CAR and binds CAR with high affinity and avidity, was used as a ligand. By contrast, whole Ad particles or even intact fiber protein were not suitable because each has been demonstrated to interact with other receptor molecules in addition to CAR, including  $\alpha_v$ -containing integrins, heparin sulfate glycosaminoglycans, and dipalmitoyl-phosphatidylcholine (45,46,52,84-86).

### **1.1. Biotinylation of Ad2 and Ad12 knob.**

Given the possible complication of using radio-labeled proteins described above, the Ad2 and Ad12 knob were labeled with biotin. Biotin is a small vitamin molecule that can be covalently bound to proteins through ester linkage to epsilon amino groups of lysine residues, under mild reaction conditions that rarely perturb protein structure or activity. Thus, biotin is bound irreversibly to target proteins and no enzymes are known which cleave the biotin-protein bond. The fate of the protein therefore can be monitored on Western blots or by microscopy using biotin-specific reagents.

The purified knob domains from Ad2 and Ad12 were mixed with biotin and incubated as described in the materials and methods section. Excess biotin was removed by overnight dialysis, and the following day the degree of biotin-labeling was determined using the HABA-EZ link assay. Typically, substitution levels ranged from 2-4 moles of biotin per mole of knob protein. A general indicator of excessive biotin labeling is retardation of the labeled protein on SDS-PAGE gels. After labeling, biotinylated knob protein was run alongside unlabeled knob on a 12% SDS-PAGE gel and no change in migration was observed.

### **1.2. Evaluation of biotinylated knob-CAR binding.**

Over-biotinylation potentially could obscure the CAR-binding interface on the knob molecule; therefore the CAR-binding activity of labeled knob preparation was evaluated post-biotinylation. The newly biotinylated knob preparations were dot-blotted alongside unlabeled knob on a nitrocellulose membrane (Schleicher and Schuell), crosslinked with 0.25% glutaraldehyde, blocked with 3% BSA and probed with FITC-conjugated recombinant CAR D1 protein. The fluorescent intensity of the blotted samples was compared using the STORM-860 fluorescence-imager (Molecular Dynamics) which revealed no decrease in CAR-binding activity post-labeling for wild-type Ad2 and Ad12 knob, while the non-CAR binding mutant counterparts exhibited minimal reactivity with CAR D1 (data not shown). In addition, the ability of the biotinylated wild-type Ad2 and Ad12 knob protein to attach to CAR expressed in cell culture was also tested. Both biotinylated knob preparations were applied to monolayers of A549 cells and spinner cultures of HeLa S3 cells. After successive washes with PBS, both biotinylated wild-type Ad2 and Ad12 knob were detected in A549 (chapter 3, figure 1) and HeLa S3 (data not shown) cells lysates probed with streptavidin-coupled to horse radish peroxidase (SA-HRP). The biotinylated S408E/P409A-Ad2 knob mutant failed to attach in cell culture, while we did observe some P417E/P418A-Ad12 knob but only with cells treated with a large

amount. This confirmed that the CAR binding activity of the wild-type knob ligands had not been negatively affected by the biotin label.

## **2. Evaluating the fate of the biotinylated knob ligand *in vivo*.**

To test the hypothesis of Awasthi et al., 2004 that the knob protein injected into the blood stream binds in the liver (67), biotinylated Ad2 and Ad12 knob were separately administered to mice by tail-vein injection. The knob protein was allowed to circulate in the animals for 10, 60, and 180 minutes. Western blots of liver tissue extracts confirmed that the Ad2 and Ad12 knob proteins accumulated in the liver, but at different rates (chapter 3, figure 2). Ad2 knob was only detected 10 minutes post-injection. Ad12 knob was detectable at 10 minutes post-injection but did not reach maximal accumulation until 60 minutes post-injection. By 180 minutes post-injection, the concentration of Ad12 knob in liver extracts decreased with the appearance of a stable knob-related degradation product. This confirmed the hypothesis that recombinant knob protein bound the liver post-injection into the mouse bloodstream. Additionally, this supplied evidence implying that knob is degraded in the liver, possibly at faster rate for the serotype 2 derived knob compared to the serotype 12 derived knob.

## **3. Hepatocytes are responsible for the apparent degradation of biotinylated knob in the mouse liver.**

Taken together, our results and those of earlier investigators suggest that knob was degraded in a CAR-dependent fashion in the mouse liver (66,67). Given the architecture of the liver, it was possible that knob degradation was mediated by other resident cell types in the liver. The liver possesses its own unique population of macrophages known as Kupffer cells which are capable of internalizing and degrading ligands in the blood by phagocytosis. The authors of both CAR biodistribution studies argued that Kupffer cells were not binding the recombinant knob proteins. Awasthi et al., 2004 had postulated that iodinated Ad2 and Ad12 knob proteins were exposed to dehalogenase enzymes, which are present within microsomal compartments of hepatocytes but not Kupffer cells (67). Zinn et.al reported that pre-injection of mice with GdCl<sub>3</sub>, which depletes Kupffer cells in the liver did not impede knob localization in the liver, thus suggesting binding occurred on hepatocytes (66). To further explore this hypothesis, primary hepatocyte cell cultures were tested for their ability to bind and degrade knob.

### **3.1. Primary rat hepatocytes.**

The difficulty in preparing clean primary cultures of mouse hepatocytes was described by specialists at Hoffman-La Roche, who recommended and generously provided primary rat hepatocyte cultures. The assay by which all subsequent assessments of knob metabolism over time were determined was developed using these cell cultures.

Initial experiments were designed taking into account the possibility of trivalent knob protein potentially facilitating the crosslinking of adjacent CAR molecules (49,87). As such, two doses of biotinylated knob were applied in these early studies: a sub-saturating dose favoring the possibility of one knob molecule binding 2-3 CAR molecules and a saturating dose favoring one knob molecule bound per CAR molecule. Extrapolating from the cell binding studies with

biotinylated Ad2 and Ad12 knob (chapter 3, figure 1), 0.04  $\mu\text{g}/\text{mL}$  was selected as a sub-saturating amount and 1  $\mu\text{g}/\text{mL}$  as a saturating amount. Briefly, primary rat hepatocytes were treated with either dose in the cold to synchronize endocytosis and were incubated at 37°C for 0 or 120 minutes (approximately the time required for knob metabolism in the animal studies). Hepatocyte cell lysates were analyzed by Western blot probing with SA-HRP for the biotin label.

The knob-specific bands detected on the Western blot showed that the concentration of cell-associated biotinylated knob protein substantially decreased with time when incubated at 37°C (chapter 3, figure 3). Control sets incubated for 120 minutes at 4°C failed to exhibit any decline in knob concentration. Quantification of protein bands on the Western blot using CCD camera imaging system and software revealed that binding a sub-saturating dose of knob increased the degree of its degradation during the 120 minute incubation with cells at 37°C, where the 1  $\mu\text{g}/\text{mL}$  dose produced a 4-fold decrease and the 0.04  $\mu\text{g}/\text{mL}$  dose saw a 9-fold decrease. Based on these results, it was concluded that the knob protein was degraded in a CAR-dependent, temperature-dependent, and concentration-dependent manner in the context of primary rat hepatocyte cell cultures. Additionally, to exclude the action of surface-associated proteases known as “secretases” or “sheddases” (88), cells were incubated at 37°C in the presence of the metabolic inhibitor sodium azide ( $\text{NaN}_3$ ) or the clathrin-coated pit inhibitor hypertonic sucrose (HS); both of which are not known to have any negative impact on sheddase activity. Both treatments resulted in a reduction in the amount of knob degradation, though neither treatment completely abolished the effect (chapter 3, figure 4B).

### **3.2. H4-II-E cell line.**

Although hepatocytes are the major cell type represented in rat liver perfusates, other constituent cell types in the liver cannot be excluded from the primary cell cultures (89). To further reinforce the contention that the degradation of knob occurs specifically in hepatocytes and not another cell type, a rat hepatocyte-derived cell line was employed. The H4-II-E hepatoma cell line was selected given its known retention of many phenotypes observed in primary hepatocytes. By contrast, the phenotype of the human HepG2 cell line differs substantially from the observed phenotypes of primary hepatocyte cultures, thus they were not used in this study. As described in the introduction section 1.2., most rodent cell lines do not express CAR, which may be due to differences in chromatin remodeling (20). Thus, it was uncertain if the H4-II-E rat hepatoma cell line exhibited CAR expression. As a first step, the biotinylated knob cell binding studies previously performed on A549 cells (chapter 3, figure 1) were repeated with the H4-II-E cell line. This investigation revealed that H4-II-E cells indeed express at levels similar to what was observed with A549 cells. To the best of our knowledge, this is the first report of a rodent cell line demonstrating CAR expression. Subsequently, H4-II-E cells were tested for the CAR-dependent knob degradation observed with the primary rat hepatocyte cultures.

Western blot analysis of H4-II-E cell lysates from 0, 120, and 180 minutes at 37°C revealed the same sharp decrease in knob concentration over time that

was observed for the primary rat hepatocytes (chapter 3, figure 4A). This phenomenon was not observed when the cells were incubated at 4°C for 120 minutes. As was done with the primary rat hepatocyte cultures, to exclude the action of sheddases, cells were incubated at 37°C in the presence of NaN<sub>3</sub> or HS (chapter 3, figure 4B). As was previously observed with the primary hepatocyte culture, treatment with these agents reduced the amount of knob degradation over time, while not completely abolishing the effect. Taken together, these results indicated that the H4-II-E cells, and by extension primary rat hepatocytes and hepatocytes *in vivo*, have the ability to bind and degrade knob protein. Furthermore, sheddases are not likely mediating the disappearance of knob protein from these cells. From this, it was concluded that the H4-II-E cell line was a suitable substitute for the primary rat hepatocytes. All subsequent studies of CAR endocytosis were performed using these cells as a positive control.

### **3.3. A549 cell line.**

The lung carcinoma A549 cell line is commonly used to propagate adenovirus. Based on the slow endocytosis of RGD-negative Ad particles by A549 cells that was reported by Bai et.al, it was presumed that CAR molecules on these cells also would exhibit limited endocytosis of knob since this ligand also lacks RGD motifs necessary for interaction with integrin co-receptors (55). Indeed, no change was observed in the concentration of the Ad knob ligand associated with A549 cells over 120 minutes at 37°C (chapter 3, figure 4A). Quantification of protein bands on blots by CCD camera showed no difference in Ad2 knob concentration over a period of 120 minutes. Similar results were obtained for control reactions where primary rat hepatocytes and the H4-II-E cells were incubated at 4°C for 120 minutes. Ad12 knob showed a slight decline in concentration by the 180 minute time point at 37°C, which likely could be attributed to dissociation of non-specific contacts.

### **3.4. HEK-293 cell line.**

Despite the designation, the human embryonic kidney-293 (HEK-293) cell line has been confirmed to be neuron-derived (90,91). Bai et.al reported limited delay in endocytosis of RGD-negative adenovirus mutants on this cell line, suggesting that CAR molecules on these cells are more active in endocytosis than on A549 cells (55). Repeating the knob degradation analysis on HEK-293 cells revealed a 3-fold and a 6-fold decrease in knob concentration by 180 minutes at 37°C, with Ad2 or Ad12 knob applied at saturating or sub-saturating doses, respectively (chapter 3, figure 4A). We concluded from this finding that high endocytic activity of CAR is not exclusive to hepatocytes, and can also be exhibited on certain human cell types.

### **3.5. HeLa S3 cell line.**

Similar to the A549 and HEK-293 cell lines, the suspension-adapted HeLa S3 cell line was frequently employed to generate large quantities of adenovirus particles (40,44). In the studies reported by Bai et.al, RGD-negative viruses were rapidly endocytosed by the HeLa S3 cell line (55). Therefore, when evaluating HeLa S3 cells for knob binding and degradation over a period of 120 minutes at 37°C, it was expected that these cells would exhibit active endocytosis of the knob

ligand. Interestingly, the HeLa S3 cells failed to degrade bound knob ligands and thus were similar to the A549 cell line in this regard (data not shown).

#### **4. Evaluating CAR potential to internalize knob protein.**

##### **4.1. Indirect immunofluorescent microscopy with acid surface-stripping.**

Given the accumulating biochemical evidence that knob is degraded after endocytosis by a CAR-dependent mechanism, we wanted to provide microscopic evidence of internalized populations of the knob protein. Typically, a ligand that has been endocytosed exhibits a punctate pattern inside of cells when probed by indirect immunofluorescent microscopy. To exclude the possible, though unlikely, involvement of the biotin modification in the CAR-dependent metabolism of knob, unlabeled Ad2 and Ad12 knob were employed in these experiments. The threshold of detection not being as sensitive as with Western blots required doses ranging from 0.1  $\mu\text{g}/\text{mL}$  to 1  $\mu\text{g}/\text{mL}$ . As with the metabolism studies, binding of the ligand was done in the cold to synchronize uptake events. After warming for designated times at 37°C, the cells were probed with fluorescently labeled anti-Ad2 knob and anti-Ad12 knob antibodies. Specified samples were washed in acetic acid, which dissociates knob-CAR complexes, enabling us to distinguish between surface-bound and internalized populations of the knob ligand.

##### **4.1.1. A549 cell line.**

At the initial time point, the knob-specific fluorescence was found to be concentrated at the cell surface in spiny filopodia-like protrusions (chapter 3, figure 5A). This same fluorescent pattern was observed at all subsequent incubation times, and the intensity of the fluorescence did not diminish even after 300 minutes at 37°C. The localization to filopodia-like structures is notable given that Hommelgaard et al., 2004 described association with such membrane structures to be responsible for the internalization resistance of the ErbB2 receptor (92). Acetic acid stripping abolished all fluorescence irrespective of the time point indicating that none of the knob ligand was endocytosed on this cell type.

##### **4.1.2. H4-II-E cell line.**

Knob-specific fluorescence produced a “cobblestone-like” pattern at the initial time point, where it traced the perimeter of each cell (chapter 3, figure 5A). By 30 minutes at 37°C, much of the perimeter pattern had been redistributed into small punctate fluorescent clusters. After 60 and 120 minutes at 37°C, the fluorescence was entirely punctate, with the latter time point showing diminished fluorescent intensity. The “cobblestone” pattern observed at the initial time point was completely abolished by acetic acid stripping. The surface-stripping technique failed to eliminate the punctate fluorescence seen in the later time points. The intensity of the punctate pattern persisted especially in the 60 minute samples. These findings supported the contention that the degradation previously observed on H4-II-E cells first required the endocytosis of the knob ligand. Additionally, the knob ligand alone caused a dramatic rearrangement of CAR on the surface of the

hepatoma cells, which had previously only been described for the whole adenovirus particles infecting the HeLa S3 cell line (93).

#### **4.2. Western blot analysis of cells surface-stripped with pronase.**

In an effort to corroborate the findings obtained through the indirect immunofluorescence assay, the cell lysates of surface-stripped H4-II-E and A549 cell lysates were compared by Western blot analysis probing with SA-HRP. Enzymatic surface-stripping was employed using subtilisin, which had previously been employed for similar purposes for the investigation of the importance of  $\alpha_v$ -integrins to adenovirus uptake (52). Unfortunately, the results obtained from subtilisin-stripping experiments proved to have low reproducibility with respect to A549 and H4-II-E cells, though it worked well in tests with the HEK-293 cell line. Pronase was chosen to replace subtilisin. Using this system, it is expected that internalized ligand will be protected from the enzyme digest as these enzyme cocktails do not negatively affect membrane integrity and cell viability. The lack of deleterious effects on cells was confirmed by trypan blue staining, where cell viability was greater than 95% after exposure to pronase treatment.

When pronase was applied to either H4-II-E or A549 cells, that had been treated with biotinylated Ad2 or Ad12 knob, at an initial  $T_0$  time point, no knob band was visualized on a blot demonstrating that without warming to 37°C knob could not be internalized. H4-II-E cells harvested at 30 minute increments after warming to 37°C exhibited pronase-resistant knob bands on a Western blot (chapter 3, figure 5B). It appears that a finite population of the CAR on H4-II-E cells is endocytically active, since approximately 25% of the knob bound at the initial time point is protected from surface-stripping at the  $T_{30}$  time point (as assessed by CCD camera quantification of the Western blot). In subsequent 30 minute increments, the amount of internalized knob is progressively reduced. Pronase-resistant knob bands were never detected at any time point for the A549 cell line. An extended time course revealed the amount of pronase-resistant knob at subsequent 30 minute time points progressively decreased suggesting that the knob protein internalized earlier was being degraded and that no new knob protein had been endocytosed (chapter 3, figure 5C).

#### **5. Route of CAR endocytosis.**

Receptor endocytosis can proceed through two different routes. Clathrin-coated pits (CCPs) characterized by the clathrin triskelion lattice lining invaginations of the cell membrane have been most heavily studied. Solutions of hypertonic sucrose (HS) and the psychotropic drug chlorpromazine (CPZ) are known to inhibit uptake through this pathway (73-75). Uptake mediated by lipid rafts, cholesterol-enriched microdomains in the cell membrane, represents an alternative pathway. Internalization by this route can proceed through flask-shaped invaginations termed caveolae which are coated with the protein caveolin-1 or by a less understood caveolae-independent route (94). This alternative pathway is particularly sensitive to disruptions in cholesterol content, which can be affected by several drug treatments. Methyl- $\beta$ -cyclodextrin depletes the cholesterol content of the cell membrane, but this has recently been shown to also have deleterious effects on CCPs thus rendering it unsuitable for delineating lipid-raft involvement. Nystatin (NYS) and filipin (FIL)

behave as cholesterol-sequestering agents that negatively impact the raft-mediated endocytosis without additional effects on CCPs (76-78). Treating cell cultures separately with these inhibitors of endocytosis was used as a means to determine which route of uptake is employed by endocytically active populations of CAR.

### **5.1. Knob degradation assay with specific inhibitors of endocytosis.**

First, the effect of the individual drug treatments on the CAR-dependent knob degradation was tested. As described in the Materials and Methods I section 5, designated plates of H4-II-E or A549 cells were pre-treated with HS, CPZ, NYS, or FIL at 37°C. Subsequently, the cells were treated with biotinylated knob followed by incubation at 37°C for 120 minutes. The resulting cell lysates were analyzed by Western blot probing with SA-HRP.

At each stage of the experiment, the cells were examined for any change in morphology or loss of adherence due the effects of each individual drug treatment. Neither CPZ nor HS produced any obvious effect at any of the doses tested. In contrast, NYS caused cell rounding with increased loss of adherence with prolonged exposure at 37°C. The FIL treatment resulted in a dramatic shrinkage in cell size without loss of adherence with the morphological effects becoming more pronounced with continued incubation at 37°C. Additionally, trypan blue staining of recovered cells prior to lysis revealed that after 120 minutes at 37°C in CPZ, NYS, or FIL resulted in greater than 60% staining positive. Whereas at the initial time point, less than 10% stained positive indicating that prolonged exposure to CPZ, NYS, and FIL at 37°C was extremely toxic to the cells. HS treatment had no adverse effects on cell viability.

### **5.2. Knob internalization assay with specific inhibitors of endocytosis.**

The severe toxicity of the endocytic inhibitors after extended incubation at 37°C negatively impacted the reproducibility of the results obtained from Western blot analysis of the samples from the knob metabolism assay. As such, an assay with shorter incubation times was desired. The pronase surface-stripping assay was selected to replace the knob metabolism assay since it requires only 30 minutes to detect a pronase-resistant knob band on Western blots. Designated samples were pre-treated with individual drugs for 30 minutes at 37°C, exposed to biotinylated Ad2K or Ad12K in the cold for 60 minutes, and designated samples were incubated for 30 minutes at 37°C. The knob treatment and subsequent time course incubation were conducted in the continued presence of each drug. Western blots revealed that CPZ-treated H4-II-E cells failed to produce a pronase-resistant knob band, while NYS did not (chapter 3, figure 6B). This indicated that the biotinylated knob protein was internalized through CCPs. Notably, the abnormal cell morphologies observed in the previous assay were not detected using this method.

To corroborate the findings from the pronase surface-stripping assay, the selected endocytic inhibitors were evaluated for their effect on the development of punctate knob-specific fluorescence on H4-II-E cells examined by indirect immunofluorescence. H4-II-E cells grown on glass coverslips were pre-treated with CPZ, HS, NYS, or FIL, bound with unlabeled Ad2 or Ad12 knob and warmed for specific durations at 37°C in the continued presence of one of the

specific inhibitors. The formation of knob-specific fluorescent puncta after 60 minutes at 37°C was blocked in the presence of CPZ and in the presence of HS (chapter 3, figure 6A). Both NYS and FIL treated samples demonstrated the knob redistribution pattern previously established for the H4-II-E cell line. This led to the conclusion that CCPs were involved in the CAR-dependent uptake of knob.

### **5.3. Co-localization with EEA-1 marker.**

Molecules internalized by cells through CCPs typically are delivered to early endosomes containing the early endosomal antigen 1 (EEA-1) marker. Using indirect immunofluorescence, co-localization of internalized knob protein with the EEA-1 marker was evaluated. When examined on H4-II-E cells, much of the knob-specific fluorescence overlapped with puncta staining positive for EEA-1 (chapter 3, figure 6C). No bleed-through of either fluorophore was observed in controls omitting either knob detection or EEA-1 detection. This established that knob was delivered to EEA-1 positive early endosomes, the destination of ligands internalized by CCPs, which strengthened the previous results with inhibitors of specific modes of endocytosis.

## **6. Site of proteolysis.**

At this point, we had established that, in the context of primary rat hepatocytes and the rat hepatoma H4-II-E cell line, CAR mediated the endocytosis of the knob ligand through CCPs with delivery to EEA-1 positive early endosomes. EEA-1 positive early endosomes have been described to gradually mature and ultimately fuse with lysosomes, where internalized proteins can be degraded (79). We wanted to confirm that the degradation observed for the knob ligand in hepatocytes and hepatoma cells occurred in the lysosome. To accomplish that goal, two different experiments were conducted using indirect immunofluorescent microscopy and the aforementioned knob degradation assay.

### **6.1. Co-localization with LysoTracker Red marker.**

LysoTracker Red marker specifically stains the lysosomal compartment of the cell. When pre-incubated with knob-treated H4-II-E cells that had not been warmed to 37°C, knob-specific fluorescence is confined to the cell surface in the already characterized “cobblestone-like” staining pattern, while LysoTracker Red stains several intracellular compartments. Knob-treated H4-II-E cells that had been warmed at 37°C for 60 minutes in the presence of the LysoTracker Red showed considerable co-localization observed between the knob-specific punctate fluorescence and intracellular compartments staining positive as lysosomes (chapter 3, figure 7A). The co-localization suggested that the knob ligand is eventually delivered to lysosomes after endocytosis.

### **6.2. Knob degradation assay with lysosome inhibitors.**

Ammonium chloride (AC) and wortmannin (WM) both impede lysosome-based ligand degradation by inhibiting endosome maturation and lysosome fusion, respectively. Knob-treated H4-II-E cells incubated at 37°C for 120 minutes has been demonstrated to be sufficient time to observe a significant decrease in knob concentration relative to knob-treated cells that were not incubated at 37°C. The time course analysis was repeated in continued presence of either AC or WM to determine if either chemical prevented knob metabolism over time. Western blots

of H4-II-E cell lysates incubated with either AC or WM do not exhibit a substantial decrease in knob concentration over time, relative to samples that were incubated without either inhibitor (chapter 3, figure 7B). Neither AC nor WM were able to completely ablate knob degradation over time. We concluded that the degradation of the knob protein that had been observed in many of the assays conducted occurred in lysosomes. This last finding was the final piece in the determination of the fate of the knob ligand when it attaches to cells expressing an endocytically active population of CAR.

## **7. Receptor crosslinking.**

In experiments described in previous sections, the importance of CAR crosslinking by homotrimeric knob for ligand endocytosis and delivery to the lysosome was tested using saturating and sub-saturating doses of the knob protein. Degradation of knob over time was observed for both primary rat hepatocytes and rat hepatoma cells with saturating amounts and those with sub-saturating amounts. However, quantification of protein bands observed on the blots revealed a 4-fold decrease in knob concentration after 120 minutes at 37°C if a saturating dose was applied, while the application of a sub-saturating dose resulted in a 9-fold reduction in knob concentration after 120 minutes at 37°C. This suggested that doses favoring the knob homotrimer interacting with 2-3 CAR molecules, likely promoted crosslinking of the receptor molecules, which increased the degree of knob degradation.

While knob alone appears to have the capability of initiating CAR redistribution and internalization within the context of hepatocytes and hepatocyte-derived cell lines, the ligand alone is clearly not sufficient for CAR expressed on the A549 cell line. Interestingly, indirect immunofluorescent analysis of knob bound to A549 cells revealed that the majority of the receptor-ligand complexes were preferentially associated with spiny filopodia-like protrusions (chapter 5, figure 3C). Hommelgaard et.al described association with such membrane projections to be responsible for the internalization resistance of the ErbB2 receptor (92). They were able to override the restriction of the ErbB2 receptor to the cell surface by antibody-induced “super crosslinking” of adjacent receptors. We examined the use of single-layer and double-layer antibody-induced crosslinking of CAR on A549 cells to determine if such higher-level crosslinking could promote the endocytosis of the otherwise internalization-resistant receptor.

### **7.1. A549 cell line.**

#### **7.1.1. Knob internalization.**

Indirect immunofluorescence analysis was used to evaluate for internalization of knob-CAR complexes. As described previously, A549 cells grown on glass coverslips were treated with unlabeled Ad2 or Ad12 knob at 4°C to synchronize endocytosis. In these experiments, after removal of excess unbound knob protein, rabbit polyclonal anti-Ad2 knob or anti-Ad12 knob was bound to the knob-treated cells in the cold. When examining the effect of single-layer crosslinking, the primary rabbit antibodies were conjugated with either AF488 for anti-Ad2 knob or AF555 for anti-Ad12 knob. In sets of samples designated for double-layer crosslinking, the primary anti-knob antibodies were not conjugated with a fluorophore and the primary antibody

treatment was followed by binding goat-anti-rabbit modified with FITC or rhodamine in the cold. After knob and the designated antibodies were sequentially applied in the cold, some samples were fixed immediately for an initial time point while others were incubated at 37°C for specified durations. Upon examination, the single-layer crosslinking of anti-knob was adequate to trigger the redistribution of the knob-CAR complexes from the membrane projections into fluorescent puncta (chapter 3, figure 8A). The punctate fluorescence persisted after acetic acid stripping, which confirmed that the receptor-ligand complexes had been internalized. Identical results were obtained with double-layer crosslinking.

Hommelgaard et al., 2004 also reported that the “super crosslinked” ErbB2 receptor had been internalized through CCPs. To ascertain if A549 CAR had been endocytosed in similar fashion, the experiment was repeated in the continued presence of hypertonic sucrose to block the assembly of the CCPs. The redistribution and uptake of the receptor-ligand complexes across the cell is observed when the cell culture media contains 0.4 M sucrose (data not shown). In addition, acetic acid surface-stripping of these samples failed to remove the punctate fluorescence demonstrating that CCPs were not associated with the antibody-induced uptake of knob-CAR on A549 cells.

#### **7.1.2. Knob degradation.**

Having established that the resistance of A549 CAR to endocytosis could be overridden by antibody-induced crosslinking, we wanted to determine if the internalized receptor-ligand complexes were being delivered to a proteolytic compartment as occurred in the H4-II-E cell line. Initial studies of the A549 cell line showed that knob was not degraded over time when incubated at either a saturating or sub-saturating concentration. A549 cells were treated with knob and antibodies for single and double-layer crosslinking as described in the section above, except that the knob ligands employed were biotinylated. To our surprise, Western blots of the resulting cell lysates showed that despite triggering endocytosis, knob was not subsequently delivered to an intracellular compartment with proteolytic activity (chapter 3, figure 8B). Additionally, indirect immunofluorescence analysis failed to detect co-localization of the internalized knob ligand with the EEA-1 marker or the LysoTracker-Red dye (chapter 3, figure 8 C and D). We concluded that higher-level crosslinking of internalization resistant species of CAR can force uptake of the “super-crosslinked” receptor-ligand complexes, but does not guarantee delivery to the lysosomes or another degradative intracellular compartment. Given the results, it appears that the “super-crosslinked” knob-CAR complexes on A549 cells have been delivered to an intracellular compartment that does not traffic to either lysosomes or proteasomes.

### **7.2. H4-II-E cell line.**

#### **7.2.1. Knob internalization.**

The “super-crosslinking” of knob-CAR complexes by sequential antibody treatments promoted the uptake of the complexes on a cell line

previously established to express a population of CAR incapable of receptor-mediated endocytosis. We wanted to evaluate the effect, if any, of “super-crosslinking” to the described CAR-mediated uptake and delivery of knob to lysosomes on the H4-II-E cell line. An examination of single-layer and double-layer crosslinking by indirect immunofluorescence of knob-treated H4-II-E cells by anti-knob antibodies did not have any observable effect on the redistribution and internalization of the knob-CAR complexes. Acetic acid surface-stripping of designated samples also confirmed that the resultant fluorescent puncta were intracellular. Additionally, the observed CAR uptake phenotype was equally sensitive to incubation with hypertonic sucrose. This confirmed that endocytosis still proceeded by CCPs when higher-level crosslinking was employed on the H4-II-E cell line.

#### **7.2.2. Knob degradation.**

As described above, cell lysates were prepared from biotinylated knob-treated H4-II-E cells subjected to “super-crosslinking” and analyzed by Western blot probing with SA-HRP. The blots revealed no impairment to the degradation of the knob ligand over time, but did indicate an increase in the fold reduction of knob concentration over time. When analyzed for co-localization with the EEA-1 marker, there was greater overlap than was previously observed when only knob was applied. The “super-crosslinking” produced no observable difference between the knob-LysoTracker-Red co-localization pattern previously seen when knob alone was bound to the cells. The increased degradation of knob and the greater EEA-1 co-localization appeared to reinforce our contention that crosslinking of CAR is an accelerating factor in its observed receptor-mediated endocytosis on hepatocytes and hepatocyte-derived cell lines.

## 8. Figures.

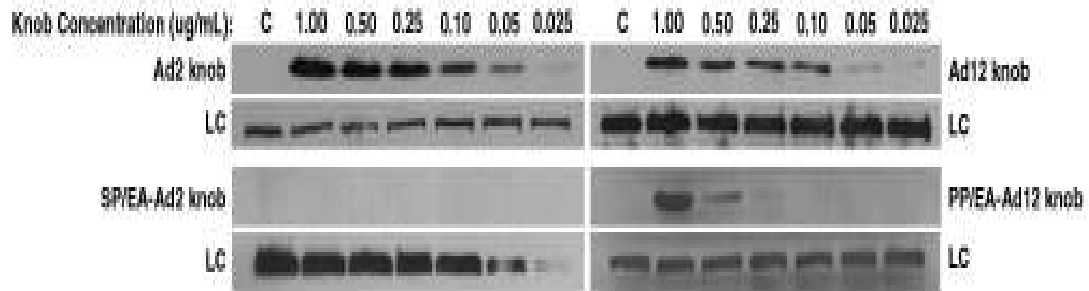


**Figure 1. Knob titration curves.** A549 (above) and H4-II-E cells (not shown) were treated with dilutions of biotinylated wild-type Ad2 knob, Ad12 knob, or one of their respective mutants with substitutions in the CAR binding site (SP/EA-Ad2 knob or PP/EA-Ad12 knob). Harvested cell lysates were blotted and probed with streptavidin-HRP. The SP/EA-Ad2 knob mutant failed to bind the cells at all concentrations tested. Lane C corresponds to untreated controls. LC corresponds to the loading control.

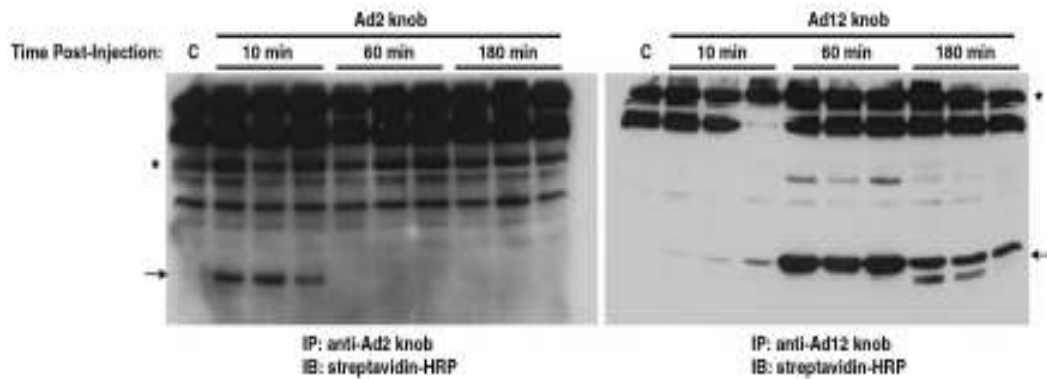


**Figure 2. Knob degradation *in vivo* in mouse liver.** Swiss-Webster mice were injected (tail-vein) with biotinylated Ad2 or Ad12 knob. Mice were euthanized at 0, 60, or 120 minutes post-injection (3 mice per time point) and their livers were excised. Liver tissue extracts were prepared, immunoprecipitated with anti-Ad2K or anti-Ad12K coupled sepharose, and analyzed by Western blot probing with SA-HRP probe. Lane C corresponds to a liver lysate prepared from a mouse injected with PBS as a negative control. Asterisks indicate protein bands used for loading controls.

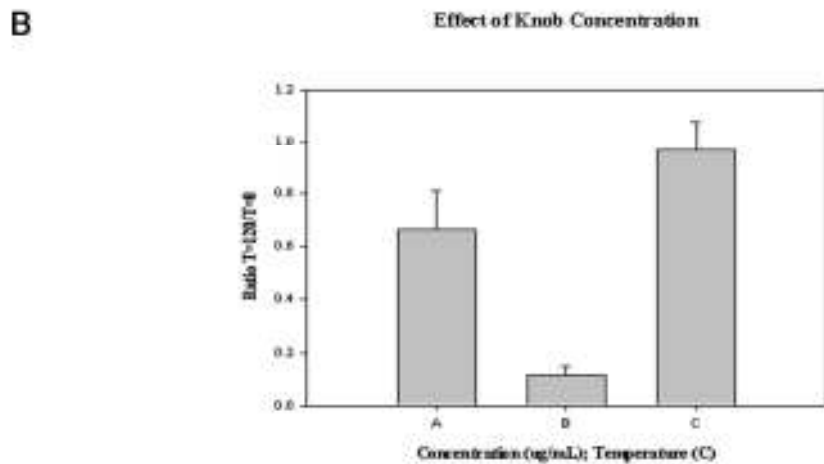
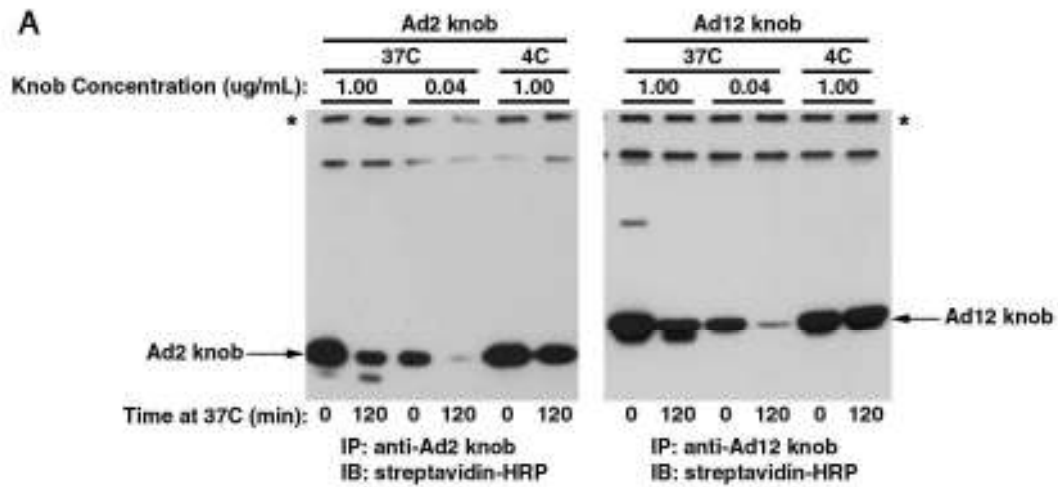


**Figure 3. Knob binding and degradation on primary rat hepatocytes.** *A*, To synchronize potential receptor endocytosis, primary rat hepatocyte cultures were treated with biotinylated wild-type Ad2 knob or Ad12 knob at saturating (1  $\mu\text{g/mL}$ ) and sub-saturating (0.04  $\mu\text{g/mL}$ ) doses at 4°C. Cells were washed in PBS to remove unbound knob. Then the cells were harvested for an initial time point. Alternatively, after washing with PBS, cells were supplied fresh media and were either incubated at 4°C or warmed to 37°C for 120 minutes. Afterwards, cells were harvested and cell lysates were analyzed by Western blot probing with SA-HRP. Asterisks indicate protein bands used for loading controls. *B*, The ratio of the relative amount of knob between the T<sub>120</sub>/T<sub>0</sub> time points from repeated experiments (n=5) was plotted with the mean and standard deviation calculated by SigmaPlot™.

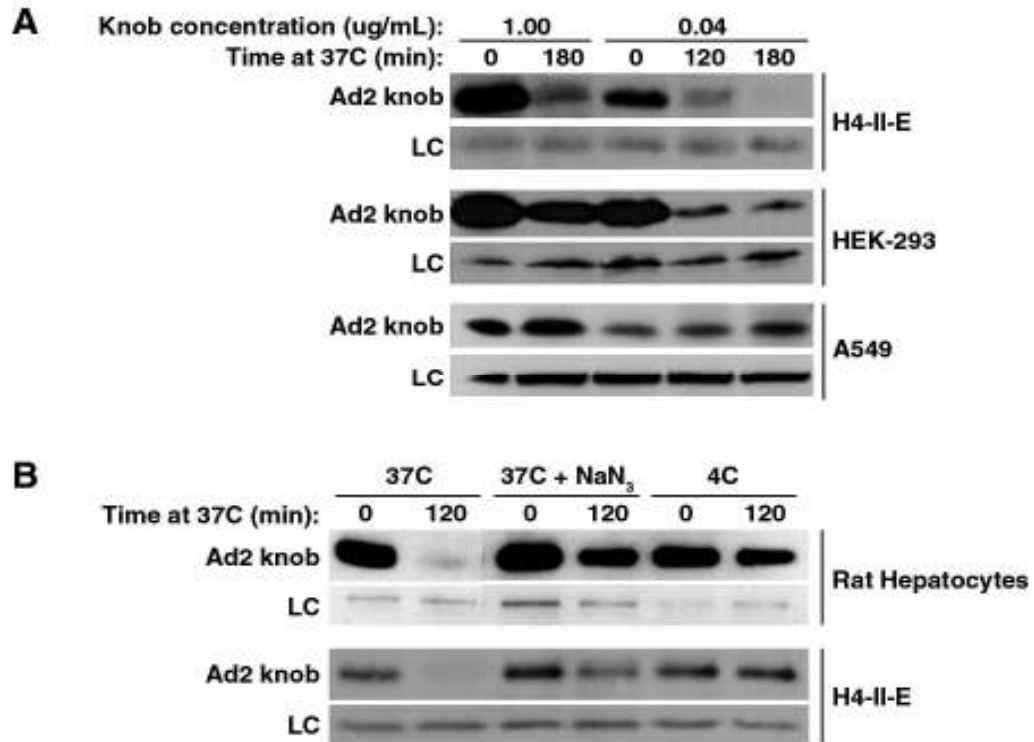


**Figure 4. Knob degradation is observed in the hepatocyte-derived H4-II-E cell line.** *A*, H4-II-E, HEK-293, and A549 cells were treated with biotinylated wild-type Ad2 knob and tested for knob degradation as described in figure 3, omitting immunoprecipitation with anti-knob sepharose. *B*, Primary rat hepatocytes and H4-II-E cells treated with 0.04 µg/mL biotinylated Ad2 knob were tested for knob degradation at 37°C in the absence or continued presence of 25 mM NaN<sub>3</sub>. Alternatively, cells were examined for knob degradation at 4°C. Cell lysates were analyzed by Western blot probing with SA-HRP. LC corresponds to the loading control.

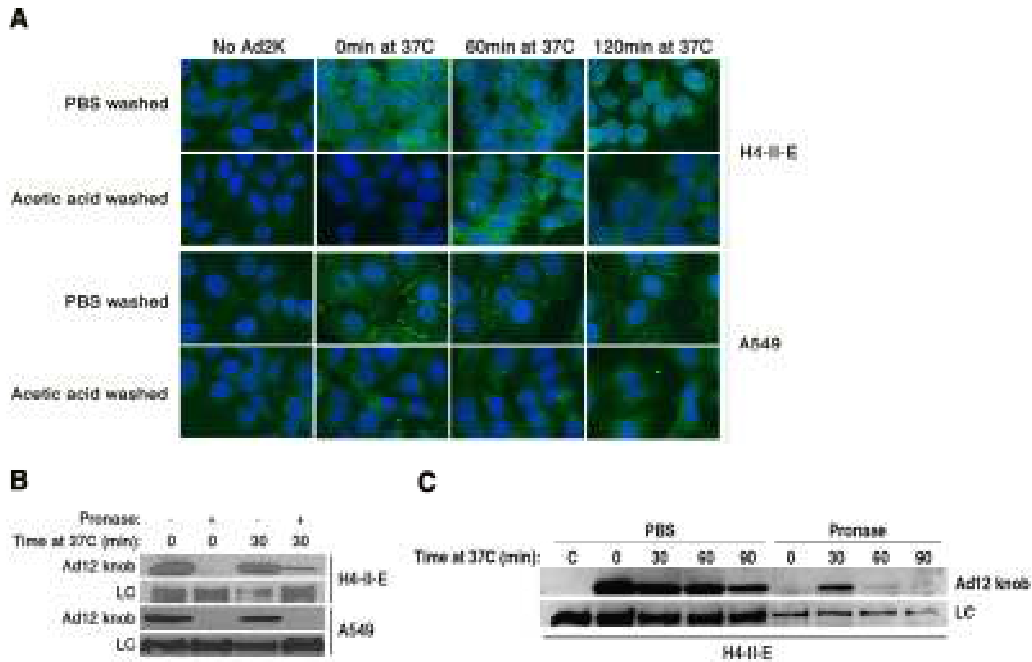


**Figure 5. Knob internalization by CAR.** *A*, H4-II-E and A549 cells grown on glass coverslips were treated with unlabeled Ad2 knob at 4°C. Excess unbound knob was removed and cells were fixed immediately for an initial time point or alternatively, cells were supplied fresh media and incubated at 37°C for 60 minutes. Designated sets of cells were surface-stripped with 0.2 M acetic acid in 0.5 M NaCl on ice. Cells were subsequently probed with rabbit anti-Ad2 knob followed by goat-anti-rabbit-FITC. Slides were examined under a 63X objective with DAPI and FITC filters. *B*, H4-II-E and A549 cells were treated with biotinylated Ad12 knob at 4°C as described previously. Cells were either fixed immediately for an initial time point or were supplied fresh media and warmed to 37°C. Post-fixation cells were treated with either 0.5 mM EDTA or 0.1 mg/mL pronase and incubated at 37°C for 30 minutes. Cell lysates were analyzed by Western blot probing with SA-HRP. *C*, The pronase surface-stripping assay described in *B* was repeated on H4-II-E cells, but with additional 60 and 90 minute time points included.

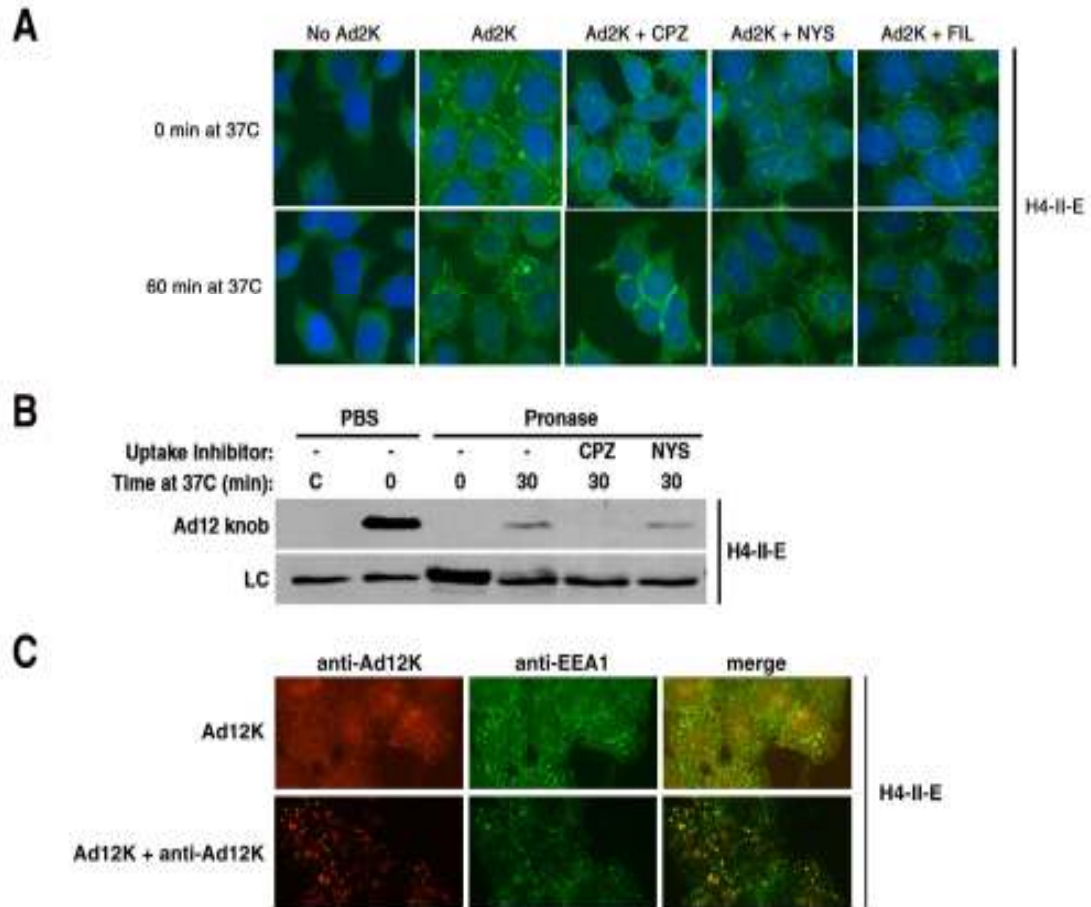


**Figure 6. CAR endocytosis of knob proceeds through clathrin-coated pits.** *A*, H4-II-E cells grown on glass coverslips were treated with unlabeled Ad2 knob and warmed to 37°C for 0 or 60 minutes in the absence or continued presence of either chlorpromazine, nystatin, or filipin. The cells were then probed with rabbit anti-knob followed by goat-anti-rabbit-FITC. *B*, H4-II-E cells were treated with biotinylated Ad12 knob and were either fixed immediately for an initial time point or were supplied fresh media and warmed to 37°C for 30 minutes as described previously. The knob treatment and incubation were performed in the absence or continued presence of either chlorpromazine or nystatin. After fixation cells were treated with either 0.5 mM EDTA or 0.1 mg/mL pronase and incubated at 37°C for 20 minutes. Cell lysates were analyzed by Western blot probing with SA-HRP. LC corresponds to the loading control. *C*, H4-II-E cells grown on glass coverslips were treated with unlabeled Ad12 knob, warmed to 37°C for 60 minutes and probed with anti-Ad12K-AF555 then mouse monoclonal anti-EEA1 followed by goat-anti-mouse-FITC (top panel). Alternatively, cells were treated successively with unlabeled Ad12 knob and anti-Ad12K-AF555, warmed for 60 minutes at 37°C, and probed with anti-EEA1 followed by goat-anti-mouse-FITC (bottom panel). Slides were examined under a 63X objective with FITC and Cy3.5 filters.

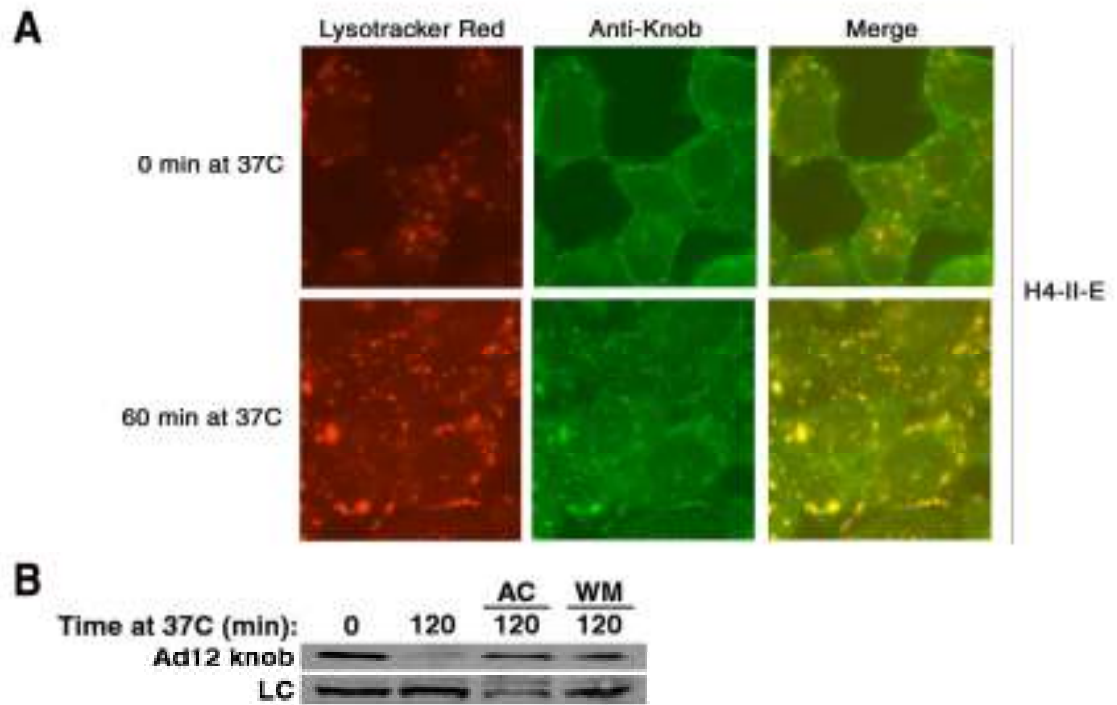


**Figure 7. Knob degradation occurs in lysosomes.** *A*, H4-II-E cells grown on glass coverslips were treated unlabeled Ad2 knob and LysoTracker Red at 4°C, warmed at 37°C for 0 or 60 minutes, and probed with rabbit anti-Ad2K followed by goat-anti-rabbit-FITC. Slides were examined under a 63X objective through FITC and Cy3.5 filters. *B*, H4-II-E cells were treated with biotinylated Ad2 knob and warmed to 37°C for 0 or 120 minutes in the absence or continued presence of 20 mM NH<sub>4</sub>Cl or 100 nM wortmannin. Cell lysates were analyzed by Western blot probing with SA-HRP. LC indicates the loading control.

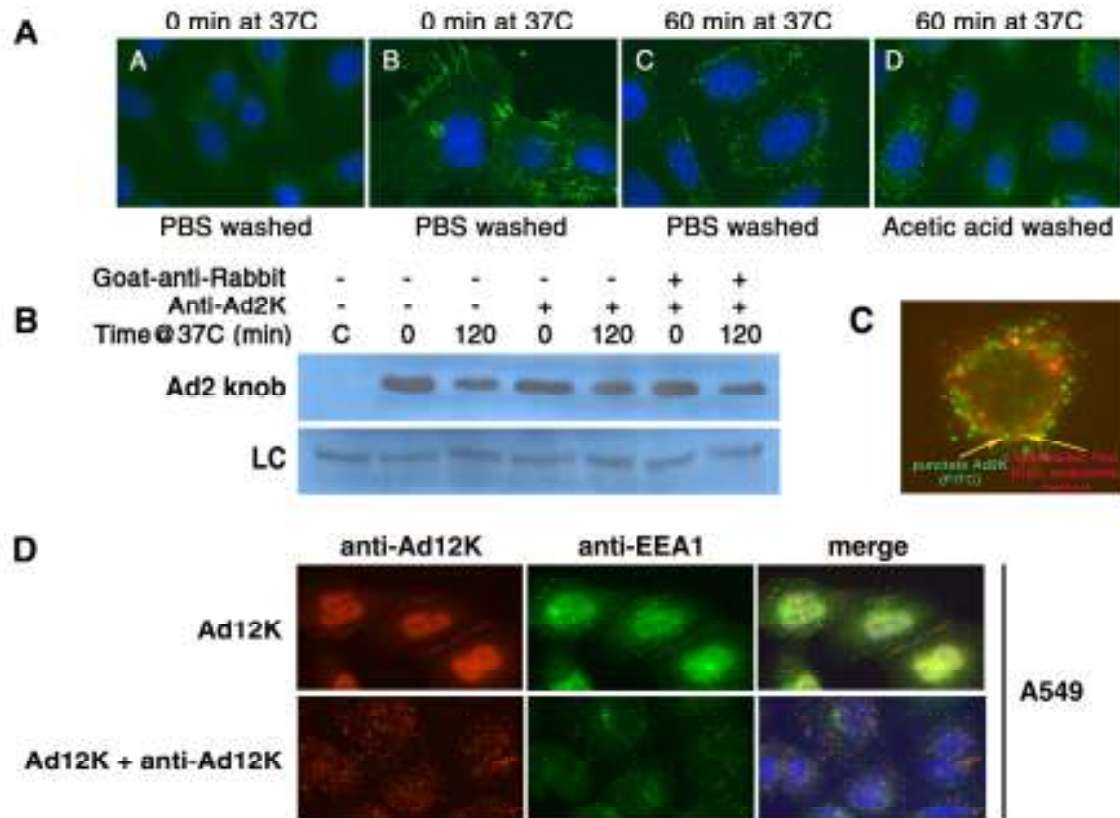


**Figure 8. Antibody-induced receptor-crosslinking overrides CAR internalization resistance on A549 cells.** *A*, A549 cells grown on glass coverslips were successively treated with unlabeled Ad2 knob, rabbit anti-Ad2K, and goat-anti-rabbit-FITC 60 minutes each at 4°C with PBS washes between each treatment. The cells were either fixed immediately for an initial time point or were warmed to 37°C for 60 minutes. Selected samples were washed with 0.2 M acetic acid in 0.5 M NaCl to remove surface-bound ligand. Slides were imaged using a 63X objective with FITC and DAPI filters. Panel A displays control cells not incubated with Ad2 knob. *B*, A549 cells were treated successively with biotinylated Ad2 knob, rabbit anti-Ad2K, and/or goat-anti-rabbit-FITC as indicated at 4°C. Subsequently, the cells were warmed to 37°C for 0 or 120 minutes. Harvested cell lysates were analyzed by Western blot probing with SA-HRP. LC indicates the loading control. *C*, A549 cells grown on glass coverslips were treated as described in *A*, except the media applied during the 60 minute incubation at 37°C was supplemented with the LysoTracker Red reagent. Slides were imaged using a 63X objective with FITC and Cy3.5 filters. *D*, A549 cells grown on glass coverslips were treated with unlabeled Ad12 knob and anti-Ad12K-AF555 successively at 4°C and warmed to 37°C as described in *A*. Cells were then probed with mouse monoclonal anti-EEA1 followed by goat-anti-mouse-FITC (bottom panel). Alternatively, cells were treated with unlabeled Ad12 knob at 4°C, warmed to 37°C, and probed with anti-Ad12K-AF555 then anti-EEA1 followed by goat-anti-mouse-FITC (top panel). Slides were examined using a 63X objective with FITC, DAPI, and Cy3.5 filters.

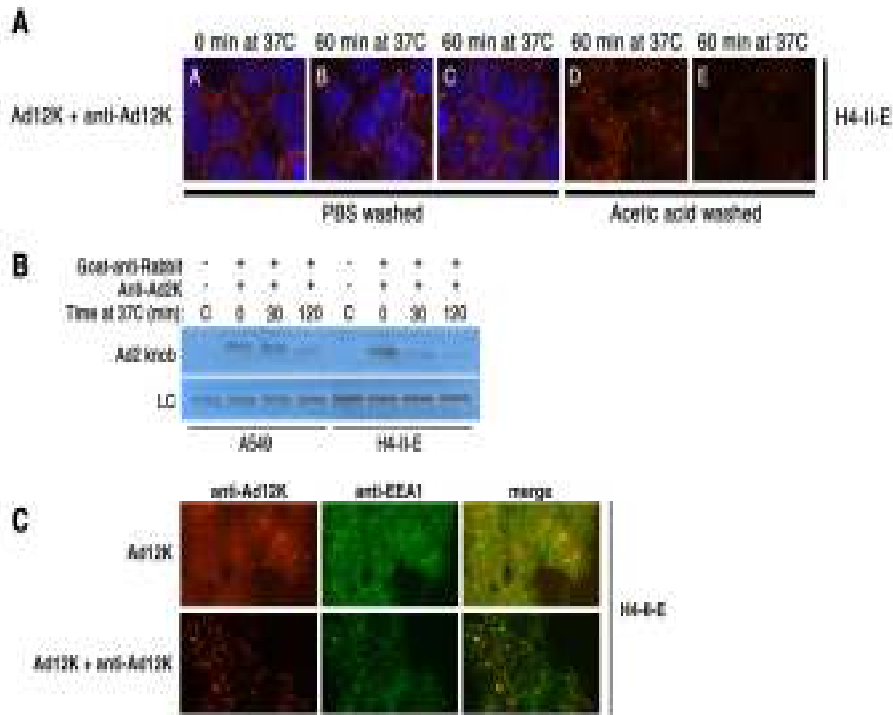


**Figure 9. Antibody-induced receptor-crosslinking accelerates CAR internalization and degradation on H4-II-E cells.** *A*, H4-II-E cells grown on glass coverslips were successively treated with Ad12K and anti-Ad12K-AF555 60 minutes each at 4°C with PBS washes between each treatment. The cells were either fixed immediately for an initial time point (panel A) or were warmed to 37°C for 60 minutes (panels B-E). Selected samples were washed with 0.2 M acetic acid in 0.5 M NaCl to remove ligand on the cell surface (panels D-E). Selected samples were tested for sensitivity to 0.4 M sucrose (panels C and E). Slides were imaged using a 63X objective with FITC and DAPI filters. *B*, H4-II-E and A549 cells were treated successively with biotinylated Ad2 knob, rabbit anti-Ad2K, and goat-anti-rabbit-FITC as indicated at 4°C. Subsequently, the cells were warmed to 37°C for 0, 30, or 120 minutes. Harvested cell lysates were analyzed by Western blot probing with SA-HRP. LC indicates the loading control. *C*, Bottom row: H4-II-E cells grown on glass coverslips were treated with unlabeled Ad12 knob and anti-Ad12K-AF555 at 4°C, warmed to 37°C for 60 minutes, and probed with mouse monoclonal anti-EEA1 followed by goat-anti-mouse-FITC. Top row: alternatively, cells were treated with unlabeled Ad12 knob at 4°C, warmed to 37°C, and probed with anti-Ad12K-AF555 then anti-EEA1 followed by goat-anti-mouse-FITC. Slides were examined using a 63X objective with FITC, DAPI, and Cy3.5 filters.

## **Chapter 4: Discussion I—CAR Hepatocyte Study**

Since its initial discovery, much of the research conducted on CAR has focused on its role in primary airway epithelial cells and epithelial-derived cell lines. This is in part due to the intense interest in utilizing adenovirus as a vector for gene therapy of lung and other epithelial tissues. Clinical trials showed the Ad vectors had surprisingly poor transduction efficiency in lung tissue (58). It was subsequently determined that CAR is localized predominantly on the basal-lateral surface of these cells, and thus is not accessible to virus particles delivered to the apical surface (lung airways). Cell culture models have demonstrated that CAR is confined to the adherens junction of cells, where it has been described to contribute to the paracellular permeability barrier through the formation of homophilic interactions with CAR expressed on adjacent cells (30). In the context of polarized epithelium, CAR has failed to exhibit a capacity to mediate the rapid internalization of bound ligand. However, a considerable amount of anecdotal evidence has accumulated implying that CAR was capable of efficient receptor-mediated endocytosis, but in a cell-type dependent basis. As previously mentioned in the Introduction section 2, CAR-binding Ad serotypes lacking the RGD motif necessary for integrin interaction are not slow to infect their respective host cells, but exhibit a tropism for enteric epithelium rather than lung epithelium (56,57). However, mutant serotypes constructed with the substitutions for the RGD motif demonstrated varying degrees of impairment of viral particle uptake (55). Similarly, the efficiency of infection of RGD-negative and wild-type Ad particles was indistinguishable with respect to primary cultures of human and rat hepatocytes relative to monolayers of HeLa cells (95).

The intent of our studies was to examine the behavior of CAR expressed on hepatocytes; specifically, to determine if hepatocyte-specific CAR mediates rapid ligand endocytosis. To achieve this aim, recombinant knob domain was employed as a CAR-specific ligand both *in vitro* and *in vivo*. As demonstrated by both the CAR biodistribution study and the LDLR study, experiments that use radioiodine or other labile radiolabels for tracking the fate of a protein *in vivo* must be interpreted with care because of potential separation of the label and protein resulting from hydrolysis of labile bonds (67,69). To circumvent that problem, the knob proteins employed in this study were labeled with biotin, a small molecule which binds to proteins by stable covalent bonds allowing detection of biotinylated protein in tissue and cell culture with streptavidin modified with peroxidase or a fluorophore.

As detailed in the introduction section 4, the best evidence in support of endocytically active CAR arose from the *in vivo* CAR biodistribution study conducted in mice by Awasthi et al., 2004 (67). In that publication, it was concluded that accumulation of radioactivity in the stomach instead of the liver probably resulted from de-iodination of the protein in liver microsomes. With the radioiodine separated from the knob domain, the ultimate fate of the protein in the liver was uncertain. Repeating the animal study with biotinylated Ad2 and Ad12 knob revealed that both proteins accumulate and appear to be degraded within the liver, though at differing rates. Western blots of the liver tissue lysates revealed that Ad2 knob was only detected in the livers of mice sacrificed 10 minute post-

injection. In contrast, Ad12 knob was seen in small amounts at 10 minutes, but continued to accumulate to a relatively high concentration by 60 minutes post-injection. By the 180 minute time point, Ad12 knob had started to diminish in concentration, and a faster migrating band was observed, which likely corresponds to a stable degradation product. The basis for the differing kinetics observed between Ad2 and Ad12 knob is not understood, but we propose three different models that potentially could account for this effect. First, the *in vivo* CAR biodistribution study conducted with radioiodinated Ad2 and Ad12 knob reported that the Ad2 trimers were less stable to SDS treatment than the Ad5 and Ad12 knob trimers (67). Degradation of Ad12 knob in the liver might require more time due to its greater inherent stability relative to Ad2 knob. Second, using fluorescent anisotropy analysis, our lab has found that Ad2 knob has a greater affinity ( $K_d$  of 35 nM) for CAR relative to Ad12 knob ( $K_d$  of 290 nM), suggesting that Ad2 knob might be depleted more quickly from the bloodstream by a higher affinity interaction with CAR (51). Lastly, side-by-side comparison of the knob crystal structures show that Ad12 knob has several hydrophobic patches displayed on its surface that are not present on Ad2 knob (96). These patches potentially could mediate low affinity non-specific contacts with unknown molecules in the bloodstream, thus delaying the delivery of Ad12 knob to CAR in the liver.

The application of biotinylated knob protein to primary rat hepatocyte cultures as well as the H4-II-E rat hepatoma cell line confirmed that the degradation of the knob ligand can occur in hepatocytes. Ad2 and Ad12 knob demonstrated similar kinetics of degradation, suggesting that the difference observed *in vivo* is at the level of attachment, not protein stability. Similar results were obtained for the human neuron-derived HEK-293 cell line demonstrating that this phenomenon extends beyond hepatocytes to other cell types and that this was not exclusive to rodents. The A549 and HeLa S3 cell lines were the only cell types tested that failed to exhibit active CAR endocytosis, thus establishing this cell line as a suitable negative control for subsequent analyses.

The observed degradation of the knob protein was completely impeded by incubation of H4-II-E cell cultures at 4°C, while it was only partially impaired when incubated at 37°C with known inhibitors of endocytosis such as hypertonic sucrose and sodium azide. Both of these results strongly suggested that the apparent degradation of the knob ligand occurred intracellularly, thus requiring prior internalization by CAR. Cell culture based surface-stripping assays were designed to demonstrate CAR-dependent internalization directly. Indirect immunofluorescent microscopy demonstrated the transformation of surface-associated knob-specific fluorescence to punctate fluorescence over the course of incubation at 37°C. The knob-specific punctate fluorescence persisted after the cells were washed in acetic acid, thus confirming that it was indeed intracellular. Western blot analysis of knob-treated cell cultures surface-stripped by an enzyme treatment revealed the presence of an enzyme-resistant knob band if incubated at 37°C for 15-30 minutes. This result corroborated the prior immunofluorescent findings, thus confirming that knob was internalized by CAR. The repetition of both assays in the continued presence of chemical inhibitors specific for

endocytosis by either clathrin-coated pits or lipid raft-mediated mechanisms demonstrated that knob internalization was blocked at the level of CCPs. Internalized populations of knob were found by immunofluorescent microscopy to co-localize with the EEA-1 marker of early endosomes, which are linked to CCP uptake. Cumulatively, these results illustrate that the degradation of knob observed both in cell culture and *in vivo* requires prior internalization of the ligand into CCPs which results in its delivery to EEA-1 positive early endosomes.

The LysoTracker Red fluorescent marker, which preferentially stains the lysosomal pathway, was incubated with knob-treated cells. The fluorescently tagged antibodies for knob frequently co-localized with the LysoTracker Red reagent indicating that knob is degraded within lysosomes. This assertion was reinforced by the apparent sensitivity of knob degradation on the hepatoma H4-II-E cell line to ammonium chloride and wortmannin, which both block lysosome-specific degradation at the level of endosomal maturation and lysosome fusion, respectively. This completed a model where, in the context of hepatocytes, knob attaches to CAR with subsequent uptake via CCPs and eventual delivery to lysosomes where knob is ultimately degraded.

In a previous study of the ErbB2 receptor, the receptor's resistance to endocytosis was attributed to its preferential association with filopodia-like membrane protrusions (92). Interestingly, the A549 cell line, the only cell type tested that failed to exhibit CAR endocytosis, demonstrated association of knob-CAR complexes in similar protrusions when examined by immunofluorescent microscopy. The authors of the ErbB2 receptor study described using successive receptor-specific antibodies to crosslink adjacent molecules, which effectively triggered the rapid endocytosis of the ErbB2 receptor via CCPs. We employed their "super-crosslinking" technique successfully to induce the endocytosis of knob-CAR complexes on A549 cells with the addition of anti-knob antibodies. Although this was able to initiate the endocytosis of knob bound to CAR on this cell line, it failed to deliver the knob ligand to a degradative compartment. Western blots of "super-crosslinked" A549 cell lysates showed that the knob concentration remained constant over time. Additionally, internalized knob-specific punctate fluorescence failed to co-localize with the EEA-1 marker and the LysoTracker Red reagent. When the same technique was tested on knob-treated H4-II-E cells, the "super-crosslinking" actually accelerated the uptake and degradation of knob. We concluded that CAR expressed on the A549 cell line, and possibly also in the context of lung epithelia, is isolated from the endocytic pathway available to CAR expressed on H4-II-E cells and by extension on hepatocytes *in vivo*.

In the first tests for the detection of knob degradation on primary hepatocyte and H4-II-E cultures, two different doses of the knob ligand were applied. This experimental design was based on evidence from the cryo-EM structure of CAR bound to CVB particles, suggesting that CVB virus particles may induce the formation of CAR dimers in the cell membrane (87). The cytoplasmic tail regions of these putative dimers formed discontinuous electron density suggesting a possible dimer interaction. Potential crosslinking of CAR by

bound coxsackievirus particles was reinforced through indirect immunofluorescent microscopy and fluorescent resonance energy transfer (FRET) experiments. Attachment of CVB particles was shown to bring two CAR molecules into close proximity, which initiated the lateral diffusion of the virus-receptor complexes into lipid rafts, where endocytosis proceeded by a raft-dependent mechanism (97). Based on these results, we wanted to determine if knob, a trivalent ligand capable of binding as many as 3 CAR molecules simultaneously, triggered CAR endocytosis by receptor crosslinking. As described in the Results I section 5, we applied saturating and sub-saturating doses of biotinylated knob, with the latter dose favoring a crosslinking event, and found that a higher degree of knob degradation over time was observed for the cell cultures treated with a sub-saturating amount of ligand. Given that the “super-crosslinking” technique further accelerated the degradation of knob, we believe that receptor crosslinking may initiate CAR-mediated ligand endocytosis, while it is certainly clear that it enhances the rate of CAR internalization on permissive cell types.

At this point, it is important to emphasize the usefulness of using recombinant knob rather than whole virus particles or purified fiber. Aside from the other receptor interactions that would confound the data, the knob domain allowed the detection of two very different uptake pathways exhibited by A549 cells and H4-II-E cells that would not have been observed had whole Ad particles been employed. Although demonstrating different rates of endocytosis, RGD-negative and wild-type Ad virions productively infect both A549 cells and hepatocytes (55,95,98). Knob ligand was internalized and degraded by hepatocytes and H4-II-E cells, but not A549 or HeLa S3 cells. Antibody-induced receptor crosslinking overrode the internalization-resistant CAR on A549 cells, but did not deliver knob to the same degradative intracellular compartment observed for hepatocytes and H4-II-E cells. Using knob as a mono-specific ligand for CAR, two different endpoints are observed depending on the cell line examined, which would not have been observed in the context of whole virus particles.

Taken together, we have provided evidence of rapid CAR-mediated ligand endocytosis in the context of hepatocytes both in cell culture and *in vivo*. To best of our knowledge, this is the first report of such behavior for CAR. Prior studies of CAR behavior have been limited to cell culture models, and in many instances were conducted with ectopically expressed CAR in cell lines that do not endogenously express the receptor molecule. Although these model systems provide valuable information regarding receptor physiology, it is uncertain whether they accurately reflect receptor activity in the context of cells and tissues *in vivo*. In our study, we have corroborative evidence that the activity we observed in cell culture translates to the animal model. These findings should be of interest to both virologists attempting to utilize adenoviruses for gene therapy vectors and to cell biologists interested in exploring the purpose of elevated levels of CAR expression in the adult liver tissue of humans and rodents.

**Future Directions.**

In future studies, we would like to explore what factors regulate the ability of CAR to catalyze rapid ligand endocytosis in hepatocytes. Here, we propose 3 models that potentially could explain the disparity in receptor function between the different cellular contexts. With the multiple splice variants that have been described for CAR (see Introduction section 1.1.), we acknowledge the possibility that the difference in behavior between lung epithelial cells and hepatocytes may be due to different splice isoforms exhibiting alternative functions. Another possible explanation resides at the level of differential post-translational modification, specifically the only known reversible fatty acid modification: palmitoylation. And lastly, given the increasing database of known cytosolic proteins known to bind CAR through its class I PDZ interaction motif, it may be possible that CAR molecules incapable of rapid uptake are locked in supramolecular lattices of PDZ interactions (32,33,35,38). Additionally, lung and liver tissue could demonstrate differential expression of PDZ domain containing proteins reported to be partnered with CAR through the PDZ interacting motif. Future research will need to discern which if any of these hypothesized model mechanisms is responsible for the regulation of CAR-mediated endocytosis of bound ligand. And it may very well be determined that the regulatory mechanism is one not yet predicted.

Another potential focus of future research would be to elucidate what is the physiological significance of endocytically active CAR in adult liver tissue. To that end, we would like to ascertain if there is a host metabolite that selectively binds to CAR in the liver. Indeed, we have already considered using CAR D1-derived affinity column to attempt to extract a novel CAR ligand from the blood or tissue extracts.

## **Chapter 5: Supplementary Data—CAR Hepatocyte Study**

In light of the potential avenues of future research described briefly in the previous discussion section, some preliminary experiments have been conducted that will be briefly described in this section.

### **1. Regulation hypothesis #1: CAR splice variants.**

In both human and rodent tissues, alternative splice variants of CAR have been reported (13,15,16). The secreted soluble isoforms of CAR lacking the transmembrane domain and cytoplasmic tail have been described to have anti-viral effects by competing for virus binding in the bloodstream. As yet, alternative functions have not been attributed to the cell-associated CAR isoforms.

A query of the Genbank nucleotide database for the CAR gene (CXADR) in humans, rats, and mice yields a curious report. Only one mRNA transcript is reported for human CAR, which gives rise to the known full-length 46 kDa protein. The mouse entries describe two isoforms: one for full-length CAR and a smaller splice variant which produces a truncated CAR protein with the last 26 acid amino acids of the cytoplasmic tail domain replaced. And lastly, only one entry for a rat CAR mRNA transcript exists, which is 96% identical to the second smaller transcript described for mice. The implication that could be derived from this online query is that the CAR endocytic phenotype that has been elucidated in mouse liver tissue, primary rat hepatocytes, and rat hepatoma cells is attributable to the second smaller CAR isoform not described for human tissues. However, this would confound the detection of the CAR-dependent knob metabolism in the human HEK-293 cell line.

To explore this possibility, we designed several primers for 3'-RACE (rapid amplification of cDNA ends) PCR analysis. Briefly, RNA was extracted and purified from H4-II-E, A549, and HEK-293 cell cultures, and mRNA molecules were reverse transcribed to cDNA. Subsequently, using a 5'-CAR-specific primer and a universal 3'-adaptor primer, CAR cDNAs were amplified by PCR. An examination of the PCR products from the three different cell lines on an agarose gel revealed several faint bands (chapter 5, figure 1, top panel). A faint band matching the expected size of the full-length CAR transcript of approximately 2.5Kb was observed in the H4-II-E and HEK-293 lanes, though we cannot rule out that such a band is not also present in the A549 lane but below detection limits.

To confirm that CAR specific transcript(s) were copied in the first strand cDNA synthesis reaction, we amplified this material using forward and reverse primers specific for human CAR D1 with the A549 and HEK-293 samples (data not shown) and forward and reverse primers specific for rat CAR D1 with the H4-II-E sample (chapter 5, figure 1, bottom panel). The D1 domain of CAR was successfully amplified for all 3 samples confirming that CAR-specific transcripts were present from the first stand synthesis and subsequent amplification.

A second set of primers relevant to the cytoplasmic tail domain of CAR was used to determine if alternative splice variants of CAR had also been

amplified by the initial 3'-RACE PCR. With respect to the alternative splicing of CAR, the splicing event occurs within exon 7 of the CAR gene, where a small fraction designated exon 7A is shared by all splice variants. After exon 7A, the 3' ends of all variants differ in nucleotide sequence resulting from either joining the splice donor at 7A to an acceptor site for exon 8, or override of the splicing event. Forward primers were designed to anneal with the exon 7A region, and unique reverse primers were prepared for each of the two major cell-associated splice variants. The amplification of 3'-RACE PCR products from the H4-II-E cell line using the cytoplasmic tail primer sets produced a band for both the full length CAR mRNA-1 and the shorter CAR mRNA-2 isoforms (chapter 5, figure 1, bottom panel). In the case of the A549 and HEK-293 cells, strong amplification was observed for the full length CAR transcript, while the primer set for the predicted short mRNA2 isoform produced a weakly-amplified product (data not shown). Although quantitative PCR will be required to say for certain, it appears only the rat hepatoma cell line exhibits detectable amounts of the smaller cell-associated CAR isoform. Further experiments will be necessary to determine if the second mRNA2 isoform observed in H4-II-E cells is responsible for the CAR endocytic phenotype.

## **2. Regulation hypothesis #2: CAR palmitoylation and raft association.**

### **2.1. Palmitoylation.**

As mentioned above, palmitoylation is the only known reversible fatty acid modification of cellular proteins. Attached palmitate moieties have been reported to anchor peripheral membrane proteins to the cytoplasmic leaflet of the phospholipid bilayer (99,100). However, palmitate-dependent anchorage of integral membrane proteins has remained controversial, though it has been reported that the reversible palmitoylation of the transferrin receptor (TfR) on two unique cysteine residues in the cytoplasmic tail regulates its permissiveness to endocytosis (101). As detailed in the Introduction section 3, CAR is known to be palmitoylated, and the abrogation of CAR palmitoylation resulted in dramatic redistribution of the receptor, which was found in approximately equal amounts intracellularly and at the cell surface (31). Notably, knob-CAR complexes on A549 cells were found to preferentially associate with filopodia-like membrane extensions (see panel C, supplemental figure 3), an association reported to render receptor molecules internalization-resistant (92). A recent publication describes that palmitoylation of the motif: Cys-Cys-X-B-B (where X represents any amino acid and B represents a basic amino acid) not only promoted association with filopodia extensions, but triggered the generation of new projections (100). The site of CAR palmitoylation Cys-Cys-Arg-Lys-Lys is such a motif, suggesting that palmitoylation of this motif is responsible for the localization of CAR on A549 cells to membrane protrusions and may contribute to the formation of additional protrusions on A549 cells.

To examine if palmitoylation is responsible for the resistance of CAR on A549 cells to receptor-mediated endocytosis, 2-bromopalmitate (2-BrP) was incorporated into a knob cell binding assay. The palmitate analogue 2-

BrP been established to significantly reduce the levels of protein palmitoylation in cell culture as well as in vivo (100). If CAR modification with palmitate restricts CAR to the cell surface of A549 cells, then it would be expected that extended exposure to 2-BrP would gradually diminish the number of available CAR binding sites on the cell surface. A549 cells were incubated in the presence of 2-BrP, and subsequently treated with biotinylated Ad2 or Ad12 knob. After knob treatment, lysates of these cells were probed with SA-HRP on a Western blot to determine if the amount of bound knob had been reduced relative to samples not incubated in the presence of 2-BrP. With increasing concentration of 2-BrP and with increasing duration of exposure, the amount of biotinylated Ad2 or Ad12 knob that was able to bind diminished. At all doses tested, 2-BrP was extremely toxic to H4-II-E cells, therefore we were unable to establish if it reduced the number of available CAR binding sites on the surface of these cells. Further analysis will be required to determine if the reduced knob binding is the result of down-regulation of CAR at the cell surface by de-palmitoylation.

## **2.2. Lipid raft association.**

Frequently, palmitoylated receptors are found preferentially associated with cholesterol-enriched lipid raft domains within the plasma membrane. Although palmitoylation is not a pre-requisite for raft association, it has been predictive of localization to such membrane microdomains. Many tight junction proteins have been reported to be embedded in lipid rafts. These findings suggest that CAR functioning as a cell adhesion molecule may be similarly anchored in lipid rafts. Raft-associated proteins often are insoluble when cells are lysed in cold non-ionic detergents such as Triton X-100 (TX-100) and Nonidet-P40 (NP40).

Knob-treated A549 and H4-II-E cells were lysed at 4°C or 37°C in TX-100. The resultant lysates were centrifuged to pellet detergent-resistant membrane (DRM) fractions from the lysates. The supernatant was recovered, and the DRM pellet predicted to contain raft-associated proteins was dispersed by sonication in TX100. The separate fractions were examined by Western blot probing with SA-HRP, which revealed that the bulk of H4-II-E associated knob-CAR complexes were soluble in the non-ionic detergent regardless of incubation temperature. However, when lysed in TX-100 in the cold, most A549 associated knob-CAR complexes were detected in the DRM fraction, suggesting CAR is localized within lipid rafts on the A549 but not the H4-II-E cell line. Sequestration of membrane cholesterol by both FIL and NYS failed to affect a redistribution of knob-CAR complexes on A549 cells observed by indirect immunofluorescent microscopy.

### 3. Supplemental Figures of Preliminary Data.

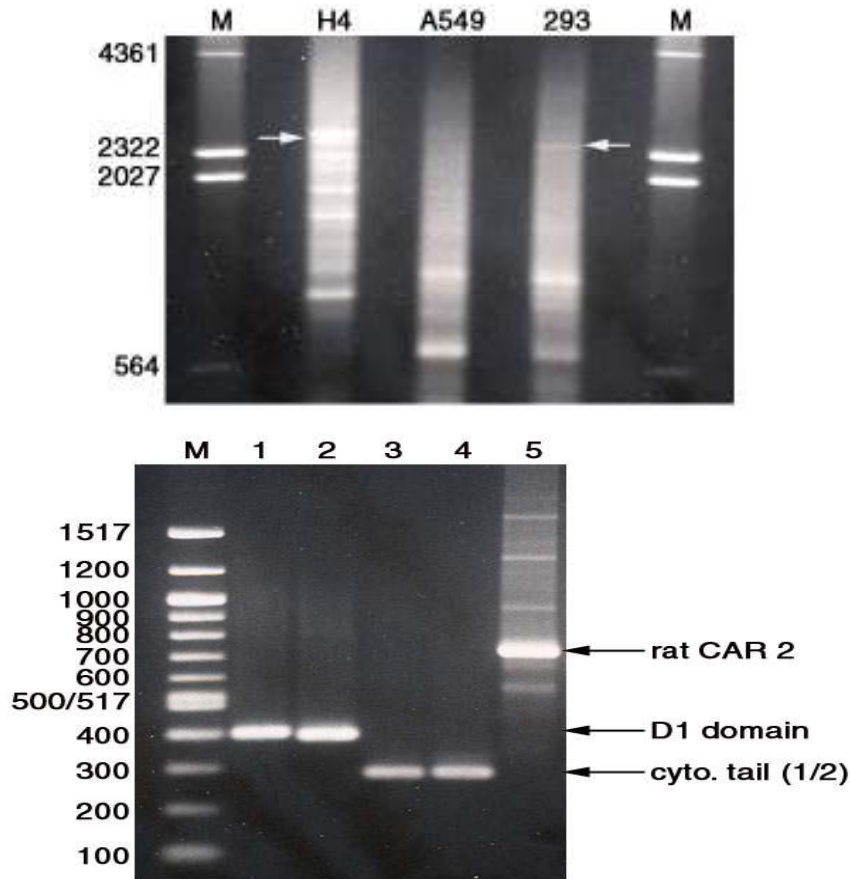


**Figure 1. The smaller cell-associated CAR isoform (rCAR2) is dominant in H4-II-E cells.** *Top panel:* agarose gel of the products of 3'RACE-PCR of RNA harvested from H4-II-E, A549, and HEK-293 cell lines (as indicated) run alongside a ladder of DNA fragments of indicated size. Arrows point to band size expected for the amplification product of the full length CAR gene (2.5 Kb). *Bottom panel:* agarose gel of PCR products amplified from prior 3'RACE PCR products. Lane 1: CAR D1 domain amplified from plasmid containing D1 fragment (positive control). Lane 2: CAR D1 domain amplified from H4-II-E 3'RACE PCR product. Lane 3: rat cytoplasmic domain specific to isoform 1 amplified from H4-II-E 3'RACE PCR product. Lane 4: rat cytoplasmic domain specific to isoform 2 amplified from H4-II-E 3'RACE PCR product. Lane 5: 3'RACE re-amplification of H4-II-E 3'RACE PCR product using cytoplasmic domain specific forward primer. M: DNA fragment ladder of indicated sizes.

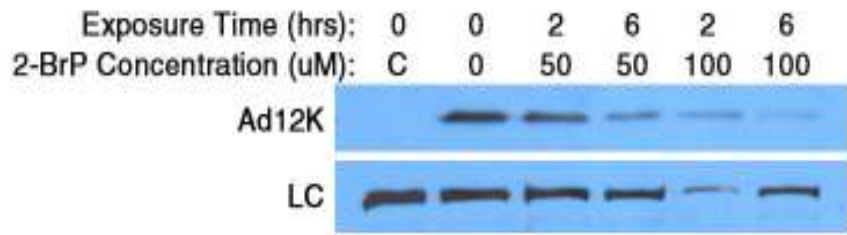


**Figure 2. Effect of reduced palmitoylation on available CAR binding sites.** A549 cells were incubated at 37°C with either 50  $\mu$ M or 100  $\mu$ M 2-bromopalmitate (2-BrP) for 2 hours or 6 hours, or without 2-BrP. After the designated incubation times, biotinylated Ad12 knob was applied for 1 hour, and residual unbound knob was removed by successive PBS washes. A549 cell lysates were examined on a Western blot probing with SA-HRP. LC indicates the loading control.

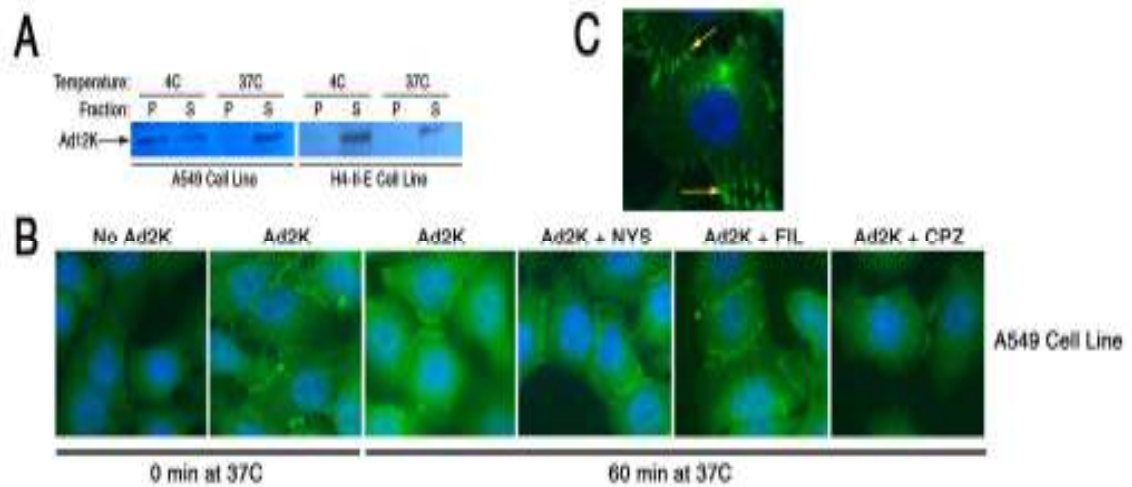


**Figure 3. A549 and H4-II-E CAR fractionate differently after cold lysis in non-ionic detergent.** *A*, A549 and H4-II-E cells were treated with biotinylated Ad12K and then lysed in 1% TritonX-100 either on ice or at 37°C. The lysates were pelleted, and the insoluble fraction was resuspended in an equivalent volume of 1% TritonX-100. The soluble and insoluble fractions were analyzed by Western blot probing with streptavidin-HRP. *B*, A549 cells grown on glass coverslips were incubated in the continued presence or absence of chlorpromazine (CPZ), nystatin (NYS), or filipin (FIL) and treated with Ad2 knob. The cells were incubated at 37°C for 0 or 60 minutes, fixed, permeabilized, and probed with rabbit anti-Ad2 knob followed by goat-anti-rabbit-FITC. Coverslips were mounted with ProLong medium containing DAPI stain. Slides were examined under 63X objective of a Zeiss microscope using DAPI and FITC filters. *C*, Ad2 knob bound A549 cell, probed for knob as described in *B* with arrows indicating preferential association with filopodia-like membrane projections.

## **Chapter 6: Materials and Methods II—CAR Prostate Study**

## **1. Materials.**

The affinity purified rabbit polyclonal anti-rat spermine binding protein (SBP) antibodies were generously provided by Drs. Richard Hiipakka and Shutsung Liao of the University of Chicago. Two different affinity-purified goat polyclonal anti-CAR antibodies, designated sc-10313 and sc-10314, were purchased from Santa Cruz Biotechnology, Inc. (Santa Cruz, CA) that were raised against two distinct CAR D1 derived peptides. The kallikrein fluorogenic peptide substrate Pro-Phe-Arg 7-amido-4-methylcoumarin (Pro-Phe-Arg-MCA) was purchased from Sigma-Aldrich Co. (Saint Louis, MO). “ImmunoPure” streptavidin horse radish peroxidase (SA-HRP) conjugate, Sulfo-NHS-LC-biotin, and EZ-link Biotin Quantification Kit were purchased from Pierce (Rockford, IL). Nitrocellulose membrane (Protran BA83, 0.2  $\mu$ m) was purchased from Schleicher and Schuell Bioscience (Keene, NH). E-PAGE MagicMark protein molecular weight standards were purchased from Invitrogen (Carlsbad, CA).

## **2. Recombinant knob domain.**

### **2.1. Constructing the recombinant knob domain.**

Previously, the genetic sequences for the knob domain of human adenovirus serotypes 2 (Ad2) and 12 (Ad12) were amplified by polymerase chain reaction (PCR) and cloned into a pET15b vector between NdeI and XhoI restriction sites. The plasmid constructs designated 3313 (Ad2 knob) and 2580 (Ad12 knob) were separately transformed into the BL21-DE3 strain of bacteria (Invitrogen) by the electroporation method. Transformed bacteria were selected using the ampicillin resistance cassette provided by the pET15b vector. Selected colonies were grown in Luria broth supplemented with penicillin shaking at 37°C for 2 hours, after which 0.4 mM IPTG was added to midlog-phase cultures to trigger overexpression of the encoded knob domains. Cells were pelleted at 6000 rpm at 4°C and the bacterial cell pellets were lysed in BugBuster™ (Invitrogen) reagent supplemented with lysozyme and benzonase™ (Invitrogen). Lysates were centrifuged at 12000 rpm at 4°C for 20 minutes. The recovered supernatant was purified by anion exchange chromatography using a DEAE-cellulose column followed by affinity chromatography using a Ni-NTA column.

### **2.2. Biotinylation of the recombinant knob domain.**

Sulfo-NHS-LC-biotin (Pierce) was diluted to 1 mg/mL in PBS, and mixed with 1mg/mL dilution of Ad2K or Ad12K. The mixture was tumbled at room temperature for 1 hour. Subsequently, the reaction was quenched by adding 15  $\mu$ L of 1 M ammonium chloride (NH<sub>4</sub>Cl) and tumbling at room temperature for an additional 30 minutes. Excess biotin was removed by dialysis of the biotin-knob solutions overnight at 4°C against 10 mM phosphate buffer. The following day the degree of biotin-labeling was evaluated using the EZ-link HABA quantification assay (Pierce), a colorimetric assay that measures the positive correlation in color change of the HABA dye from orange to yellow in response to the concentration of biotin.

## **3. Animal studies.**

### **3.1. Swiss-Webster mice.**

Male Swiss-Webster mice were purchased from Jackson Laboratories (Maine). In accordance with the Brookhaven National Laboratory Institutional Animal Care and Use Committee protocols (Upton, NY), mice were injected (tail-vein) with 5-20  $\mu\text{g}$  of biotinylated knob protein in 0.1 mL of PBS. Mice were then euthanized in CO<sub>2</sub> atmosphere in triplicate sets at 10, 60, and 180 minutes post-injection. Specific organs were dissected, washed in Hanks balanced salt solution, snap frozen in liquid nitrogen, and stored for later analysis at -60°C.

### **3.2. Preparation of tissue lysates.**

Frozen tissue was thinly sliced with a razor blade in a Petri-dish, and then solubilized in RIPA buffer (1X PBS, 1% Nonidet-P40, 0.5% sodium deoxycholate, 0.1% SDS) supplemented with a protease inhibitor cocktail (Invitrogen). The mixture was transferred to a glass Dounce homogenizer and homogenized with 3-4 strokes. The homogenate was then transferred to a 1.5 mL eppendorf tube and centrifuged at 12000 x g at 4°C for 30 minutes. The supernatant was transferred to a new 1.5 mL eppendorf tube and centrifuged a second time to remove any residual particulates. The final supernatant is representative of the total tissue lysate.

### **4. Urinary protein analysis.**

Urine samples were diluted 1  $\mu\text{L}$  into 8  $\mu\text{L}$  PBS and 5  $\mu\text{L}$  of Laemmli sample buffer, and boiled. The urine dilutions were analyzed for protein content by SDS-PAGE alongside E-PAGE MagicMark molecular weight standards. In some experiments, boiling or the reducing agent were omitted prior to gel loading. After gel electrophoresis, gels were stained by boiling in coomassie blue solution (0.25% coomassie blue reagent in 8% glacial acetic acid) and subsequently de-stained by boiling in 8% glacial acetic acid.

### **5. Kallikrein fluorescence assay and zymogram.**

Urine samples were diluted 1:320 in enzyme dilution buffer (50 mM Tris-HCl, 100 mM NaCl, 0.4% BSA, pH 8.8), and triplicate 100  $\mu\text{L}$  aliquots were mixed in black, non-binding 96-well plates (Nunc) with 100  $\mu\text{L}$  of 50 mM of the fluorogenic Pro-Phe-Arg-MCA substrate diluted in reaction buffer (50 mM Tris-HCl, 100 mM NaCl, pH 8.8). The fluorescence intensity was measured for 10 cycles at 60 second intervals using a Tecan Ultra 384 plate reader set to excitation and emission wavelengths of 360 and 465 nm, respectively, and manual gain of 25. Linear regression analysis showed the increase in fluorescence was linear for all samples over a period of analysis. Microsoft Excel was used for analysis and plots. For zymogram analysis, 1  $\mu\text{L}$  urine samples were diluted in Laemmli sample buffer without reducing agent, and were loaded onto a SDS-polyacrylamide gel without prior boiling. After gel electrophoresis, the gel was incubated for 30 minutes in 2.5% Triton X-100, rinsed briefly in distilled water, and then incubated for 10 minutes in 50  $\mu\text{M}$  Pro-Phe-Arg-MCA substrate dissolved in the reaction buffer. The gel was then briefly de-stained with distilled water and imaged by long wavelength UV trans-illumination.

### **6. Western blot analysis.**

Of the total tissue lysate, 5  $\mu$ L was diluted with 5  $\mu$ L of distilled water and 5  $\mu$ L of 3X Laemmli sample buffer (72); and then boiled for 10 minutes. The lysate was separated on a 12% SDS-PAGE gel and then electro-blotted onto nitrocellulose by semi-dry blotting rig (CBS Scientific, Del Mar, CA) using the discontinuous Tris-CAPS buffer method described by BioRad (Hercules, CA). The nitrocellulose membrane was blocked in 3% solution of bovine serum albumin (BSA) in PBS-T for 30 minutes at room temperature, and then probed with SA-HRP or specified primary antibody HRP conjugates for 60 minutes at room temperature. The blot was washed successively in PBS-T, and reacted with West-Dura chemiluminescent reagent (Amersham Biosciences). X-ray film was exposed to the blot for various durations, developed, and fixed.

#### **7. Mass spectrometry and protein identification.**

Proteins in isolated bands excised from SDS-polyacrylamide gels stained with coomassie blue were identified by LC MS/MS analysis at the Keck Mass Spectrometry Facility at Yale University Medical School (New Haven, CT). Briefly, gel slices were washed sequentially in 50% acetonitrile/50% water; 50% acetonitrile/50 mM ammonium bicarbonate; and 50% acetonitrile/10 mM ammonium bicarbonate for 1 hour, and then were vacuum dried. The dried gel slices were re-hydrated with an equal volume of 6.7  $\mu$ g/mL trypsin and digested at 37°C for 18 hours. Using a Waters Q-ToF mass spectrometer, HPLC-purified peptides were subjected to MS/MS analysis. The “MASCOT” search algorithm ([www.matrixscience.com](http://www.matrixscience.com)) was used to correlate the sequences of tryptic peptide masses to known proteins in the mouse proteome.

## **Chapter 7: Results II—CAR Prostate Study**

In the course of our analysis of knob-CAR interaction *in vivo* described above in chapter 4, we made the unexpected observation that many animals that were injected with 20  $\mu\text{g}$  of knob protein in 0.1 mL of PBS exhibited lethargic behavior. Upon dissection many of the mice had unusually large bladder volumes. Urine was collected from these mice as well as from mice that were injected with PBS alone as negative controls. Analyses of the protein content of urine samples by SDS-PAGE revealed an apparent knob-induced selective proteinuria, where two proteins migrating at 28 kDa and 6 kDa were found at elevated levels. In our experiments we sought to answer the following two questions. First, what are the identities of the 28 kDa and 6 kDa proteins that are observed at elevated levels in the urine of mice injected with knob protein? How does the knob protein stimulate the appearance of these two proteins in the urine?

### **1. Large bladder volumes.**

As described in Results I, recombinant knob domain derived from CAR-binding Ad serotypes was expressed, purified, and labeled with biotin (see Materials and Methods I, section 3). The knob protein was injected in the tail-vein of male Swiss-Webster mice. It was reported that approximately 3  $\mu\text{g}$  of knob protein was sufficient to saturate all available CAR binding sites in the liver (66). To exceed this level, mice were injected with 5-20  $\mu\text{g}$  of knob protein in 100  $\mu\text{L}$  total of PBS. Several of mice exhibited lethargic behavior approximately 1 hour after injection. When dissected, these animals were found to have unusually large bladder volumes (chapter 6, figure 1). Urine samples were collected from both knob-injected mice and PBS-injected controls. Additionally, kidney, and in later experiments the prostate gland were dissected, washed, and frozen for later analysis.

### **2. Urinary protein analysis.**

#### **2.1. Protein gel electrophoresis.**

The collected urine samples were analyzed by gel electrophoresis to assess protein content. The 20 kDa major urinary protein-1 (MUP-1), a normal constituent of rodent urine (102), was detected in all knob-injected and PBS-injected control samples. However, in addition to MUP-1, two unknown proteins with molecular weights of approximately 28 kDa and 6 kDa were frequently observed in about half the mice injected with recombinant knob protein (chapter 6, figure 2A). Furthermore, 10 of 11 urine samples containing high concentration of the unidentified 28 kDa and 6 kDa proteins came from animals that had large bladder volumes. By contrast, all of the urine samples where little or no 28 kDa or 6 kDa was observed came from mice that had normal, small bladder volumes, suggesting a correlation between the appearance of these proteins and abnormally large bladder volume.

The biochemical properties of the 28 kDa and 6 kDa proteins were examined in an effort to determine their identity. We looked for an effect of reduction of disulfide bonds and heat denaturation on the electrophoretic mobilities of these proteins (chapter 6, figure 2B). First, it was observed that when DTT was omitted, MUP-1 produced a faster-migrating band, indicative

of an internal disulfide bond which has been reported for MUP-1 (102). The absence of DTT retarded the migration of the 6 kDa protein slightly, but had a considerable effect on the 28 kDa protein whose mobility was slowed to produce a 55 kDa band. Omitting heat denaturation had the same effect on the 28 kDa protein, but did not affect the 6 kDa protein. The similar effect of both heat denaturation and DTT treatment suggests that the 28 kDa protein may exist as a dimer, where the two monomers are linked via a disulfide bond. The slowed mobility of 6 kDa by omission of DTT implies that the molecule may contain an internal disulfide bond.

## **2.2. Knob assessment.**

The heat stability of the putative 28 kDa protein dimer was reminiscent of knob trimers, which are resistant to dissociation in SDS at temperature below 50°C (103). Assembled knob trimers migrate in SDS gels with an apparent molecular weight of ~ 60 kDa. However, unlike the 28 kDa protein, knob trimers do not have inter-subunit disulfide bonds nor do the subunits contain internal disulfide bonds (104). Urine samples were examined on Western blots with a SA-HRP probe to directly determine if the 28 kDa protein was related to biotinylated knob. The SA-HRP probe failed to detect any biotinylated knob protein in the sample, thus confirming that the 28 kDa protein and knob were unrelated. Ponceau-S staining of the immunoblot membrane confirmed that the 28 kDa protein was present at high concentration in most samples (chapter 6, figure 3B).

## **2.3. Kallikrein assessment.**

We also examined the possibility that the 28 kDa protein was urinary kallikrein is a ~ 30 kDa protease that liberates kinin by proteolysis of the kininogen precursor (105). Kinin peptide has been reported to participate in the regulation of both blood pressure and tissue inflammation (106,107). Examination of urine from knob-injected and PBS-injected mice revealed no significant difference in the level of kallikrein activity as determined in a protease assay using a fluorogenic substrate. These findings were corroborated by the different electrophoretic mobilities observed for the 28 kDa protein and kallikrein on a zymogram.

## **2.4. CAR assessment.**

Several studies have described soluble forms of CAR that can be generated by alternative splicing or proteolytic cleavage by sheddases (15,16,108), which might correspond to the 28 kDa and/or the 6 kDa protein detected in mouse urine samples. However, two different anti-CAR antibodies failed to react with any proteins in any urine samples on Western blots, thus eliminating CAR as the source of the 28 kDa and 6 kDa proteins.

# **3. Identification of SBP and P12.**

## **3.1. Mass spectrometry analysis.**

LC MS/MS analysis was employed to directly determine the identities of the 28 kDa and 6 kDa bands observed at elevated levels in the urine sample from knob-injected mice. The amino acid sequences of tryptic peptides generated from gel-purified 28 kDa and 6 kDa proteins were determined, and

were used to query the mouse protein database. This analysis identified the 28 kDa protein as the spermine binding protein (SBP) and the 6 kDa protein as the Kazal-type protease inhibitor P12. Previous publications described both proteins as products of the ventral lobe of the mouse prostate gland, which normally are secreted into seminal fluid (109,110). Antibodies specific for the rat homologue of SBP were used to corroborate the results from the mass spec analysis (111). We were confident that the rat anti-SBP IgG would cross-react with the mouse SBP given the high level of sequence similarity between the two homologues. Indeed, the anti rat SBP strongly reacted with the 28 kDa band on blots where Ponceau-S staining had confirmed its presence at high concentrations. At the time of these studies, no antibodies against the P12 Kazal-type protease inhibitor were available to corroborate the mass spec results. We are confident in the identification of the 28 kDa protein as SBP given the reinforcement of the mass spec results by the confirmed Western blot detection.

### **3.2. Western blot analysis with anti-spermine binding protein.**

Having established that the anti rat SBP cross-reacts with mouse SBP in the recovered urine samples, additional urine samples were analyzed by Western blot analysis with anti-SBP (111). In about half of the urine samples obtained from PBS-injected mice, SBP also was detected though the relative signal intensity was low when compared to knob-injected samples. Indeed, blots of urine from the majority of knob-injected mice exhibited high concentrations of SBP. Urine samples were also collected from mice injected with P417E/P418A, an Ad12 knob mutant with specific amino acid substitutions in the CAR binding site have lowered its affinity for CAR relative to wild-type Ad12 knob. Of these samples, only 1 exhibited high levels of SBP on a Western blot. Table II contains the summary of these Western blot analyses. The accumulated results suggested that the secretion of high levels of SBP into the urine was triggered by IV administration of knob protein. It is interesting to note that knob proteins derived from Ad serotypes 5 and 12 was considerably more effective at stimulating secretion of SBP into the urine than knob derived from Ad serotype 2.

### **4. Phosphate enhances knob effect.**

Knob proteins in the analysis described above were diluted in PBS. The specific constituents of this PBS solution were 2.7 mM KCl, 9.2 mM phosphate buffer, and 138 mM NaCl (Dulbecco's recipe). We wanted to ascertain if any of these components of the diluent contributed to the secretion of SBP and P12 into the mouse urine. To that end, animal experiments were repeated where knob protein diluted in normal saline solution (0.9% NaCl) alone was injected into mice. The urine collected from these animals was analyzed by SDS-PAGE as described above. To our surprise, very little SBP was observed in the urine of knob-injected mice relative to the saline injected controls. Similar results were obtained when knob was diluted in saline containing 2.7 mM KCl, where there was no detectable difference in the SBP and P12 secretion relative to controls. However, knob diluted in 9.2 mM phosphate buffer in normal saline stimulated

secretion of high levels of both SBP and P12 into mouse urine, while diluent-injected control mice exhibited little secretion of SBP or P12. Based on these findings, we concluded both knob and phosphate acted synergistically to stimulate the secretion of SBP and P12 from the ventral lobe of the mouse prostate.

## 5. Figures and Tables.

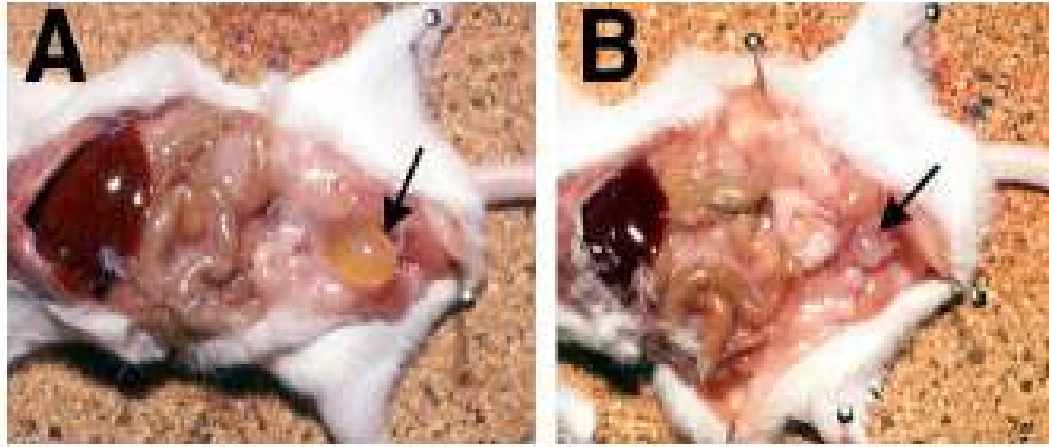


**Figure 1. Increased bladder volume in knob-injected mice.** *A*, male Swiss-Webster mouse 60 minutes after IV injection (tail vein) of biotinylated Ad12 knob protein (10  $\mu$ g protein in 100  $\mu$ L PBS). *B*, control male Swiss-Webster mouse 60 minutes post-injection of 100  $\mu$ L PBS. Bladders are indicated by arrows.

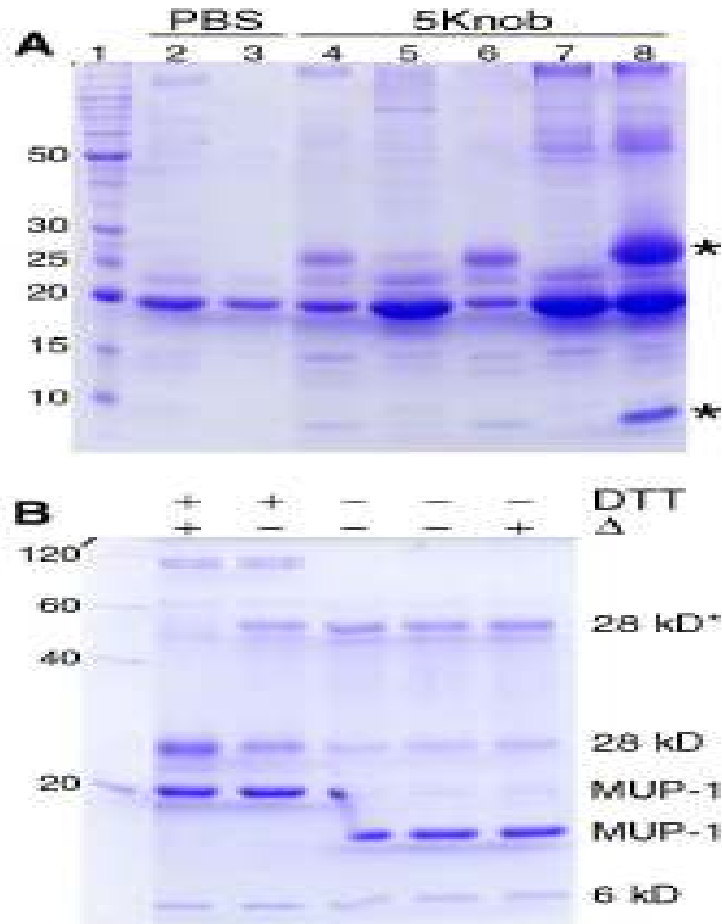


**Figure 2. Appearance of novel proteins in urine of knob-injected mice.** *A*, SDS-PAGE of urine (2  $\mu$ L per sample) from male Swiss-Webster mice injected with either 100  $\mu$ L PBS (lanes 2 and 3) or 10  $\mu$ g of biotinylated Ad5 knob protein in 100  $\mu$ L PBS (lanes 4-8). Novel proteins of  $\sim$  28 kDa and  $\sim$  6 kDa that appeared in knob-injected urine samples are indicated with an asterisk (\*). *B*, replicates of a urine sample that contained 28 kDa and 6 kDa proteins were mixed (2  $\mu$ L each) with reducing or non-reducing SDS-PAGE sample buffer (+, -DTT, respectively) and incubated at 100°C or at room temperature for 3 minutes (+, - $\Delta$ , respectively) before loading on the gel. Omitting either heat treatment or reducing agent decreased the mobility of the 28 kDa protein, as indicated (28 kDa\*), while omitting reducing agent increased the mobility of the 20 kDa major urinary protein (MUP-1) as indicated (MUP-1\*). The apparent molecular weights of protein standards (in kDa) loaded in the first lane of each gel are indicated. Proteins in both gels were visualized by staining with coomassie blue.

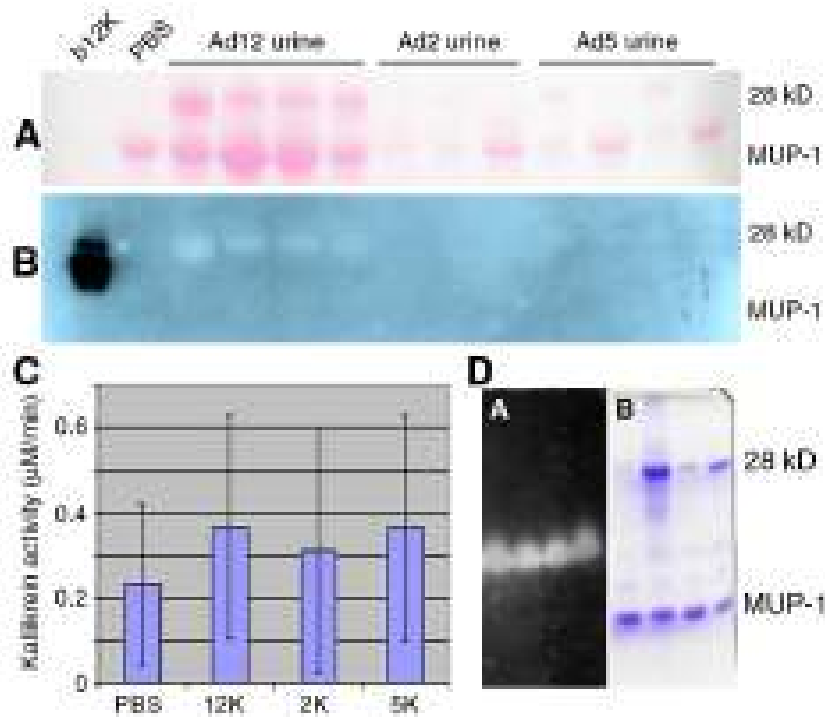


**Figure 3. The novel 28 kDa protein is not related to knob or kallikrein.** *A*, Ponceau-S stained PVDF membrane after transfer of proteins from an SDS gel of urine samples (2  $\mu$ L each) from male Swiss-Webster mice injected with PBS or with biotinylated Ad12, Ad2, or Ad5 knob proteins (as indicated); or with a control sample of biotinylated Ad12 knob protein (b12K). The positions of the MUP-1 and 28 kDa proteins are indicated. *B*, autoradiogram of the same PVDF membrane shown in *A* after probing with streptavidin-HRP and chemiluminescent visualization. *C*, hydrolytic activity of urine samples against the fluorogenic substrate Pro-Phe-Arg-MCA, which typically is used to assay the 28 kDa kallikrein protease. *D*, panel A: zymogram of urine samples (unheated and unreduced) after electrophoresis on SDS-PAGE. The gel was incubated with the fluorogenic substrate indicated in *C*, and then photographed under long wave UV light. *D*, panel B: same gel shown in panel A, after staining with coomassie blue. The positions of MUP-1 and the 28 kDa protein are indicated.

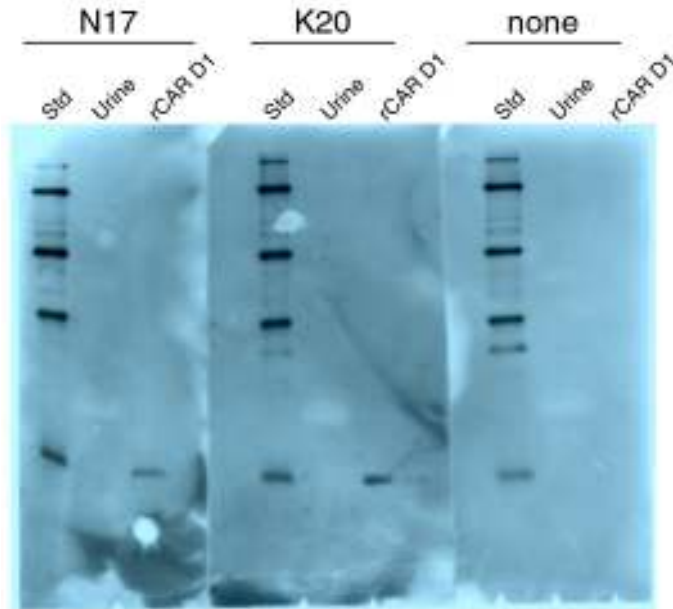


**Figure 4. CAR fragments are not detected in mouse urine.** Urine collected from knob-injected mice was analyzed by Western blot probing with two different affinity-purified goat polyclonal anti-CAR antibodies, designated N17 (left panel) and K20 (middle panel). Recombinant rat CAR D1 domain was analyzed alongside the urine samples as a positive control for antibody reactivity. Blots were also probed with secondary antibody alone as a negative control (right panel). *Std* represents the E-PAGE MagicMark (Invitrogen) molecular weight standard.

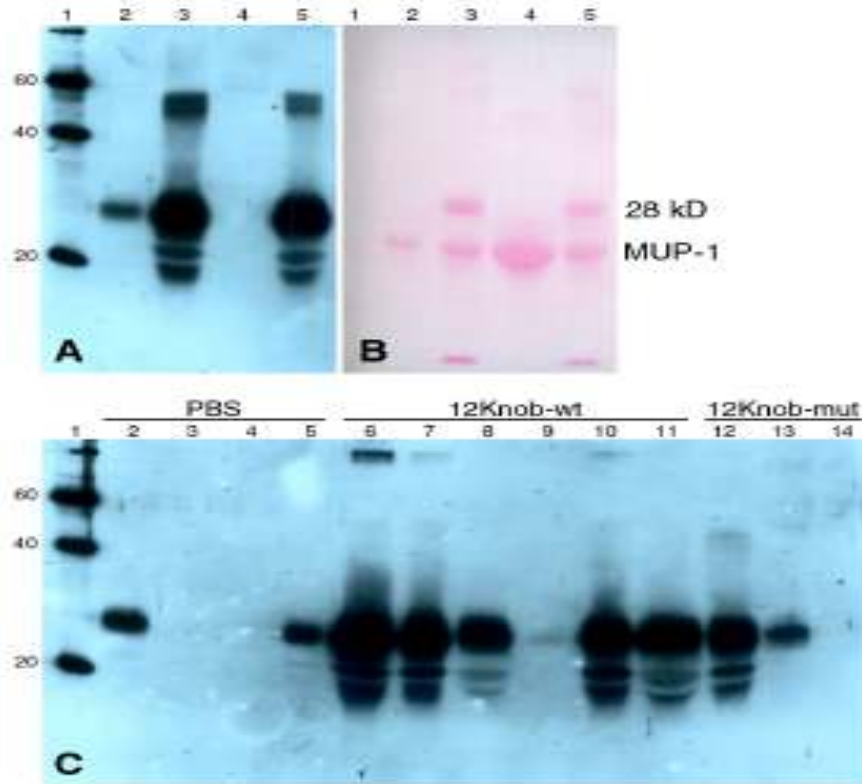


**Figure 5. The 28 kDa protein reacts with antibodies specific for rat spermine binding protein.** *A*, Western blot analysis of urine proteins probed with rabbit antibodies specific for rat spermine binding protein. *B*, same PVDF membrane that was used for autoradiogram in *A*, stained with Ponceau-S. The positions of the 28 kDa and MUP-1 proteins are indicated. *C*, Western blot analysis of urine samples from male Swiss-Webster mice injected with either 100  $\mu$ L PBS (lanes 2-5), biotinylated wild-type Ad12 knob protein (lanes 6-11), or with biotinylated mutant Ad12 knob P417E/P418A protein that has decreased binding affinity for CAR, the coxsackie and adenovirus receptor. The blot was probed with rabbit antibodies specific for the rat spermine binding protein.

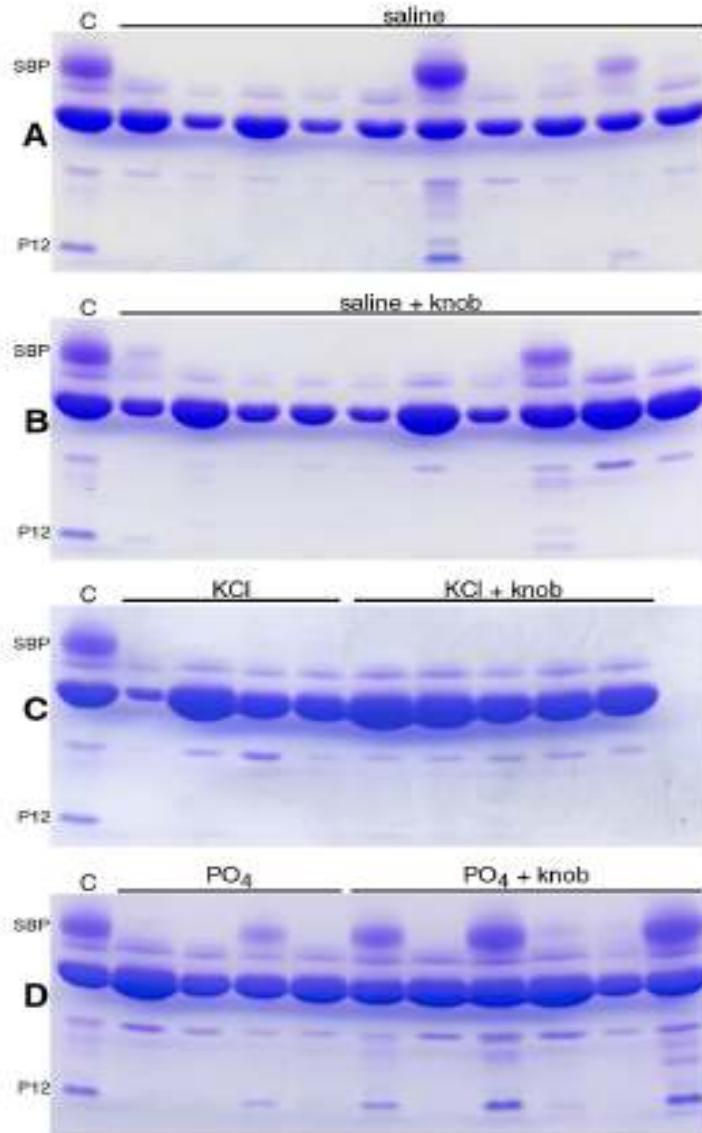


**Figure 6. Knob protein and phosphate buffer synergistically promote secretion of spermine binding protein and P12.** *A* and *B*, SDS-PAGE of urine samples from mice injected with 100  $\mu$ L normal saline (panel *A*) or with 20  $\mu$ g Ad12 knob protein in 100  $\mu$ L of normal saline. *C*, SDS-PAGE of urine samples from mice injected with 100  $\mu$ L saline containing 2.7 mM KCl, or with 20  $\mu$ g Ad12 knob protein in 100  $\mu$ L saline containing 2.7 mM KCl. *D*, SDS-PAGE of urine samples from mice injected with 100  $\mu$ L saline containing 9.2 mM phosphate buffer or with 20  $\mu$ g Ad12 knob protein in 100  $\mu$ L saline containing 9.2 mM phosphate buffer. The knob protein that was used in all experiments shown in this figure was not labeled with biotin.

Table I. Protein ID from mass spectrometry analysis of tryptic peptides.

Sample <sup>1</sup>	ID (accession)	# peptides matched	MOWSE score <sup>2</sup>
28 kD	SBP (6755402)	4 <sup>3</sup>	192
6 kD	p12 (6678105)	2 <sup>4</sup>	60

<sup>1</sup> protein bands were excised from a coomassie blue-stained polyacrylamide gel and digested with trypsin. Sequences of peptides isolated by HPLC were then determined by MS/MS analysis

<sup>2</sup> proteins in the mouse protein database that contain the observed tryptic peptides were identified using the MASCOT search algorithm ([www.matrixscience.com](http://www.matrixscience.com)). MOWSE scores >49 are considered significant (probability of random match <3 per 10e6).

<sup>3</sup> sequences of matching tryptic peptides: YFSDTGGSDK, DADNKDADNK, YFYVQGEDQGQLK, DDGDEDDDGNDDDDDQKDES.

<sup>4</sup> sequences of matching tryptic peptides: RIEPVLIR, EASCHDAVAGCPR.

Table II. Spermine binding protein concentration in urine from knob-injected<sup>1</sup> and control mice.

SBP concentration <sup>2</sup>	Ad12 knob <sup>3</sup>	Ad5 knob <sup>3</sup>	Ad2 knob <sup>3</sup>	PBS <sup>3</sup>
High	18 (72%)	9 (56%)	1 (20%)	0
Low	4 (16%)	5 (31%)	1 (20%)	2 (50%)
ND <sup>3</sup>	3 (12%)	2 (13%)	3 (60%)	2 (50%)

<sup>1</sup> all knob protein injections were delivered in 100  $\mu$ L of PBS.

<sup>2</sup> relative SBP concentrations were determined on Western blots by comparison to concentration standards similar to lanes 2 and 3 of Figure 4A.

<sup>3</sup> not detectable.

Table III. Knob and phosphate together promote prostatic secretion.

Treatment	number of mice (total)	number SBP positive <sup>1</sup>	% SBP positive
saline	9	2	22
saline + 12K	10	2	20
KCl <sup>2</sup>	4	0	0
KCl + 12K	5	0	0
PO <sub>4</sub> <sup>3</sup>	4	1	25
PO <sub>4</sub> + 12K	5	4	80

<sup>1</sup> positive samples contained SBP and P12 at levels detectable by coomassie blue-staining.

<sup>2</sup> saline (0.9% NaCl) containing 2.7 mM KCl.

<sup>3</sup> saline containing 9.2 mM phosphate buffer.

## **Chapter 8: Discussion II—CAR Prostate Study**

Contrasting the results we have presented of a novel endocytic phenotype for CAR in hepatocytes, the *in vivo* data we have collected in the context of prostate epithelium reinforces the traditional model of CAR acting as an intercellular adhesion molecule. When we administered knob protein at concentrations in excess of the saturation level for available CAR binding sites in the liver (3  $\mu$ g) (72), the knob ligand potentially could interact with CAR localized to other tissues in the mouse. Many of these animals exhibited lethargic behavior, which was unexpected. Upon dissection, we discovered that many of the knob-injected mice had unusually large bladder volumes.

We first analyzed the urine for possible proteinuria induced by knob injection. With the exception of MUP-1 (102), protein concentrations in urine of male mice are very low, usually undetectable by coomassie blue staining. However, two unknown proteins migrating at approximately 28 kDa and 6 kDa were present at high concentration in the urine of many knob-injected mice. A variety of biochemical analyses were conducted to determine the identities of these proteins, including an examination of the effect of omitting heat denaturation or reducing agents on electrophoretic mobility. Western blot analyses determined that the two proteins were neither knob nor proteolytically shed fragments of CAR (108). We had also considered that the 28 kDa protein might be urinary kallikrein, a  $\sim$  30 kDa protease that potentially could increase urine volume through release of kinin, a peptide with diuretic properties (105). Two different assays utilizing an artificial kallikrein substrate demonstrated that the 28 kDa protein was not urinary kallikrein. Ultimately, by mass spectrometry the 28 kDa and 6 kDa proteins were identified as the mouse spermine binding protein (SBP) and the Kazal-type protease inhibitor P12, respectively (109,110). The identity of 28 kDa protein as SBP was corroborated by Western blot analysis of mouse urine with rabbit anti-rat SBP antibodies.

Given the distended bladders, we had initially believed that knob was exerting this effect at the level of the kidney, where it is known that CAR is expressed within the adherens junction of glomerular podocytes (112). Indeed, we were able to detect biotinylated knob in kidney tissue lysates. However, identification of the 28 kDa and 6 kDa proteins as SBP and P12 indicated that knob was in some way triggering secretion of prostatic proteins. This was not entirely unexpected given the relatively high levels of CAR expression in prostate epithelium (chapter 1, figure 3) (65). More specifically, SBP and P12 are reported to be produced solely in the ventral lobe of the mouse prostate (109,110). As described in the Introduction section 3, CAR down-regulation is coincident with cancer progression in many tissues including the prostate (61-63,113). Intriguingly, when prostate tumors are experimentally-induced in mice, the tumors rarely are derived from the ventral lobe epithelium (114). This suggests that CAR expression may be higher in the ventral lobe epithelium relative to other lobes of the mouse prostate. Additionally, the secretion of these proteins into the urine occurred rapidly after injection of knob protein, indicating that CAR in the prostate is readily accessible to the knob ligand. This is consistent with

histochemical analysis indicating high concentration of CAR on basal and apical surfaces as well as in lateral tight junction region (65).

Within the context of the polarized epithelium of lung tissue, CAR has been detected in the adherens junction, where it has been described to mediate homotypic contacts through the D1 domains of CAR expressed on adjacent cells (36,39,59). These homophilic interactions have been experimentally demonstrated to contribute to the blockage of ions and other solutes through the paracellular space. Indeed, trans-epithelial resistance was considerably reduced when knob protein was applied to the basal surface of polarized lung epithelium (36,60). It has been inferred that the Ad-derived knob protein, which exhibits ~1000-fold higher affinity for CAR than the homophilic interaction of CAR D1 domains (39,51), competitively reduces CAR homotypic contacts resulting in an increased flux of ions and solutes through the paracellular space. This potentially explains the impact of CAR binding in the prostate epithelium, as a previous study reported that the experimentally-induced prostatic secretion in dogs was accompanied by the paracellular flux of sodium ions (115). However, the mechanism for the increase in ion flow through paracellular space of prostate epithelium has yet to be described.

Notably, the Ad5 and Ad12 knob proteins were considerably more effective at stimulating the release of SBP and P12 into the urine than the Ad2 knob. While fluorescence anisotropy experiments have calculated relatively CAR binding affinities for all three knob serotypes, they also exhibit a variety of differences in relative trimer stability, isoelectric point, amino acid sequence, and surface-exposed hydrophobic patches (50,51,96). Within the *in vivo* context, many of these factors could contribute to the inability of Ad2 knob to stimulate SBP and P12 release into the mouse urine. The substituted amino acids reside in a region critical to knob-CAR interaction, which was found to considerably reduce CAR affinity (27,50). However, cell binding assays (chapter 3, figure 1) have indicated that the mutant Ad12 knob retains some CAR affinity, which may be sufficient to trigger secretion, in light of the relatively weak affinity demonstrated for dimers of recombinant CAR D1 (39,50).

We also demonstrated that the presence of 9.2 mM phosphate buffer enhances the amount of SBP and P12 released into the mouse urine, but only in the presence of either Ad5 or Ad12 knob. This finding suggests that knob and phosphate work in concert to affect the secretion of these proteins from the ventral lobe. It has been demonstrated that the IV administration of phosphate results in precipitation of free calcium in the bloodstream causing an acute hypocalcaemia (116). Notably, free calcium is required to maintain homophilic interactions between E-cadherins, which like CAR are expressed in prostate epithelium and contribute to intercellular adhesion in the adherens junction (117-120). Thus, we hypothesize that the disruption of the paracellular permeability barrier in prostate epithelium requires disruptions of homophilic interactions between both CAR and E-cadherins. This is in contrast to cell culture models where knob alone was capable of opening the paracellular space between cells by disrupting CAR-CAR homotypic contacts. Potentially, the integrity of the

epithelium *in vivo* may be fortified by additional factors that are not reproduced in the cell culture model such as interactions with smooth muscle, stroma, and extracellular matrix. In absence of phosphate buffer, knob may be able to compromise the permeability barrier of the prostate epithelium, but not to a level sufficient to stimulate the secretion of SBP and P12.

Taken together, our results suggest that IV injected knob protein in concert with phosphate buffer rapidly decrease intercellular adhesion mediated by both CAR and E-cadherins in the ventral lobe prostate epithelium. The resulting disruption in the ion gradient normally maintained by the paracellular permeability barrier stimulates the secretion of the SBP and P12 proteins into the urine. The enlarged bladders suggest that secretion of additional prostatic proteins occurs, specifically clotting agents known to be present in rodent seminal fluid that coagulate to form a copulatory plug in the vaginal cavity (121). These so-called semenoclotin proteins are expressed in and secreted by the seminal vesicle, suggesting that knob and phosphate together may stimulate secretion from that organ as well. The fact that semenoclotin proteins were not observed in urine in our experiments is consistent with the insolubility of these proteins. In our experiments, urine samples were clarified by centrifugation before analysis, which likely would remove any residual semenoclotin proteins from the supernatant fraction. The experimentally-induced formation of such a plug in the urethra would effectively prevent the passage of urine, which would explain the large bladder volumes observed in mice.

### **Future Directions.**

Here, we have provided *in vivo* evidence of CAR functioning in a capacity similar to that observed in cell culture models, where CAR contributes to the maintenance of intercellular adhesion between polarized epithelial cells. We have hypothesized from the presented data that disruption of CAR-CAR homotypic contacts by knob protein in prostate epithelium, increases paracellular permeability of the prostate epithelium, thus stimulating the release of specific proteins into the mouse urine. Our efforts to directly detect biotinylated knob protein in prostate tissue lysates were not successful; however, the Western blot technique may lack sufficient sensitivity, considering the small size of the prostate and consequently the much smaller total number of CAR receptors in comparison to the liver, where knob is readily detected by this method. In future studies, we intend to confirm that the knob protein is present in the prostate after tail-vein injection into mice, and will likely have to develop a more sensitive assay with which to detect knob in the small amount of prostate tissue that can be dissected from mice, possibly using radio-labeled protein. Additionally, we will use co-immunoprecipitation to demonstrate that knob binds CAR in the prostate. We will also need to confirm that the effect of phosphate is the result of disruption of E-cadherin connections in the prostate. Parallel studies in primary prostate cell cultures and prostate-derived cell lines also could be informative in regard to the potential synergistic effects of CAR and E-cadherins on cell adhesion.

In the context of both liver and prostate epithelia, knob protein is able to readily access CAR after IV injection. This implies that the knob trimer could be potentially useful for the detection and imaging of CAR in these and other tissues. A knob-based agent for imaging and therapy of prostate tumors is an attractive potential application of this research; however, as noted earlier, CAR expression is down-regulated in prostate tumors which might lessen its utility as a target for such treatments.

## References

1. Chretien, I., Marcuz, A., Courtet, M., Katevuo, K., Vainio, O., Heath, J. K., White, S. J., and Du Pasquier, L. (1998) *Eur J Immunol* **28**, 4094-4104
2. Fechner, H., Haack, A., Wang, H., Wang, X., Eizema, K., Pauschinger, M., Schoemaker, R., Veghel, R., Houtsmuller, A., Schultheiss, H. P., Lamers, J., and Poller, W. (1999) *Gene Ther* **6**, 1520-1535
3. Bergelson, J. M., Krithivas, A., Celi, L., Droguett, G., Horwitz, M. S., Wickham, T., Crowell, R. L., and Finberg, R. W. (1998) *J Virol* **72**, 415-419
4. Carson, S. D. (2001) *Rev Med Virol* **11**, 219-226
5. Bergelson, J. M., Cunningham, J. A., Droguett, G., Kurt-Jones, E. A., Krithivas, A., Hong, J. S., Horwitz, M. S., Crowell, R. L., and Finberg, R. W. (1997) *Science* **275**, 1320-1323
6. Roelvink, P. W., Lizonova, A., Lee, J. G., Li, Y., Bergelson, J. M., Finberg, R. W., Brough, D. E., Kovesdi, I., and Wickham, T. J. (1998) *J Virol* **72**, 7909-7915
7. Asher, D. R., Cerny, A. M., Weiler, S. R., Horner, J. W., Keeler, M. L., Neptune, M. A., Jones, S. N., Bronson, R. T., Depinho, R. A., and Finberg, R. W. (2005) *Genesis* **42**, 77-85
8. Dorner, A. A., Wegmann, F., Butz, S., Wolburg-Buchholz, K., Wolburg, H., Mack, A., Nasdala, I., August, B., Westermann, J., Rathjen, F. G., and Vestweber, D. (2005) *J Cell Sci* **118**, 3509-3521
9. Kashimura, T., Kodama, M., Hotta, Y., Hosoya, J., Yoshida, K., Ozawa, T., Watanabe, R., Okura, Y., Kato, K., Hanawa, H., Kuwano, R., and Aizawa, Y. (2004) *Virchows Arch* **444**, 283-292
10. Chen, J. W., Zhou, B., Yu, Q. C., Shin, S. J., Jiao, K., Schneider, M. D., Baldwin, H. S., and Bergelson, J. M. (2006) *Circ Res* **98**, 923-930
11. Tomko, R. P., Xu, R., and Philipson, L. (1997) *Proc Natl Acad Sci U S A* **94**, 3352-3356
12. Tomko, R. P., Johansson, C. B., Totrov, M., Abagyan, R., Frisen, J., and Philipson, L. (2000) *Exp Cell Res* **255**, 47-55
13. Chen, J. W., Ghosh, R., Finberg, R. W., and Bergelson, J. M. (2003) *DNA Cell Biol* **22**, 253-259

14. Mayr, G. A., and Freimuth, P. (1997) *J Virol* **71**, 412-418
15. Dorner, A., Xiong, D., Couch, K., Yajima, T., and Knowlton, K. U. (2004) *J Biol Chem* **279**, 18497-18503
16. Thoelen, I., Magnusson, C., Tagerud, S., Polacek, C., Lindberg, M., and Van Ranst, M. (2001) *Biochem Biophys Res Commun* **287**, 216-222
17. Yanagawa, B., Spiller, O. B., Proctor, D. G., Choy, J., Luo, H., Zhang, H. M., Suarez, A., Yang, D., and McManus, B. M. (2004) *J Infect Dis* **189**, 1431-1439
18. Dorner, A., Grunert, H. P., Lindig, V., Chandrasekharan, K., Fechner, H., Knowlton, K. U., Isik, A., Pauschinger, M., Zeichhardt, H., and Schultheiss, H. P. (2006) *J Mol Med* **84**, 842-851
19. Goodfellow, I. G., Evans, D. J., Blom, A. M., Kerrigan, D., Miners, J. S., Morgan, B. P., and Spiller, O. B. (2005) *J Virol* **79**, 12016-12024
20. Pong, R. C., Lai, Y. J., Chen, H., Okegawa, T., Frenkel, E., Sagalowsky, A., and Hsieh, J. T. (2003) *Cancer Res* **63**, 8680-8686
21. Solecki, D., Gromeier, M., Harber, J., Bernhardt, G., and Wimmer, E. (1998) *J Mol Recognit* **11**, 2-9
22. Mendelsohn, C. L., Wimmer, E., and Racaniello, V. R. (1989) *Cell* **56**, 855-865
23. Bella, J., and Rossmann, M. G. (1999) *J Struct Biol* **128**, 69-74
24. Campbell, J. A., Schelling, P., Wetzell, J. D., Johnson, E. M., Forrest, J. C., Wilson, G. A., Aurrand-Lions, M., Imhof, B. A., Stehle, T., and Dermody, T. S. (2005) *J Virol* **79**, 7967-7978
25. Prota, A. E., Campbell, J. A., Schelling, P., Forrest, J. C., Watson, M. J., Peters, T. R., Aurrand-Lions, M., Imhof, B. A., Dermody, T. S., and Stehle, T. (2003) *Proc Natl Acad Sci U S A* **100**, 5366-5371
26. Stehle, T., and Dermody, T. S. (2004) *Viral Immunol* **17**, 129-143
27. Bewley, M. C., Springer, K., Zhang, Y. B., Freimuth, P., and Flanagan, J. M. (1999) *Science* **286**, 1579-1583

28. Walters, R. W., van't Hof, W., Yi, S. M., Schroth, M. K., Zabner, J., Crystal, R. G., and Welsh, M. J. (2001) *J Virol* **75**, 7703-7711
29. Excoffon, K. J., Traver, G. L., and Zabner, J. (2005) *Am J Respir Cell Mol Biol* **32**, 498-503
30. Cohen, C. J., Gaetz, J., Ohman, T., and Bergelson, J. M. (2001) *J Biol Chem* **276**, 25392-25398
31. van't Hof, W., and Crystal, R. G. (2002) *J Virol* **76**, 6382-6386
32. Jelen, F., Oleksy, A., Smietana, K., and Otlewski, J. (2003) *Acta Biochim Pol* **50**, 985-1017
33. Fanning, A. S., and Anderson, J. M. (1999) *J Clin Invest* **103**, 767-772
34. Coyne, C. B., Voelker, T., Pichla, S. L., and Bergelson, J. M. (2004) *J Biol Chem* **279**, 48079-48084
35. Excoffon, K. J., Hruska-Hageman, A., Klotz, M., Traver, G. L., and Zabner, J. (2004) *J Cell Sci* **117**, 4401-4409
36. Cohen, C. J., Shieh, J. T., Pickles, R. J., Okegawa, T., Hsieh, J. T., and Bergelson, J. M. (2001) *Proc Natl Acad Sci U S A* **98**, 15191-15196
37. Sollerbrant, K., Raschperger, E., Mirza, M., Engstrom, U., Philipson, L., Ljungdahl, P. O., and Pettersson, R. F. (2003) *J Biol Chem* **278**, 7439-7444
38. Coyne, C. B., and Bergelson, J. M. (2005) *Adv Drug Deliv Rev* **57**, 869-882
39. van Raaij, M. J., Chouin, E., van der Zandt, H., Bergelson, J. M., and Cusack, S. (2000) *Structure* **8**, 1147-1155
40. Philipson, L., Lonberg-Holm, K., and Pettersson, U. (1968) *J Virol* **2**, 1064-1075
41. Gaggar, A., Shayakhmetov, D. M., Liszewski, M. K., Atkinson, J. P., and Lieber, A. (2005) *J Virol* **79**, 7503-7513
42. Segerman, A., Atkinson, J. P., Marttila, M., Dennerquist, V., Wadell, G., and Arnberg, N. (2003) *J Virol* **77**, 9183-9191
43. Sirena, D., Lilienfeld, B., Eisenhut, M., Kalin, S., Boucke, K., Beerli, R. R., Vogt, L., Ruedl, C., Bachmann, M. F., Greber, U. F., and Hemmi, S. (2004) *J Virol* **78**, 4454-4462

44. Pettersson, U., Philipson, L., and Hoglund, S. (1968) *Virology* **35**, 204-215
45. Dehecchi, M. C., Tamanini, A., Bonizzato, A., and Cabrini, G. (2000) *Virology* **268**, 382-390
46. Dehecchi, M. C., Melotti, P., Bonizzato, A., Santacatterina, M., Chilosi, M., and Cabrini, G. (2001) *J Virol* **75**, 8772-8780
47. Devaux, C., Adrian, M., Berthet-Colominas, C., Cusack, S., and Jacrot, B. (1990) *J Mol Biol* **215**, 567-588
48. Seiradake, E., Lortat-Jacob, H., Billet, O., Kremer, E. J., and Cusack, S. (2006) *J Biol Chem* **281**, 33704-33716
49. Lortat-Jacob, H., Chouin, E., Cusack, S., and van Raaij, M. J. (2001) *J Biol Chem* **276**, 9009-9015
50. Howitt, J., Anderson, C. W., and Freimuth, P. (2003) *Curr Top Microbiol Immunol* **272**, 331-364
51. Howitt, J., Bewley, M. C., Graziano, V., Flanagan, J. M., and Freimuth, P. (2003) *J Biol Chem* **278**, 26208-26215
52. Wickham, T. J., Mathias, P., Cheresch, D. A., and Nemerow, G. R. (1993) *Cell* **73**, 309-319
53. Chiu, C. Y., Mathias, P., Nemerow, G. R., and Stewart, P. L. (1999) *J Virol* **73**, 6759-6768
54. Stewart, P. L., Chiu, C. Y., Huang, S., Muir, T., Zhao, Y., Chait, B., Mathias, P., and Nemerow, G. R. (1997) *Embo J* **16**, 1189-1198
55. Bai, M., Harfe, B., and Freimuth, P. (1993) *J Virol* **67**, 5198-5205
56. Albinsson, B., and Kidd, A. H. (1999) *Virus Res* **64**, 125-136
57. Chillon, M., and Kremer, E. J. (2001) *Hum Gene Ther* **12**, 1815-1823
58. Walters, R. W., Grunst, T., Bergelson, J. M., Finberg, R. W., Welsh, M. J., and Zabner, J. (1999) *J Biol Chem* **274**, 10219-10226
59. Raschperger, E., Thyberg, J., Pettersson, S., Philipson, L., Fuxe, J., and Pettersson, R. F. (2006) *Exp Cell Res* **312**, 1566-1580

60. Walters, R. W., Freimuth, P., Moninger, T. O., Ganske, I., Zabner, J., and Welsh, M. J. (2002) *Cell* **110**, 789-799
61. Okegawa, T., Pong, R. C., Li, Y., Bergelson, J. M., Sagalowsky, A. I., and Hsieh, J. T. (2001) *Cancer Res* **61**, 6592-6600
62. Kim, M., Sumerel, L. A., Belousova, N., Lyons, G. R., Carey, D. E., Krasnykh, V., and Douglas, J. T. (2003) *Br J Cancer* **88**, 1411-1416
63. Okegawa, T., Li, Y., Pong, R. C., Bergelson, J. M., Zhou, J., and Hsieh, J. T. (2000) *Cancer Res* **60**, 5031-5036
64. Huang, K. C., Altinoz, M., Wosik, K., Larochelle, N., Koty, Z., Zhu, L., Holland, P. C., and Nalbantoglu, J. (2005) *Int J Cancer* **113**, 738-745
65. Rauen, K. A., Sudilovsky, D., Le, J. L., Chew, K. L., Hann, B., Weinberg, V., Schmitt, L. D., and McCormick, F. (2002) *Cancer Res* **62**, 3812-3818
66. Zinn, K. R., Douglas, J. T., Smyth, C. A., Liu, H. G., Wu, Q., Krasnykh, V. N., Mountz, J. D., Curiel, D. T., and Mountz, J. M. (1998) *Gene Ther* **5**, 798-808
67. Awasthi, V., Meinken, G., Springer, K., Srivastava, S. C., and Freimuth, P. (2004) *J Virol* **78**, 6431-6438
68. Josefsson, M., Grunditz, T., Ohlsson, T., and Ekblad, E. (2002) *Acta Physiol Scand* **175**, 129-137
69. Vallabhajosula, S., Paidi, M., Badimon, J. J., Le, N. A., Goldsmith, S. J., Fuster, V., and Ginsberg, H. N. (1988) *J Nucl Med* **29**, 1237-1245
70. Ashbourne Excoffon, K. J., Moninger, T., and Zabner, J. (2003) *J Virol* **77**, 2559-2567
71. Berry, M. N., and Friend, D. S. (1969) *J Cell Biol* **43**, 506-520
72. Laemmli, U. K. (1970) *Nature* **227**, 680-685
73. Kanerva, A., Raki, M., Ranki, T., Sarkioja, M., Koponen, J., Desmond, R. A., Helin, A., Stenman, U. H., Isoniemi, H., Hockerstedt, K., Ristimaki, A., and Hemminki, A. (2007) *J Gene Med* **9**, 3-9
74. Wang, L. H., Rothberg, K. G., and Anderson, R. G. (1993) *J Cell Biol* **123**, 1107-1117

75. Heuser, J. E., and Anderson, R. G. (1989) *J Cell Biol* **108**, 389-400
76. Santos, N. C., Ter-Ovanesyan, E., Zasadzinski, J. A., Prieto, M., and Castanho, M. A. (1998) *Biophys J* **75**, 1869-1873
77. Silva, L., Coutinho, A., Fedorov, A., and Prieto, M. (2006) *Biophys J* **90**, 3625-3631
78. Torgersen, M. L., Skretting, G., van Deurs, B., and Sandvig, K. (2001) *J Cell Sci* **114**, 3737-3747
79. Rubino, M., Miaczynska, M., Lippe, R., and Zerial, M. (2000) *J Biol Chem* **275**, 3745-3748
80. Li, E., Stupack, D., Klemke, R., Cheresch, D. A., and Nemerow, G. R. (1998) *J Virol* **72**, 2055-2061
81. Mousavi, S. A., Brech, A., Berg, T., and Kjekken, R. (2003) *Biochem J* **372**, 861-869
82. Rodriguez, E., and Everitt, E. (1996) *J Virol* **70**, 3470-3477
83. Kjekken, R., Mousavi, S. A., Brech, A., Griffiths, G., and Berg, T. (2001) *Biochem J* **357**, 497-503
84. Balakireva, L., Schoehn, G., Thouvenin, E., and Chroboczek, J. (2003) *J Virol* **77**, 4858-4866
85. Li, E., Brown, S. L., Stupack, D. G., Puente, X. S., Cheresch, D. A., and Nemerow, G. R. (2001) *J Virol* **75**, 5405-5409
86. Smith, T. A., Idamakanti, N., Marshall-Neff, J., Rollence, M. L., Wright, P., Kaloss, M., King, L., Mech, C., Dinges, L., Iverson, W. O., Sherer, A. D., Markovits, J. E., Lyons, R. M., Kaleko, M., and Stevenson, S. C. (2003) *Hum Gene Ther* **14**, 1595-1604
87. He, Y., Chipman, P. R., Howitt, J., Bator, C. M., Whitt, M. A., Baker, T. S., Kuhn, R. J., Anderson, C. W., Freimuth, P., and Rossmann, M. G. (2001) *Nat Struct Biol* **8**, 874-878
88. Chow, F. L., and Fernandez-Patron, C. (2007) *IUBMB Life* **59**, 44-47
89. Ihrke, G., Neufeld, E. B., Meads, T., Shanks, M. R., Cassio, D., Laurent, M., Schroer, T. A., Pagano, R. E., and Hubbard, A. L. (1993) *J Cell Biol* **123**, 1761-1775

90. Campbell, S. A., Lin, J., Dobrikova, E. Y., and Gromeier, M. (2005) *J Virol* **79**, 6281-6290
91. Shaw, G., Morse, S., Ararat, M., and Graham, F. L. (2002) *Faseb J* **16**, 869-871
92. Hommelgaard, A. M., Lerdrup, M., and van Deurs, B. (2004) *Mol Biol Cell* **15**, 1557-1567
93. Everitt, E., and Rodriguez, E. (1999) *Arch Virol* **144**, 787-795
94. Pike, L. J. (2004) *Biochem J* **378**, 281-292
95. Hautala, T., Grunst, T., Fabrega, A., Freimuth, P., and Welsh, M. J. (1998) *Gene Ther* **5**, 1259-1264
96. Durmort, C., Stehlin, C., Schoehn, G., Mitraki, A., Drouet, E., Cusack, S., and Burmeister, W. P. (2001) *Virology* **285**, 302-312
97. Triantafilou, K., and Triantafilou, M. (2004) *Virology* **326**, 6-19
98. Bai, M., Campisi, L., and Freimuth, P. (1994) *J Virol* **68**, 5925-5932
99. El-Husseini Ael, D., Craven, S. E., Brock, S. C., and Brecht, D. S. (2001) *J Biol Chem* **276**, 44984-44992
100. Gauthier-Campbell, C., Brecht, D. S., Murphy, T. H., and El-Husseini Ael, D. (2004) *Mol Biol Cell* **15**, 2205-2217
101. Alvarez, E., Girones, N., and Davis, R. J. (1990) *J Biol Chem* **265**, 16644-16655
102. Cavaggioni, A., and Mucignat-Caretta, C. (2000) *Biochim Biophys Acta* **1482**, 218-228
103. Hong, J. S., and Engler, J. A. (1996) *J Virol* **70**, 7071-7078
104. Cusack, S. (2005) *Curr Opin Struct Biol* **15**, 237-243
105. Marceau, F., and Regoli, D. (2004) *Nat Rev Drug Discov* **3**, 845-852
106. Chao, J., Li, H. J., Yao, Y. Y., Shen, B., Gao, L., Bledsoe, G., and Chao, L. (2007) *Hypertension* **49**, 490-497

107. Imamura, T., Kobayashi, H., Khan, R., Nitta, H., and Okamoto, K. (2006) *J Immunol* **177**, 8723-8729
108. Carson, S. D. (2004) *Biochemistry* **43**, 8136-8142
109. Mills, J. S., Needham, M., and Parker, M. G. (1987) *Embo J* **6**, 3711-3717
110. Mills, J. S., Needham, M., and Parker, M. G. (1987) *Nucleic Acids Res* **15**, 7709-7724
111. Hiipakka, R. A., Chen, C., Schilling, K., Oberhauser, A., Saltzman, A., and Liao, S. (1984) *Biochem J* **218**, 563-571
112. Nagai, M., Yaoita, E., Yoshida, Y., Kuwano, R., Nameta, M., Ohshiro, K., Isome, M., Fujinaka, H., Suzuki, S., Suzuki, J., Suzuki, H., and Yamamoto, T. (2003) *Lab Invest* **83**, 901-911
113. Bruning, A., and Runnebaum, I. B. (2004) *Exp Cell Res* **298**, 624-631
114. Economides, K. D., and Capecchi, M. R. (2003) *Development* **130**, 2061-2069
115. Smith, E. R., Miller, T. B., and Pebler, R. F. (1983) *Am J Physiol* **245**, F470-477
116. Hebert, L. A., Lemann, J., Jr., Petersen, J. R., and Lennon, E. J. (1966) *J Clin Invest* **45**, 1886-1894
117. Shapiro, L., Fannon, A. M., Kwong, P. D., Thompson, A., Lehmann, M. S., Grubel, G., Legrand, J. F., Als-Nielsen, J., Colman, D. R., and Hendrickson, W. A. (1995) *Nature* **374**, 327-337
118. Pokutta, S., Herrenknecht, K., Kemler, R., and Engel, J. (1994) *Eur J Biochem* **223**, 1019-1026
119. Chitaev, N. A., and Troyanovsky, S. M. (1998) *J Cell Biol* **142**, 837-846
120. Umbas, R., Isaacs, W. B., Bringuier, P. P., Schaafsma, H. E., Karthaus, H. F., Oosterhof, G. O., Debruyne, F. M., and Schalken, J. A. (1994) *Cancer Res* **54**, 3929-3933
121. Bradshaw, B. S., and Wolfe, H. G. (1977) *Biol Reprod* **16**, 292-297